UNCLASSIFIED

AD NUMBER

AD360851

CLASSIFICATION CHANGES

TO: unclassified

FROM: confidential

LIMITATION CHANGES

TO:

Approved for public release, distribution unlimited

FROM:

Distribution: Controlled: All requests to Naval Research Lab., Washington, DC.

AUTHORITY

NRL ltr, 20 Dec 2002; NRL ltr, 20 Dec 2002

THIS PAGE IS UNCLASSIFIED

AD NUMBER
AD360851
CLASSIFICATION CHANGES

TO

confidential

FROM

secret

AUTHORITY
OCA; 31 Dec 1976 IAW document markings

CONFIDENTIAL

CONFIDENTIAL

SECRET

360851L

DEFENSE DOCUMENTATION CENTER

FOR

SCIENTIFIC AND TECHNICAL INFORMATION

CAMERON STATION, ALEXANDRIA, VIRGINIA

Progress Report No. 17
Volume I
Hypervelocity Kill Mechanisms Program
[Unclassified Title]

Sponsored by

Advanced Research Projects Agency
Ballistic Missile Defense Systems Branch
ARPA Order No. 149

Semiannual Technical Progress Report
for period ending 30 September 1964

December 1964

U.S. NAVAL RESEARCH LABORATORY
Washington, D.C.

CONTRIBUTORS

Aeronautical Research Associates of Princeton
AVCO – RAD
General Electric Company – MSD
U.S. Naval Research Laboratory

SECURITY

This document contains information affecting the national defense of the United States within the meaning of the Espionage Laws, Title 18, U.S.C., Sections 793 and 794. The transmission or the revelation of its contents in any manner to an unauthorized person is prohibited by law.

DDC AVAILABILITY NOTICE

All distribution of this report is controlled. Qualified DDC users shall request through Director, U.S. Naval Research Laboratory, Washington, D.C. 20390.

CONTENTS
Volumes I and II

PROBLEM STATUS

This progress report covers the work of the participants in the Hypervelocity Kill Mechanisms Program. Work on this problem is continuing.

Authorization

NRL Problem No. F04-11

ARPA Order No. 149-60 - Amendments 1 thru 9

SUMMARY

W.W. Atkins - M.A. Persechino
U.S. Naval Research Laboratory

INTRODUCTION

Progress Report No. 17 is a semiannual technical progress report covering the work of the participants in the Hyper-velocity Kill Mechanisms Program for the period beginning 31 March 1964 to 30 September 1964. Reports covering the work completed during and prior to this reporting period are listed in Section Y.

The work of this program has involved comprehensive studies designed to evaluate the feasibility of defeating the mission of an intercontinental ballistic missile by fragment impact and/ or by subsequent re-entry heating effects. These effects include: direct kill by impact, extent of aggravation or in-crease in damage caused by aerothermal effects on an R/V during re-entry, aerodynamic instability of nose cones caused by damage to the heat shield and structure, impact and thermal damage to internal components and warheads, and perturbations on the performance of ICBM booster vehicles. The HKM Program is divided into the following four phases of work:

1. <u>Impact Damage</u>. Initially BRL, NRL, AVCO and the Canadian Armament Research and Development Establishment were selected to study the effects of hypervelocity impacts on re-entry body materials and structures. Aerojet-General was selected to study the impact effects on propulsion systems. The work of Aerojet has been completed and the final report has been distributed. The impact work performed by AVCO has also been completed and a final report was included in Progress Report No. 13. The work completed by CARDE was reported in Progress Report No. 11. BRL is preparing a final report for their work on impacts into ablative structures. Only NRL is presently engaged in impact work for the HKM Program.

2. <u>Aerothermal</u>. In the early stages of the program, AVCO performed a multitude of experiments on cratered heat shield materials using rocket exhaust and plasma jet facilities in order to determine the thermodynamic effects on a damaged vehicle during re-entry. In the later stages of the program, punctured vehicles (vented and unvented) were analyzed. GE

and AVCO performed analytical and experimental studies on coupled and uncoupled flows, jet impingement, jet diffusion, and the determination of orifice coefficients for perforated re-entry vehicles. GE conducted an analytical study to determine the aerodynamic effects on a damaged vehicle during re-entry (the aeroballistic ranges and the wind tunnels of NOL and AEDC were utilized to provide experimental data). An effective kill mechanism did not evolve from these studies. During the latter part of the second year's effort ARAP was added to the participants in the aerothermal work and, at this time, a strong fundamental research effort on internal heating was established to determine a rationale for coupled and uncoupled flows, impinging jets, and wall jets. A flight test program employing a NASA propulsion and recovery system has been completed and the details of this program are described in Item 21 in the list of reports of Section Y. These tests provided both external and internal heating data under actual and simulated environmental conditions.

3. **Vehicle Vulnerability.** The vulnerability work initially conducted to determine the vulnerability of re-entry body, warhead, and associated arming and fuzing components by BRL and Picatinny Arsenal has been terminated. A final report on the vulnerability of nuclear warheads to aerothermal effects has been prepared by Picatinny Arsenal and distributed (See Item 22, Section Y).

Aerojet-General, under the technical management of the Weapons Laboratories, Detachment 4, RTD, Eglin AFB has completed the investigations to determine the vulnerability to fragment impact of both liquid and solid rocket propulsion systems. An analysis of the vulnerability of both the United States and other vehicles is included in the Aerojet final report (See Items 24, 25 and 26).

4. **Intelligence.** The intelligence phase of the work was designed to provide information and guide lines for the work performed in the other phases of the HKM Program. A report entitled "Soviet ICBM Re-Entry Body Study" has been prepared by Raytheon. This report provides a description of the Soviet ICBM based on early Soviet missile tests in the Pacific (See Item 1). Additional intelligence data are described in Section T of previous HKM Progress Reports.

PROGRESS

The work described below is a summary of the technical progress in the remaining phases of the HKM program for the period ending 30 September 1964.

1. Impact Damage Phase

The investigation by the Ballistic Research Laboratories of impact damage to composite targets utilizing jet pellets fired from an inhibited jet charge is completed and a final report describing this work will be included when available.

The impact work conducted at NRL during this reporting period has been directed primarily toward the development of a theoretical understanding of the mechanisms involved in hyper-velocity impact damage to the ablative structure of re-entry vehicles. Two-dimensional wave analysis, utilizing hand calculations, was applied to obtain wave diagrams of shock transmission through the structure and energy and momentum transfer from projectile to target. Pressure-time recordings were also made in large scale ablative experiments at impact angles of 45° in order to guide the theoretical approach into more realistic impact situations.

In the experimental aspects of the program comparisons were made of large and small scale impacts of steel and aluminum projectiles fired into various thickness phenolic-refrasil targets with steel back-up structures. In general it was found that gross damage effects on flat-plate ablative structures can be extrapolated from smaller scale experiments. However, extension of hole-size data to large scale impacts at high angles of impact indicates a sizable change in trends.

Three energy regimes for producing holes in ablative structures have been analyzed. These regimes are the low energy regime where only the ablative is perforated; the transition region where both the ablative and the metallic back-up structure are perforated but little or no energy is dissipated behind the target; and the excess energy region where the hole size in the back-up is equal to or greater than the hole size in the ablative. The power of the energy-thickness ratio in the hole size correlation varies from about two-thirds to one-third depending upon the energy regimes considered. The excess energy regime is of the greater importance because impact damage to components located inside a realistic target is considered lethal only for the excess energy perforation condition. It is significant to note that in this regime the power of the energy-thickness term is considerably less than the power for this term in the transition region, indicating that once the excess energy region is reached considerably more energy per unit thickness of material is required to produce

the same size hole. It is only in this region that significant energy is contained in the residual or spall fragments to cause serious damage to re-entry vehicle components; and as a consequence, a smaller percentage of the initial impact energy is transferred to the ablative structure.

In the scaling experiments conducted for 45° angles of impact in the excess energy regime, the results show that the power of the energy-thickness term is greater than that for 90° impacts indicating that:

a. At angles of obliquity larger holes are produced in the ablative than for normal impacts.

b. More of the initial impact energy is transferred to the ablative structure and less into residual or spall fragments. In these experiments it was also noted that for ablative thickness to projectile diameter ratios of 0.7 more energy per unit thickness was required to produce the same size hole in structures with thickness ratios equal to 1.4, indicating a thin plate effect.

The results for 90° impacts (excess energy regime) into astrolite targets with steel back-up structure were in good agreement with the hole-size correlation presented by NRL at the Sixth Symposium for steel impacts into various ablative materials.

2. Aerothermal Phase

A seven test program was recently completed in the Malta Rocket Exhaust Facility to determine internal heat transfer to re-entry vehicle models with large perforations. Machined holes were varied to simulate hypervelocity impact damage and these results were compared with actual impact damage. Relatively large perforated models were tested in the high pressure, high enthalpy, ablating environment. Details of the first five tests were discussed in Section H of HKM Semiannual Progress Report, No. 15, for the period ending March 31, 1964. A summary report on all seven tests has been published and appears as Item 29 in the list of ARPA 149 technical reports in Section Y.

Details of the sixth and seventh tests are presented in Section H of this report and will be briefly summarized below. The Malta Rocket Exhaust Internal Heating Test Program was completed with Tests No. 6 and 7. The principal objective of these two tests was to determine the heat protection

characteristics of a lightweight 3 lb/cu ft rigid urethane
foam when used as a filler material in a re-entry vehicle.
Pre-test and post-test photographs of the models are shown
in Figures 4 thru 7 of Section H. Temperature-time histories
are shown in Figures 8 and 9, and plots of foam recession vs
time are shown in Figures 10 and 12.

The thermal performance of the foam was character-
ized by an effective heat of ablation $Q^* = \Delta E/\Delta M$, where
ΔE = total energy entering perforation cavity and
ΔM = weight of foam removed by ablation. Values of Q^* for
two different density foams were determined from tests Nos.
5, 6 and 7. These values are about 2000 Btu/lb for densities
of 3.0 lb/cu ft and 3000 Btu/lb for 7.8 lb/cu ft.

A principal achievement of the internal heating
program was the establishment of a correlation of the rate of
energy influx through a heat shield perforation. The applica-
tion of the correlation to a high-performance unfoamed R/V
indicates that an internal heating load of about 200 Btu per
square inch of perforation area is accumulated by 50,000 feet
altitude for a perforation occurring at 100,000 feet altitude.
The final correlation equation for the rate of energy ab-
sorption by a re-entry vehicle structure is:

$$dE/d\theta = 0.0105 \frac{\gamma}{\gamma - 1} \frac{PUA}{J}$$

γ = ratio of specific heats

P = local external static pressure, psia

U = local external velocity, ft/sec

A = perforation area, in^2

J = 778 ft-lb/Btu

The equation in this form neglects the effect of per-
foration enlargement during re-entry, hence calculations for
energy absorption by the R/V are considered conservative.
The above empirical correlation is in good agreement with the
results obtained by Donaldson using a turbulent shear layer
mixing analysis and is good over a range of three decades in
the correlating parameter and for two widely different test
environments as well as for irregularly shaped holes.

An initial study was begun in August 1964 with the
objective of developing an understanding of the heat pro-
tection characteristics of large variety of lightweight foams

of densities less than 15 lb/cu ft. Impact tests have shown that foam fillers placed behind ablative structures are also effective in absorbing the impact energy, therefore the use of internal foam will serve a dual purpose. Since no thermal performance data for this class of material are presently in existence, the study is being conducted in two separate but related phases. Phase 1 is a concentrated effort on the basic understanding of ablation phenomena associated with cavity heating and phase 2 is a study in the GE 5-megawatt air arc of the response of selected foams with simulated impact cavities. The foam response for two densities of urethane foam will also be determined in three different facilities in order to determine the effects of widely varying test environments.

A thermostructural kill study is also being conducted by GE to formulate a simplified computational model for determining thermostructural kill of perforated re-entry vehicles (both hardened and unhardened). Seven vehicle configurations with ballistic coefficients from 1700 to 4400 lb/ft^2 have been selected for investigation.

A major analytical study of the characteristics of free shear flow was completed by ARAP during this reporting period. Expressions have been derived for a free shear flow which develops when a free stream of gas moving at some velocity passes over a cavity of stagnant gas. A shear which develops between the moving and still gas causes a mixing region to develop downstream of the initial encounter of the two gases. It is now possible to solve problems of this type with two different gases, one in the mainstream and the other in the cavity. A principal part of this experimental program has been the thorough investigation of jet impingement. Detailed results of this investigation will be presented in two reports. The first of these reports is complete and appears as Volume II of this Report. It covers the free jet and normal impingement studies. A second report covering results for oblique impingement is nearing completion and will be published and distributed at a later date. Most of the pertinent results of both these reports have been reviewed in previous status reports.

The work reported in Section K by AVCO is in the area of instrumentation and investigation of instabilities in the high temperature 1.5 megawatt air arc. Apparatus constructed for measurement of gas enthalpy, composition, velocity and density of a free compressible, turbulent, high enthalpy jet are discussed. Experimental results from this high velocity facility will be utilized by ARAP in evaluating the associated mixing parameter, K, by means of the two-gas mixing analysis described in Section L.

NRL MEMORANDUM REPORT 1578

HYPERVELOCITY KILL MECHANISMS PROGRAM
ARPA ORDER 149-60

Impact Damage Phase

Semiannual Progress Report for Period
Ending 30 September 1964

C.D. Porter

This research was supported by the Advanced
Research Projects Agency, Ballistic Missile
Defense System Branch

NOTE: This report is for inclusion in the
overall HKM Report. The page
Designation for this Section of the
Report is the letter "B".

U.S. NAVAL RESEARCH LABORATORY
WASHINGTON, D.C.

CONTENTS

SUMMARY

The theoretical understanding and prediction of damage both to the ablative skin and to the interior structure of a re-entry vehicle for any impact situation is currently being studied at NRL. In the experimental phase of this program projectile masses (saboted steel and aluminum) range from a few grams to about 366 grams. Impact energies are as high as four megajoules. In general gross damage to flat plate ablative structures extrapolates quite well from smaller scale experiments; however, extension of impact data at angles of obliquity into the megajoule range indicates a sizable change in trends.

A hole-size theory is given which compares favorably with an empirically determined equation. To reinforce this study, wave analysis is used to deduce relative distribution between axial and radial momentum in the developing impact situation. The theoretical shock wave components are studied in impact experiments where pressure sensors are placed at various points in and around the composite skin.

PROBLEM STATUS

This is a Semiannual Technical Progress Report. Work on this project is continuing.

AUTHORIZATION

HYPERVELOCITY KILL MECHANISMS PROGRAM
ARPA ORDER NO. 149-60

IMPACT DAMAGE PHASE
[Unclassified Title.

INTRODUCTION

The U.S. Naval Research Laboratory under sponsorship of the Advanced Research Projects Agency and Office of Naval Research has been engaged in a study of hypervelocity impacts in various re-entry vehicle materials and structural elements. Information about the basic deformation process and formulas predicting damage under a wide range of impact conditions have resulted. The objectives of this work are twofold. The first goal is to determine the feasibility of hypervelocity fragment impact as a kill mechanism, and the second goal is to provide criteria for hardening or increasing the resistance of re-entry vehicle structures to impact damage. The work discussed in this paper is also directly applicable to space vehicle technology. Much of the previous hypervelocity ablative work at NRL was conducted using projectile masses of only a few grams. Some doubt as to the validity of extrapolation of these data to large mass impacts has existed in view of different empirical formulas which were developed from small scale work at various laboratories (1-3). In order to obtain data for large mass projectiles, an 8-inch hypervelocity light-gas gun range was designed and installed at the U.S. Naval Research Laboratory (see Figure 1). A total of seven shots in the megajoule range have been made to date into spaced structure elements and into ablative targets.

This paper will deal with both large and small scale impacts with particular emphasis on phenolic refrasil targets and steel and aluminum projectiles.

WAVE ANALYSIS FOR HYPERVELOCITY IMPACT INTO A COMPOSITE STRUCTURE

The problem of normal impact of a plastic cylinder on an ablative surface backed up by a steel plate (Figure 2) was chosen as a first step in the theoretical consideration for ablative structure impacts.

This impact problem is considered as a wave propagation problem in three dimensions. If the projectile has an axis of symmetry coincident with the velocity vector and normal to the target surface, then the problem can be ideally reduced to a two-dimensional case. The methods outlined in References 4 and 5 could then be applied if the variation in stream line cross section with time during the impact process is known (convenient shock wave relations for immediate characteristic treatment of the materials desired were not available; in addition, steel has unique multiple-valued wave transmission properties at high pressure). As a first approximation, it was decided to use acoustic approximations of linear superposition of amplitudes (6) assuming Equations (1) and (2) to be usable approximations of the true physical situation where ΔP_i and Δu_i were determined from Hugoniot curves:
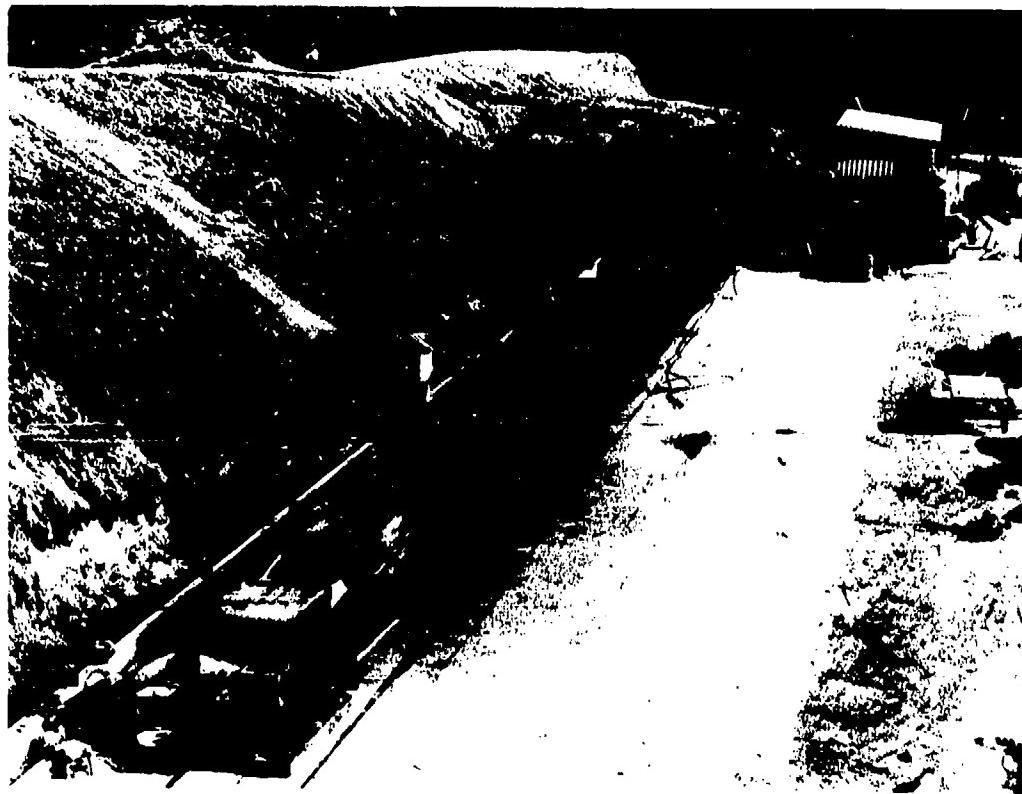
Figure 1 - Light-inch hypervelocity light-gas gun range
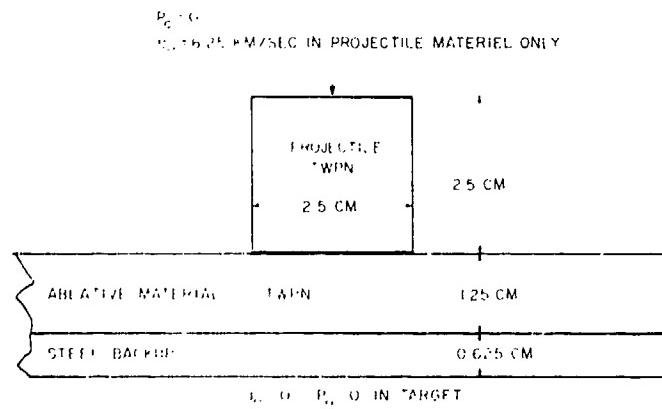
Figure 2 - Model of ablative-composite
impact for wave study

$$P \quad P_o \cdot \sum_{i=1}^{n} \, {}^{\cdot}P_i \tag{1}$$

$$u \quad u_o \cdot \sum_{i=1}^{n} \, {}^{\cdot}u_i \, \cdot \tag{2}$$

It is to be noted that Equation (2) is in vector form and as inclined waves develop due to finite boundary conditions u and ${}^{\cdot}u_i$ will consist of both normal components $u_\perp$ and radial components u_r. The Hugoniot relating pressure and the density function of oblique tape wound phenolic nylon (TWPN) and steel were taken or computed from References 7 and 8. The impact model is shown in Figure 2.

Consideration of Tape Wound Phenolic Nylon

A tape wound phenolic nylon ablative (TWPN) was assumed for both a square cylindrical projectile and the ablative surface. A Hugoniot Curve was not available for this material but Reference 7 gives the following equations from which shock equations can be used to generate the applicable Hugoniot Curves shown in Figures 3 and 4:

$$U \quad a' \cdot b'u \tag{3}$$

$$P \cdot \cdot_o Uu \tag{4}$$

$$\cdot \quad \cdot \cdot_o \quad \cdot \cdot \cdot 1 \tag{5}$$

$$P \quad \frac{A(\cdot - 1) \cdot}{(K - \cdot^2)} \tag{6}$$
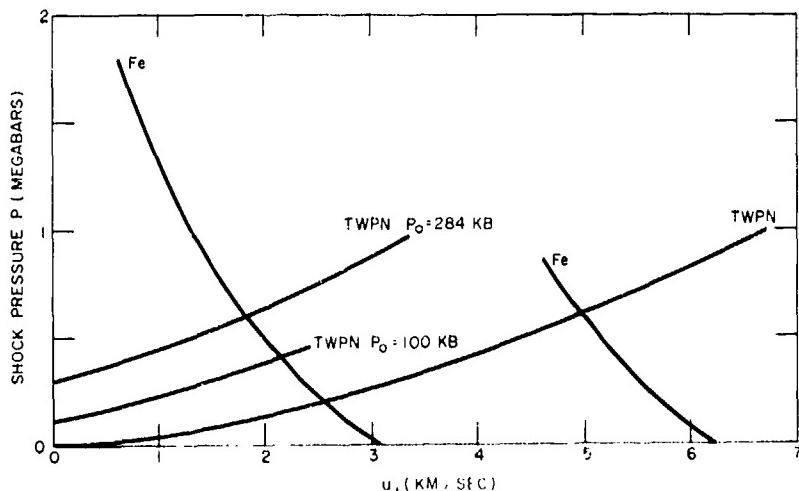
Figure 3 - Shock pressure vs particle velocity
(Hugoniot for pressure determinations)
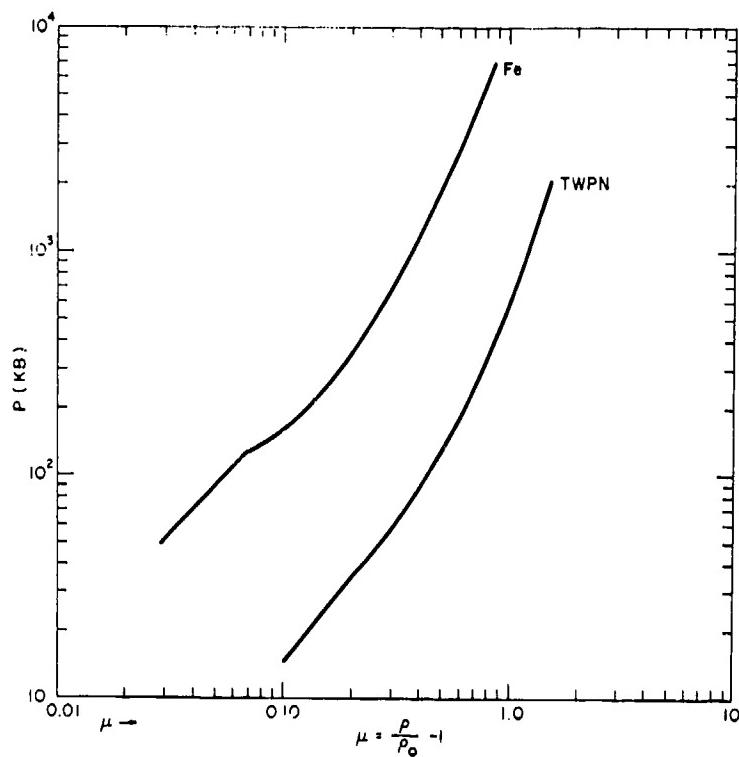
Figure 4 - Pressure vs fractional change
in density (Hugoniot relationships)

for TWPN the above constants are:

$$a' = 3.17 \text{ (km/sec)} \qquad A = 1020 \text{ (KB)}$$
$$b' = 1.35 \qquad K = 3.88.$$

The relationship connecting shock pressure with particle velocity for iron and TWPN was plotted as Figure 3. The Hugoniot for iron copied from Reference 8 was plotted in reversed form (right to left) from origin points at values of particle velocity $u = 3.125$ and 6.25 km/sec. Also the Hugoniot for TWPN was plotted with initial pressures of 100 and 284 KB at the origin $u = 0$. Standard procedures were used to deduce sound velocity from the curves relating pressure and u (Figure 4) with the help of Equation (7). Considering the material as a compressible fluid the sound velocity a_0 is given by:

$$a_0 \quad \sqrt{\frac{\partial P}{\partial \rho}\, g} \tag{7}$$

since

$$\mu \quad \frac{\rho}{\rho_0} - 1 \qquad d\mu \quad \frac{d\rho}{\rho_0} \tag{8}$$

$$a_0 = \sqrt{\frac{\partial P g}{\rho_0 \partial \mu}}, \tag{9}$$

SECRET

From Figure 4, P ... was determined and Equation (9) was solved for the velocity of sound over the range of values of ... shown in Figure 5 for both iron and TWPN. An interesting feature of the curve for iron is the discontinuity in sound velocity at 5.9 km/sec exhibited ... = 0.054 which would be reached at a pressure of about 130 KB in iron. When ... is 0.21, or the iron pressure is about 380 KB, a sound velocity of 5.9 km/sec is again attained. The shaded region in which sound velocity falls below that in unpressurized iron can lead to interesting consequences in wave propagation as reported by other observers (11). In the study of wave transmission through the steel back-up it was felt that little physical departure from reality would be experienced if the boundary rarefaction was assumed to be a single shock traveling at the local speed of sound through the plate. The plate is relatively thin compared to the model projectile and ablative covering and furthermore the spalling criterion which would result from a more exact study is not the objective of this analysis.

Stepwise wave solution of the impact model shown in Figure 2 is now undertaken. For impacts of like materials u (1 2)u$_0$ 3.125 km/sec. Referring to Figure 3, it is observed that a shock pressure of 284 KB is necessary for a particle velocity of 3.125 km/sec to be developed in stationary TWPN. From Equation (10) (conservation of mass)
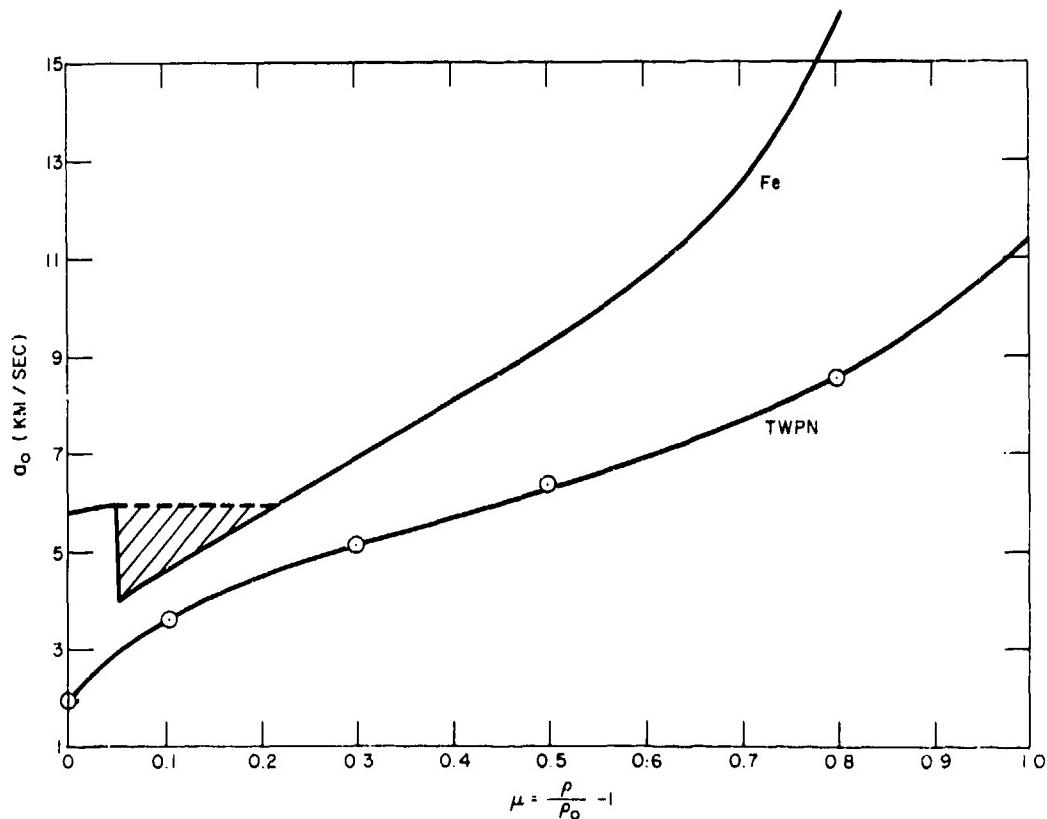

Figure 5 - Dilatational wave velocity vs density increase for Fe and TWPN

$$(u_n - U)\ (u - U)\ \quad ,\ \cdot_0\ \quad 1.737.\tag{10}$$

Hence, in the fixed coordinate system, the shock velocity in the projectile is $U = 1.125$ km/sec, and $U_{TWPN} = 6.25$ km/sec $+ 1.125$ km/sec $= 7.375$.

Figure 6 shows the shock situation which has developed 0.8 μsec after impact. The wavy line A in this figure is the contact surface separating the projectile from the impacted target ablative material. A compression shock is traveling back in the projectile as a plane wave B (edge effects are neglected) and into the ablative material as a plane wave designated by the straight line C. Since tensile forces are negligible, a rarefaction wave (assumed to be a rarefaction shock to simplify calculation) originates at the surface and proceeds inward radially as shown by E. The radial rarefaction originating at the junction of the shock B and the cylindrical surface of the projectile induces a solenoidal radial expansion motion which is normal to the rarefaction wave E and may be at any angle depending upon the angle of the wave E. The components of velocity of the contacting materials perpendicular to the curved surface of contact are finite so there is an effective collision velocity of 2.22 km/sec which must be restrained (after initial reduction of pressure to zero) in order to avoid overlap of projectile and ablative materials. This region is shown as a dark triangular region in Figure 6. A transient pressure wave E' of about 120 KB is generated in this region by the interference and maintained until Bernoulli flow, necessary to maintain boundary pressure over the flow region, is established. Below the region of free expansion of the projectile in the interference zone there exists a high velocity hydrodynamic flow region where the projectile and target material are subjected to a series of expansion waves until Bernoulli velocity u_e
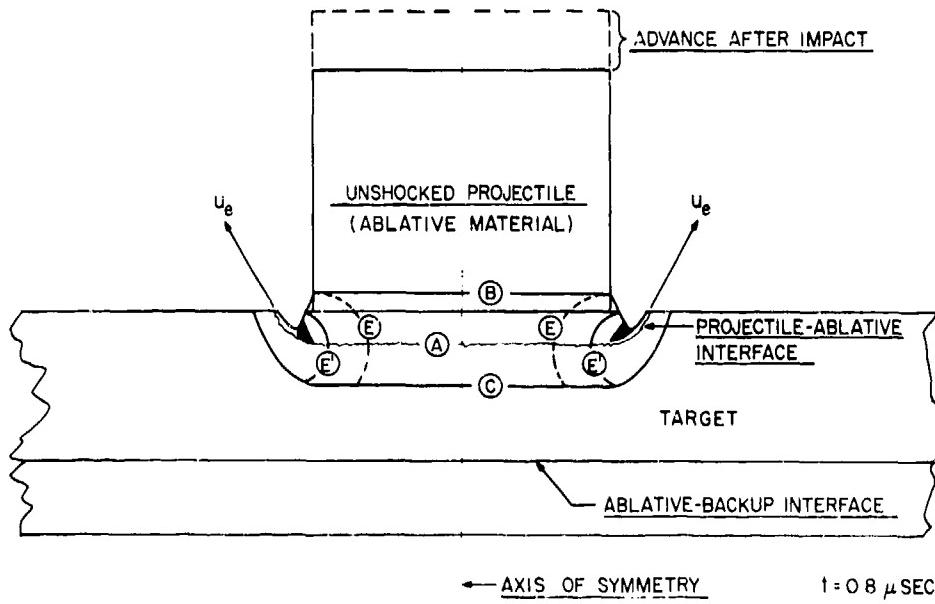
Figure 6 - Early stage of wave study, t = 0.8 μsec

satisfies the Bernoulli equation $\rho_0 u_e^2 / 2 \sim P$ is reached by the ejecting material. Computation shows u_e to be 6.79 km/sec.

The total change of velocity Δu_e of ejecta when the ejecta velocity is normal to the original ablative surface is 6.25 - (-6.79) km/sec or 13.04 km/sec. A sample calculation on mass flow of ejecta to maintain the initial 280 KB of pressure over the interference ring follows from Newton's law.

$$\dot{W} = \frac{PA_r}{\Delta u_e} = \frac{280 \text{ gm} \cdot 9.81 \text{ cm} \cdot 10^8 \cdot 3.1416 \cdot 0.625 \text{ cm}^2}{\text{cm}^2 \cdot \text{sec}^2 \cdot 13 \cdot 10^5 \text{ cm/sec}} = 4.15 \cdot 10^5 \text{ gm sec}$$

where

A_r = Area of interference ring = $2 \pi r \cdot \Delta r$ = 0.625 cm²

r = 1.25 cm (radius of projectile)

$\Delta r \cong 0.25$ cm.

After 1.7 μsec (Figure 7) the approximate average mass of ejecta $\cong \dot{W} \cdot t$ = 4.15 · 1.7 · 10^{-1} = 0.71 gm (where the mass flow rate is the average between time zero and 1.7 μsec). This sample calculation was carried out for each figure and gives a reasonable check with computed mass loss from the computation from observed momentum augmentation. This enlarging propagation pattern continues from about 1.7 μsec when the compression wave reaches the steel back-up surface as shown in Figure 7.
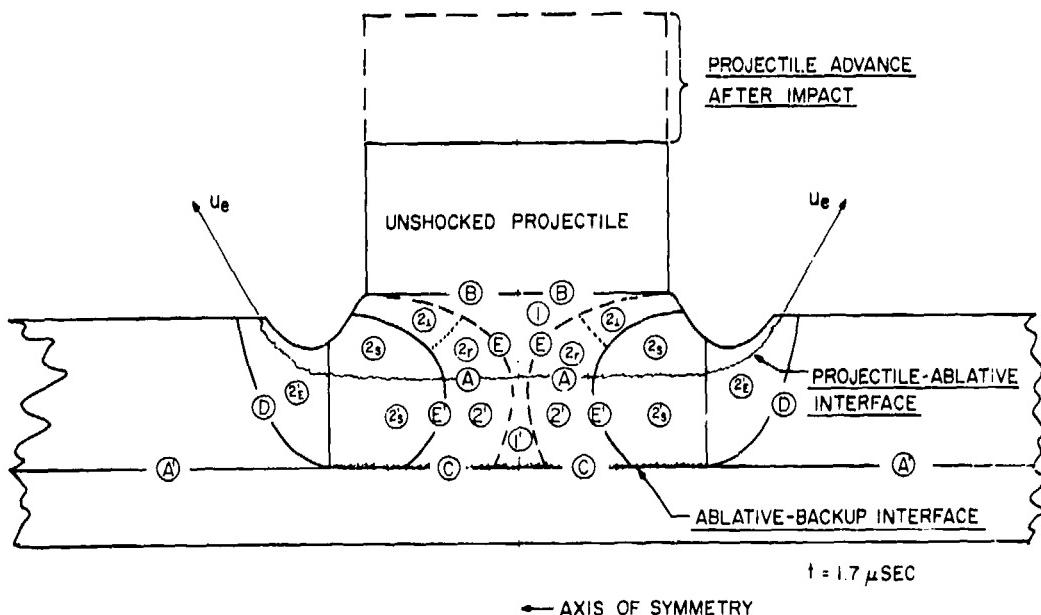
Figure 7 - Wave study (shock arrival at back-up) t = 1.7 μsec

A sample of the dynamic values 1.7 μsec after impact in the numbered regions of Figure 7 are given in Table I. Initial conditions just prior to impact are W_o = 14.9 gm, E_o = 291 kj, M_o = 93.1 gm-km/sec. At the laminate rear surface one has an interface problem which must be reduced to a pure impact problem to apply methods of Reference 8. This condition is satisfied if one pictures a statically compressed ablative which is then impacted by the steel back-up plate moving at the particle velocity u, as only the frame of reference is changed in the situation considered. This situation is shown in the two curves for TWPN and Fe and are plotted in Figure 3 in the manner for impacts with dissimilar materials with TWPN starting at the precompressed pressure of 284 KB. For the area marked 1' in Figure 7, the intersection of the two curves in Figure 3 is at 610 KB which is the predicted pressure wave which must propagate into the iron at about 9.3 km/sec. It is noted that this is exactly the pressure attained if steel were impacted directly with TWPN at 6.25 km/sec. (Right r e intersection, Figure 3). This is greater than the 284 KB incident wave, so an additional compressive shock G of 326 KB must be propagated back into the ablative surface as shown in inner part of shock front F in Figure 8. For the area between E, O and E' and above F, the ablative pressure is approximately zero. The intersection of the bottom TWPN curve of Figure 3 is at about 200 KB which is the amplitude of the reflected pressure wave around G. In the region below F bounded by E' and K a pressure of 120 KB is added to raise the total pressure in this area to 320 KB. The reflected component F traveling in a direction normal to the target surface at a shock velocity consistent with the local speed of sound of the region generates from its free end an expanding oblique compression wave J and a rarefaction K assuming the applicability of Huygens principle (these lines assumed to be straight for simplification of calculations would not exist with a sharp gradient but there would be rather a rarefaction front originating at the reflection boundary). The central inner
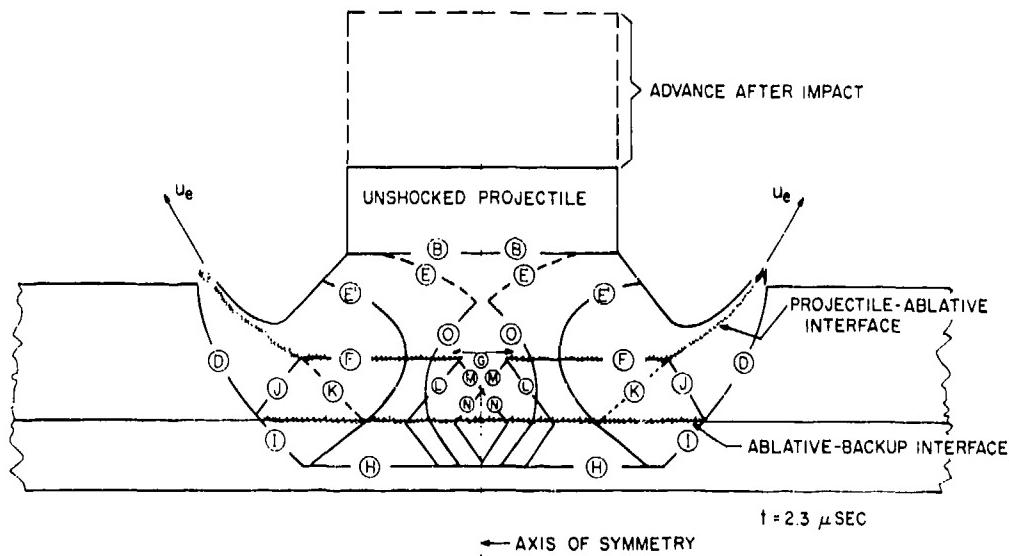
Figure 8 - Wave study (reflected shock at projectile-ablative interface) t = 2.3 μsec

TABLE I
(From Wave Analysis)

Region (Fig. 7)	P (KB)		a_o (km/sec)	U (km/sec)	$u_\perp$ (km/sec)	u_r (km/sec)	W_i (gm)	M_i (gm-km/sec)	E_i (kj)	M_{ir} (gm-km/sec)
Unshocked Projectile	0	0	5.8	NA	6.25	0	7.26	45.45	142.03	0
1	284	0.737	7.95	1.12	3.125	0	1.03	3.25	5.08	0
2	0	0	3.00		3.125	2.91	0.62	1.97	5.74	1.83
2	0	0	3.00	1.12	5.775	0.5	1.35	7.85	22.67	0.68
2$_s$	120	0.424	5.90		3.125	1.325	4.56	14.31	26.38	6.07
Subtotals (projectile material)							14.82	72.83	201.90	8.58
1'	284	0.737	7.95	7.37	3.125	0	0.05	0.17	0.27	0
2'	0	0	3.00	7.37	3.125	2.91	1.68	5.25	15.32	4.89
2'$_s$	120	0.424	5.90	7.27	3.125	1.325	8.13	25.41	46.83	10.77
2'$_E$	160	0.55	6.64	7.37	1.56	1.56	10.65	16.61	25.91	16.61
Subtotals (ablative surface affected)							20.51	47.44	88.33	32.27
Totals (all affected material)							35.33	120.27	290.23	40.85

counterpart of these radial moving oblique waves are the respective components M and L originating at the ends of G which are the junctions of the 326 and 200 KB reflected shock waves. Oblique wave components are considered negligible between a 200 and 280 KB junction along F. The radial momentum of the material is increased by this oblique wave action. In Figure 8 another significant wave action occurs. The amplitude (negative) of the solenoidal converging wave E rises as the inverse of the radius (similar to a convergent cylindrical wave) (6) so that a point near the center is reached where tensile forces break down the material and a cavity starts to form. From this point an inner boundary is continually formed, and the wave is returned as a compression shock whose initial amplitude must fall off as the inverse of the radius. The amplitude of the advancing wave D also falls off as the inverse square of the radius. The cavity must grow as the material gains radial momentum outward.

New regions which arose due to growing intersecting wave patterns were numbered, and computations were made of their volume, mass, kinetic energy, and momentum (both normal and radial). Resultant values were summed for each wave diagram for graphical presentation. The numbers and tabular details have been deleted in order that wave details can be presented with greater clarity.

In Figure 9, 3.3 sec after impact, the compression wave in the back-up plate has reached the back boundary and was reflected as a rarefaction wave which has just reached the junction between the ablative and the back-up accelerating the back-up to 2.25 km/sec at the impact center. Shock F (originated at ablative-steel boundary) has just reached the expanding cone of the projectile surface which was initially cylindrical. The cavity in the TWPN continues to grow as decomposed gas and particles fill the void with high pressure.
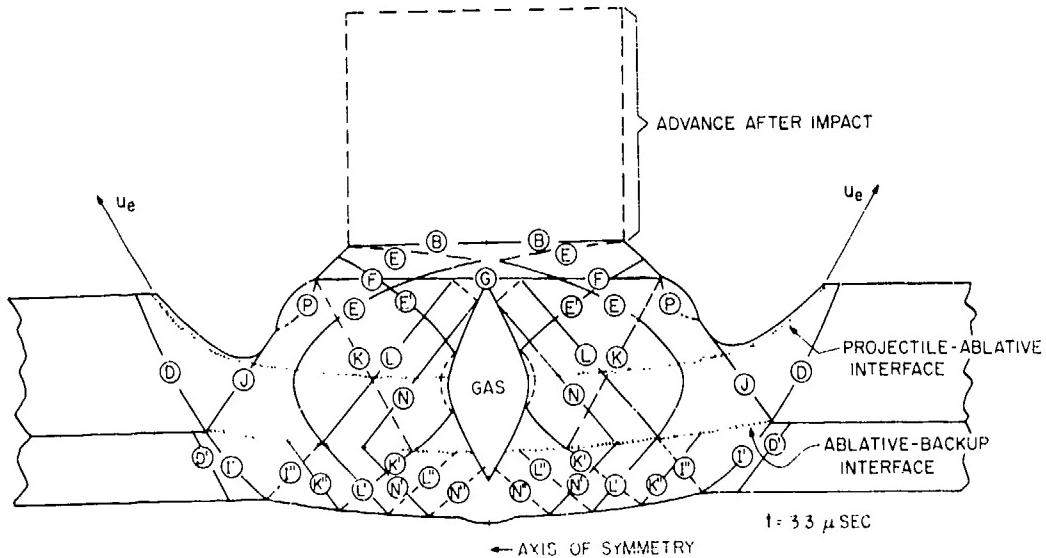

Figure 9 - Wave study (cavity formation) t = 3.3 sec

In the final wave diagram, Figure 10, at 3.6 sec after impact the plate moves away from the nearly stationary ablative as the gas in the cavity continues to be produced and expands into the voids with high pressure. At this point, the wave 'ensity of D in the ablative has fallen (due to radial attenuation) to about 103 KB wher .1ock velocity is less than that in steel where the low amplitude shock continues at about 7 km/sec. This tends to loosen the steel from the ablative bonding and allows further pressure action by the captive gas in the expanding void. The dimensionless subtotals of energy and momentum for the projectile, ablative, and back-up material are presented in graphic form in Figure 11 along with the overall totals. These values are plotted in terms of percent of initial energy and momentum against the fractional time in terms of the time it takes the projectile to advance a distance of one diameter using its initial velocity. The energy and momentum of the projectile material falls off at an increasing rate as the projectile advances into the target. The energy and momentum in the ablative increase rapidly at first then rise more gradually. The energy in the ablative falls slightly when the projectile has advanced 0.9 diameters, $\cdot = 0.9$. The back-up plate momentum rises to 0.7 of the original projectile momentum when the projectile has advanced 0.8 diameters. About 19% of the original projectile energy appears in the back-up material at $\cdot$ 0.9.

The total momentum is about 145% of M_o which is about that to be expected experimentally from impacts into relatively thick, low-strength materials. Total energy falls slowly at first and then quite steeply to about 65% of the original projectile energy when the projectile has advanced 0.9 diameters. This is to be expected since about 10% of the initial kinetic energy has been carried off in ejecta which leaves about 25% of the energy in the ablative and trapped gases in the form of potential energy, which is still increasing.

In Figure 12 consideration is next given to the increase of the value of scalar summation of radial momentum in the projectile, ablative, and back-up material. The growth
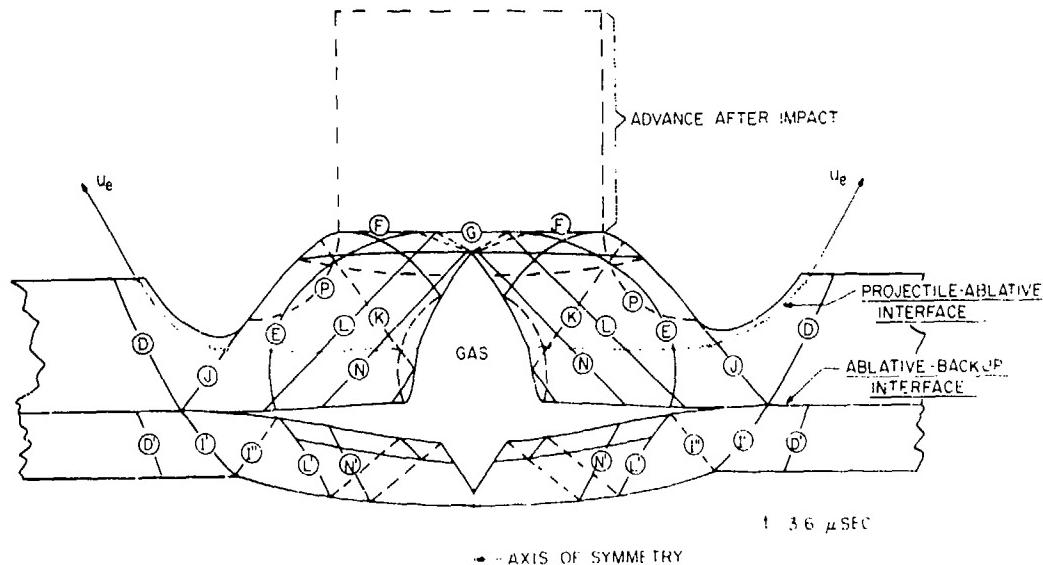

Figure 10 - Wave study (back-up ablative separation) t - 3.6 sec
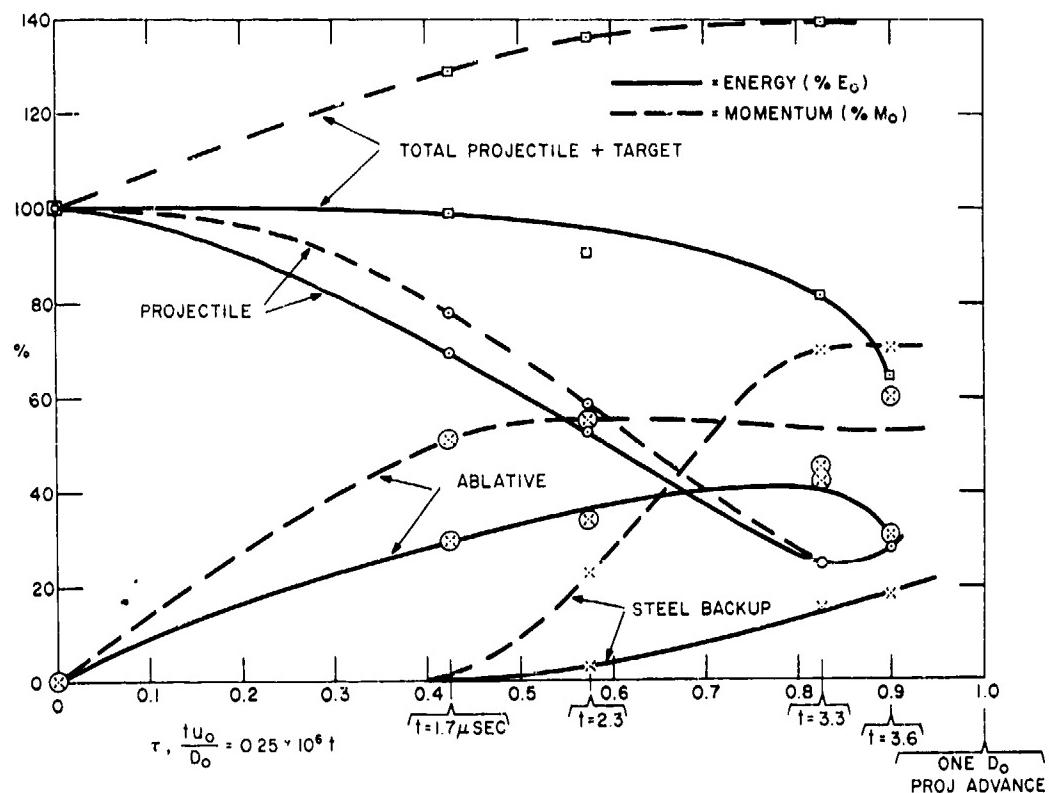
Figure 11 - Energy and momentum vs time (wave study summations)

in the value of this scalar summation of radial momentum is most rapid in the ablative due to immediate high-pressure radial propagation of the initial shock. A maximum of 62.5 gm-km/sec of scalar radial momentum is reached when the projectile has advanced 0.85 D_o. The rise in scalar radial momentum in the projectile is less rapid, reaching slightly over 50 gm-km/sec when the projectile has advanced 0.9 D_o. It appears that the back-up may attain a maximum of 20 gm-km/sec sometime later. In Figure 13 consideration is given to the growth of total scalar radial momentum whose rise is at first gradual with 50% of the original value reached when the projectile has advanced 0.5 D_o. The growth in scalar radial momentum is then quite rapid with a maximum of nearly 140% M_o being reached after advance of 0.9 of the projectile. This is in agreement with radial momentum in spall observations on moderately thick, low-strength targets (1,9).

To conclude the wave portion of the study, it is noted that, in spite of extremely simplifying assumptions (i.e., rarefaction shock, linear superposition, amplitudes proportioned per inverse of radius) the wave study gives good results in predicting momentum multiplication, observed forward ejection of material back along the trajectory at high velocity, and growth in radial momentum leading to opening of the target skin. The growth of a large pocket of heated ablative gas between the ablative and back-up which will later propel bits of the shattered ablative back along the trajectory is certainly in accord with photographic observations of impacts on ablative targets. There can be no doubt of the
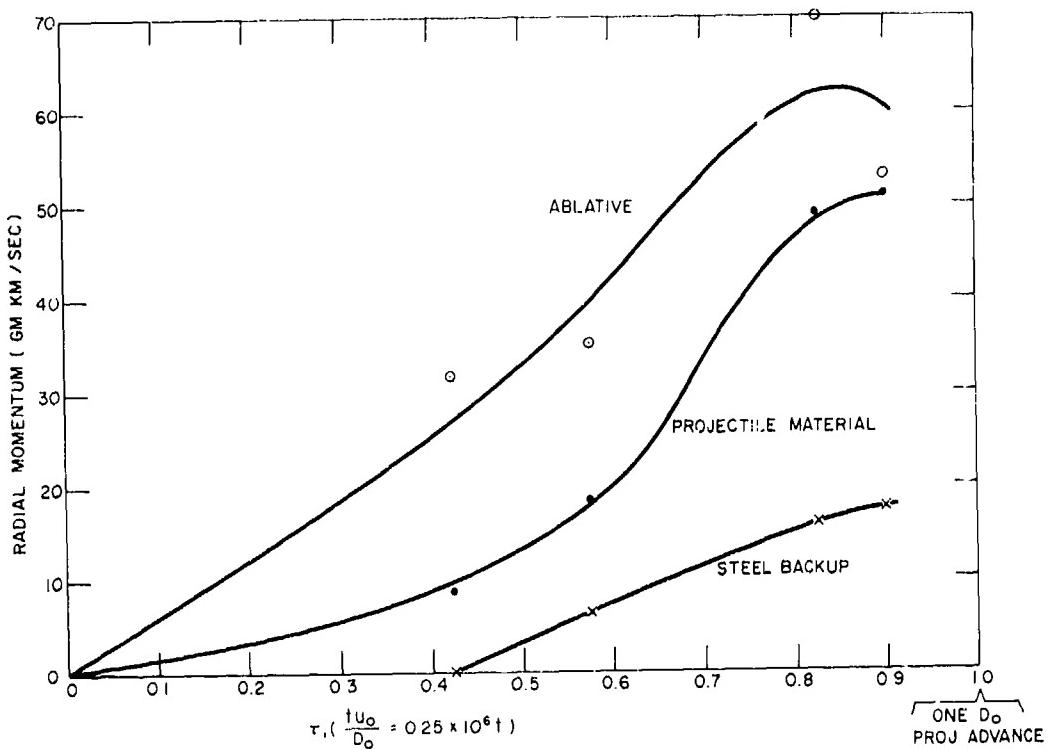
Figure 12 - Increase of radial momentum with time

extensive chemical decomposition of the phenolic compounds under the action of high amplitude multiple shocks. The extensive deposition of condensed carbon following a massive ablative shot indicates that there was abundant carbon freed from hydrogen-carbon bonding so there should also be released corresponding amounts of free hydrogen.

Seven models of the cracking out of ablative beyond the extreme pressure zone close to the impact point have been considered. One model of a developing petaling action and ablative shearout is shown in Figure 14. The trapped gas cavity B developed by wave processes (also shown in Figure 10) has continued to expand and to eject material through the central impact zone where small ruptures developed in both the ablative and back-up structure. The ablative and back-up plate are pushed apart by the high pressure gas developed in the immediate impact zone, by ablative breakdown into gaseous constituents and by the energy absorbed from the high-pressure shock. It is assumed that though small cracks develop in the accelerating ablative, they interlock so that gas is still contained and forces are transmitted to maintain an effective plate area for the gas to act against. The force F developed by gas pressure P_g is held by shear resistance S of the ablative in the growing gas pressurized ablative disk until some critical diameter equal to D_n is reached at which cracking and shearout of the shock conditioned material occurs. This situation may be described mathematically by Equation (11).

$$ F \qquad P_g \frac{D_n^2}{4} \qquad D_n T_n S . \tag{11} $$

$\tau, \left(\frac{\uparrow u_o}{D_o} = 0.25 \times 10^6 \uparrow \right)$

ONE D_o
PROJ ADVANCE
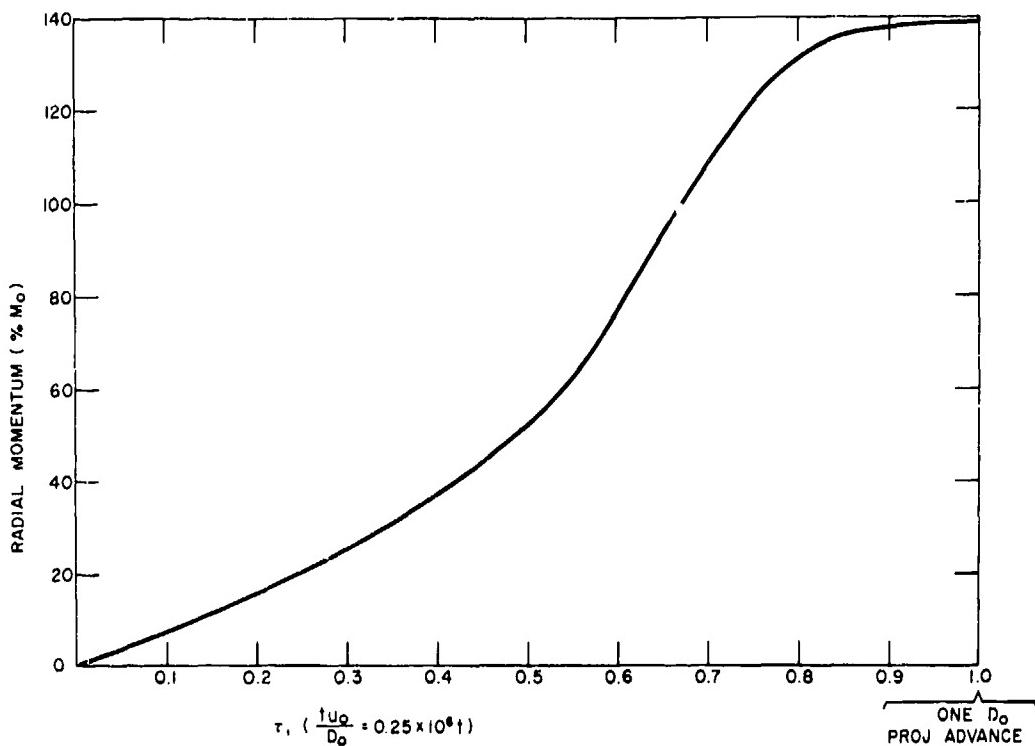
Figure 13 - Percentage increase in radial momentum
during projectile advance
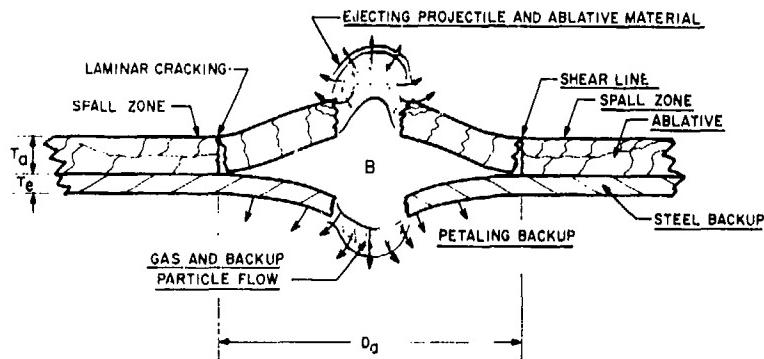
Figure 14 - Shock-gas cavity model of
ablative hole formation

Since E_o is the only source of energy to release ablative gas, this leads to expressions in Equation (12), where there is sufficient excess energy to cause rupture of the back-up in time to allow hemispherical gas expansion prior to ablative failure

$$PV_p \quad k_1 E_o \quad \text{and} \quad V_g \quad k_2 D_n^3 . \tag{12}$$

Solving Equations (11) and (12) and D_n gives Equation (13).

$$D_n \quad \left[\frac{K_2 K_1}{4S}\right]^{\frac{1}{3 \cdot 1}} \left[\frac{E_o}{T_n}\right]^{\frac{1}{3 \cdot 1}} \quad K_3 \left[\frac{E_o}{T_n}\right]^{\frac{1}{3 \cdot 1}} . \tag{13}$$

There are transition cases where the back-up does not rupture in time to allow effective hemispherical gas expansion because the shock is overtaken by the rarefactions originating first at the sides and then at the back of the projectile. Usually in this regime the plate is given a strong shock pulse which is attenuated at some stage before the shock can make the entire traverse through the plate and then back as a rarefaction to enable the plate to acquire the full velocity necessary to quickly achieve a full petaling type of rupture needed to achieve the hemispherical type of gas expansion postulated in the excess energy theory for ablative hole formation. Deep rounded bowing of the back-up including moderate petaling occurs in the final stages of this energy-thickness regime for a given ablative thickness. It appears that in this case shear and viscous forces restrain the high velocity center and a high velocity transverse wave is generated which moves out radially augmenting the impulse from the ablative wave so that in the early stages a disk-shaped cavity is opened such that the volume can be approximated by

$$V_g \quad \frac{\cdot \cdot}{4} D_n^2 . . \tag{14}$$

Solving Equations (11), (12) and (14) as before gives Equation (15) for the low energy transition regime.

$$D_n \quad k_4 (E_o T_n)^{1 \ (2 \cdot 1)} . \tag{15}$$

EXPERIMENTAL RESULTS

When the wave model was conceived the only complete set of Hugoniot curves available for ablative materials was for TWPN. The wave development, however, is valid qualitatively for any ablative up to Equation (11), except for metallic projectiles where there will be a set of reflection interactions which will raise the pressure of the interposed ablative by a set of step increments. This is shown experimentally in pressure recordings in a later discussion. The multiple extreme-pressure shocks can raise the temperature of the interposed region in excess of decomposition temperatures for most ablative components. Most phenolics under this condition will release hydrogen and gaseous carbon in amounts which will vary directly with the size of the impact and also with ablative characteristics. Choosing astrolite as an ablative material fixes S and K_1 to values valid only for astrolite. In the preliminary examination concerned with getting a gross answer covering the general class of ablatives, the scatter in data was as great as the variations in the factors

$$\left[K_2 K_1 \ 4S\right]^{\frac{1}{3 \cdot 1}}$$

so that for '........' e considerations, the best fit for the whole of the ablative data (2)
for impacts in th excess energy regime and angles over $30°$ was

$$D_n \quad 2 \left(\frac{E}{T_n}\right)^{.16} . \tag{16}$$

As more data are accumulated for vulcanized rubber bonds between astrolite and
back-up, much of the scatter is being eliminated. With these data, the effects arising
from change of backing material, incidence angle, and ablative material are more appar-
ent. From the more recent astrolite data, the best fit for hole sizes resulting from nor-
mal impacts is given by Equation (17) from which the value of · for decomposed astrolite
can also be determined

$$D_n \quad 1.55 \left(\frac{E_o}{T_n}\right)^{.41}$$

$$\frac{1}{3. \cdot 1} \quad .41 \quad . \quad 1.15 . \tag{17}$$

Substituting this value of · in Equation (15) gives

$$D_n \quad K_3 \cdot (E_o \cdot T_n)^{.76} \tag{18}$$

a relationship which was derived for determining hole sizes only in the low energy tran-
sition regime.

The combination shock and ablative-gas pressure type of ablative removal from an
approximately circular region following a $90°$ impact is only one of several removal ac-
tions observed, but is perhaps the most common in the excess energy regime. This
regime is of primary interest in the study because it is only in this regime that signifi-
cant impact damage can be accomplished behind the structure. Ablative hole size pre-
diction is also very important in the evaluation of thermal damage to components behind
the structure. This is a complex task due to the many different ablatives with different
cratering characteristics and types of holes created, as shown in Figure 15.

A case of a low energy impact, insufficient to penetrate the back-up is shown at the
top of Figure 15. Noting the right side of the ablative hole, it is seen that holes were
opening up in the laminate structure a little behind the projecting tips and indicate a near
rupture at th's point. Only a slight increase in projectile energy would have made con-
siderable difference in observed hole size. The center inset also shows a rupture section
at the right and underneath a thin, easily broken ledge indicating possible onset of fracture
at this point. Both of these cases show why scatter on observed values of hole size for
identical shot parameters can be plus or minus 10%. A type of back-up failure, charac-
teristic of magnesium back-ups, is shown in the lower inset. Large front spalls, shown
in the lower two insets, occur in the low energy regime for certain ablative-projectile
combinations.

There are three main energy regimes of ablative hole damage and are shown sche-
matically in Figure 16. The first two sketches (a and b) show nonpenetrated ablative
structures with holes formed primarily by cratering. In the minimum energy case, the
hole is formed by the intersection of the crater and rear spall, which is usually pulverized
and expelled by back-up rebound. Sketch b shows the cratering-spall hole created just
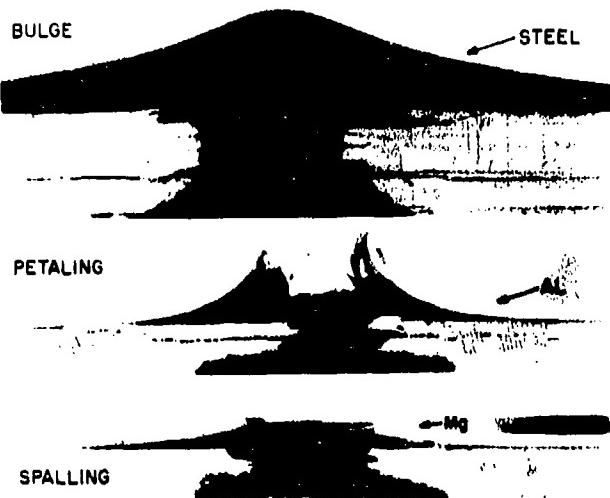
Figure 15 - Photograph of the various effects of hypervelocity impacts on ablative structures for complete performation of the ablative
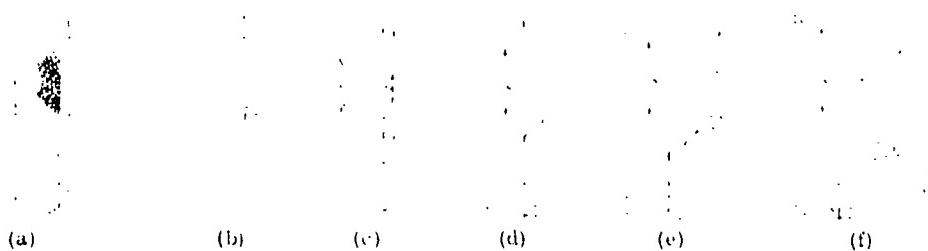
Figure 16 - Sketch of various energy regimes in hypervelocity impact: (a) start of cratering regime at V_0, (b) beginning of transition regime at V_1, (c) model of backup motion during transition, (d) transition regime hole, (e) start of excess energy regime, (f) excess energy regime

before the cratering region touches the back-up. In both cases, the high amplitude portion of the incident shock has been relieved by side rarefactions from the projectile before the shock can enter the back-up.

The two center sketches (c and d) illustrate essential features of a transition zone, where high pressure gas is created by a shock unattenuated by projectile rarefactions. The decomposition products are confined to a radial expanding zone between the ablative and a slowly receding back-up which does not rupture or open up until after the gas propelled ablative fractures over a high force gradient zone. The back-up does not acquire

high velocity because the unattenuated pressure pulse traversing the back-up plate is overtaken in the back-up by the side and end rarefactions from the projectile. This regime is characterized by very prominent bulges and cracking up to a minimum type of petaling where $D_c \backsim D_n$. The resulting radial type of gas expansion has been discussed in the preceding section on theory and leads to an energy-thickness ratio exponent of about 0.7 in the ablative hole size relationship.

The sketches e and f show the excess energy regime where $D_c > D_n$ and the back-up velocity was sufficiently high to insure rupture and approximately hemispherical gas expansion before full, effective radial expansion of the ablative gases could occur. This brief analysis then leads to consideration of ablative hole-size versus energy-thickness ratio for the various energy regimes.

The ablative hole size versus energy-thickness ratio for 90° impacts into astrolite with steel back-up is shown in Figure 17. First to be considered is the establishment of the maximum hole size limit curve for low and minimum energy impacts. From Reference 2, a minimum perforation energy was obtained for a steel projectile impacting astrolite with a steel back-up, for ablative thicknesses of 1.27 and 2.54 cm. Under minimum perforation conditions several hole sizes in the ablative were examined for the two thickness. This approximately established the end of the low energy or cratering regime and the beginning of the transition regime, shown at the upper right of the shaded zone of scatter in Figure 17. The left-hand limit point was established by considering that spall
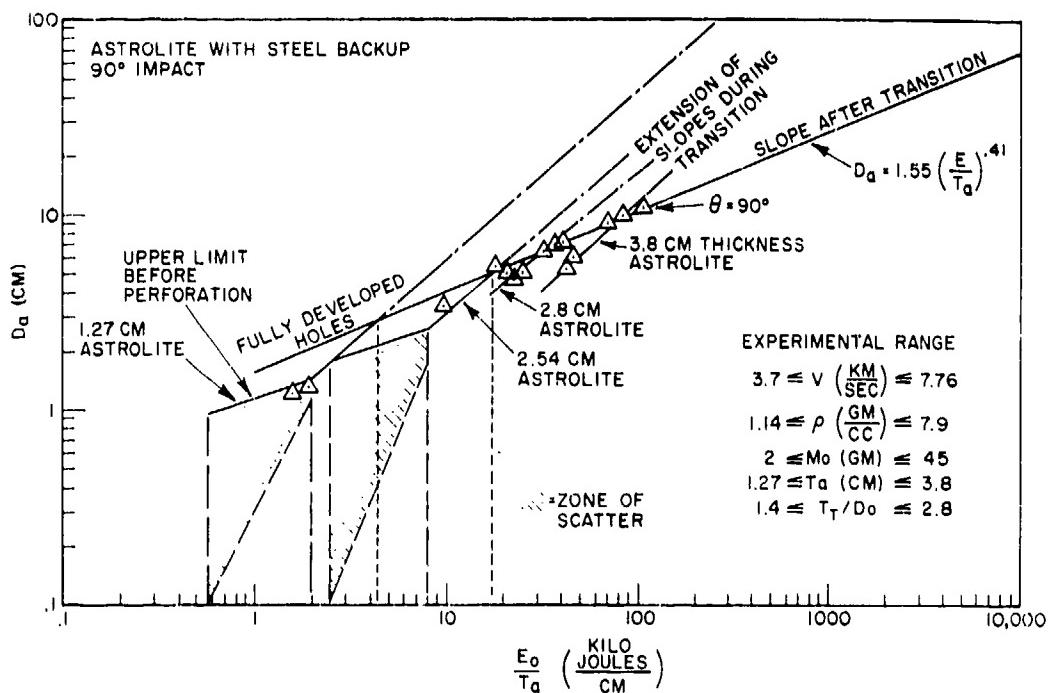

Figure 17 - Hole size vs energy-thickness ratio for steel-backed astrolite (90° impacts)

formation would complete the ablative hole with impact energy sufficient to form a crater depth about 0.7 of the ablative thickness, and hole size was assumed to vary as $(E T_n)^{-11}$. The high energy curve was then drawn in to give the best fit with data for fully developed petals. The transition curve was then constructed to connect each of the upper left-hand points (beginning of transition regime) with the experimental excess energy curve. The transition curve was constructed with a slope determined by the energy thickness ratio to the 0.7 power per Equation (18). It is to be noted that if the transition curves were inappropriately extended above the excess energy regime intercept, considerable error would be made in hole size predictions. The excess energy curve for 90° impacts on astrolite with aluminum and steel projectiles is given by Equation (17) in which hole size is proportional to energy-thickness ratio to the 0.41 power. There appears to be one curve within present experimental error for ablative thickness ratios of $T_n D_o$ above 1.5 in the excess energy regime as contrasted with a curve for each thickness in the low energy and transition regimes. The formula for the excess energy region for astrolite impacts at 90° for energy-thickness ratios ranging from 25 to 125 kj. cm gives hole size predictions in good agreement with the general ablative gross effect formula presented at the Sixth Symposium (2).

Large Mass Impacts

A four-foot square roller-mounted ablative target is shown in Figure 18. The ablative was 4.2-cm thick with a 0.63-cm thick steel rubber-bonded back-up mounted 45 to the trajectory. The impact produced a 35-cm ablative hole and the back-up received extensive petaling damage as shown by the photo at the left. The center edges of the front and rear photo show matching edges of the target and petaling can be seen to be asymmetric in the direction of the projected component of projectile motion along the plane of the back-up.

ASTROLITE COMPOSITE

BACK   FRONT
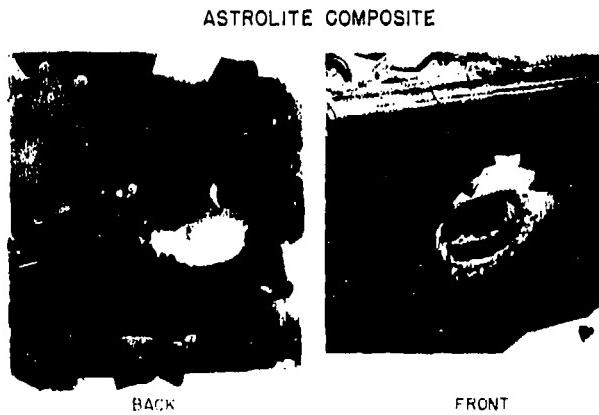
Figure 18 - Massive impact (4.1 megajoules) into steel-backed astrolite target at 45°

In Figure 19 is presented a graphical summary of 45° impacts into astrolite bonded to a steel back-up with vulcanized rubber. The upper points are the 4.1 and 1.2 megajoule impacts with respective 366-gm aluminum and 100-gm steel spheres. The lower points each represent shots where target and projectile dimensions were scaled by a factor of
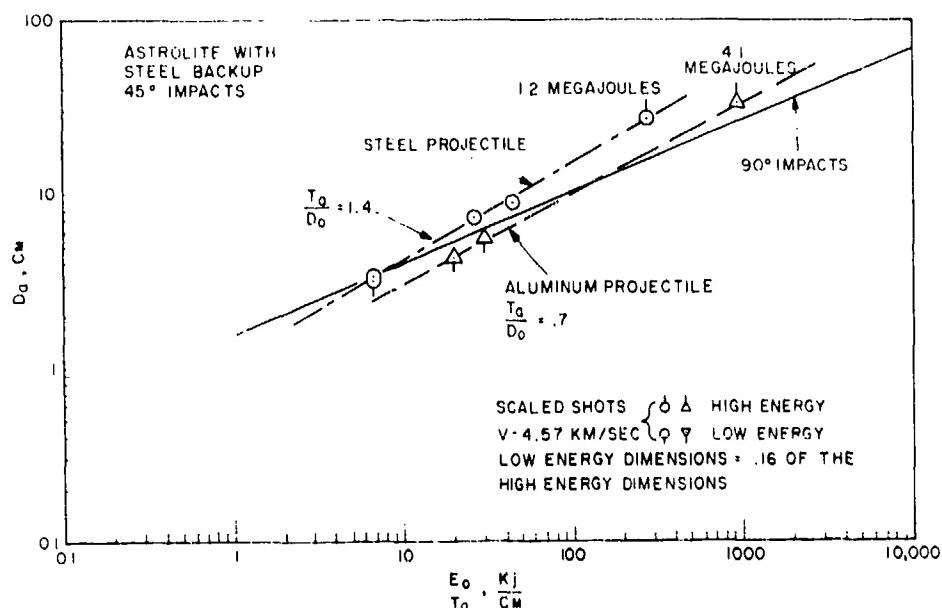
Figure 19 - Hole size vs energy-thickness ratio for
astrolite targets (45° impact)

0.16 of the corresponding massive impacts. Considering the line for the steel projectiles
first, it is noted that the intermediate energy shots fell very near the connecting line even
though they represented impacts at a higher velocity (7.8 km/sec) and an ablative-thickness
ratio of about 2.5. The line connecting the massive and the scaled aluminum shots did not
fall upon the line for the steel shots even though they all are in the excess energy regime.
This could be attributed to a thin plate effect for the low ablative thickness ratio ($T_a D_o$ =
0.68), or the effect of change in projectile material or a combination of these effects. Of
major interest is the fact that the hole diameters for these angled shots appear to be pro-
portional to the energy thickness ratio taken to about the 0.54 power. This represents a
departure from the excess energy curve for 90° impacts. One change which would occur
in angled impacts would be that multiple wave reflections between the back-up and the
metal projectile would no longer be normal to each surface. Another effect is that the
point of the projected collision between the projectile and the back-up is not at a point of
maximum back-up velocity from the preceding wave action.

Pressure Instrumentation in Ablative Material

    Though the theoretical model discussed previously is for TWPN impact by a TWPN
cylinder at 90°, the model and methods outlined in the graphical wave representation can
be approximated to apply to an impact such as the large aluminum projectile impacting
at 45° and 4.57 km/sec into the astrolite target. In this experiment, pressure data were
obtained using carbon-resistor pressure gages (10) placed in the center of the ablative
about 2.11 cm in from the ablative face and about 25.4 cm from the impact center at 90°
from the trajectory (see front of target in Figure 18). To properly evaluate the pressure
recorded, reference is made to the model shown in Figure 8. Had the projectile in this

figure been of a higher specific acoustical impedance, an increase of pressure would have occurred when the reflected shock wave component from the back-up interacted with the projectile material interface. This reflected component then would have been propagated in a spherical manner back toward the steel back-up. When this projectile reflected shock component reached the steel back-up, a second shock component reflection will occur and will propagate back into the ablative. The actual massive impact problem is further complicated by the 45° angle of attack so that no attempt is made to predict pressure wave values and the effect of all possible ray paths of propagation. The pressure-time record of these waves in the massive impact experiment does show pressure magnitude and arrival time of these components. In Figure 20, P_1 represents the maximum value of the direct pressure wave from the impact already under the influence of the rarefaction ray from the surface. Rarefaction attenuation continued to predominate until shock reflection from the back-up started to act at P_2 just 0.405 ,,sec after the main wave arrival or scope triggering. At about 1.1 ,,sec after the scope triggered, signals from the projectile reflection of the back-up reflection wave started to act and reduce the rarefaction effects. Pressure rose slightly to a maximum value P_4 before surface rarefactions again predominated. The final compression wave from the back-up reflection of the projectile reflection component reached a maximum value of P_5.

CONCLUSIONS

It has been shown that a simple two-dimensional wave analysis can be applied to gain a good idea of momentum transfer from the projectile to the target. Augmentation ratios predicted are consistent with observed momentum augmentation, and radial momentum determined from behind the target cratering studies (1,9) are in line with early stage predictions based on wave analysis. Future work is necessary to adapt wave analysis techniques to impacts made at incidence angles less than 90°, and experimental pressure-time recordings can do much to guide the theoretical approach into these more realistic modes of attack.
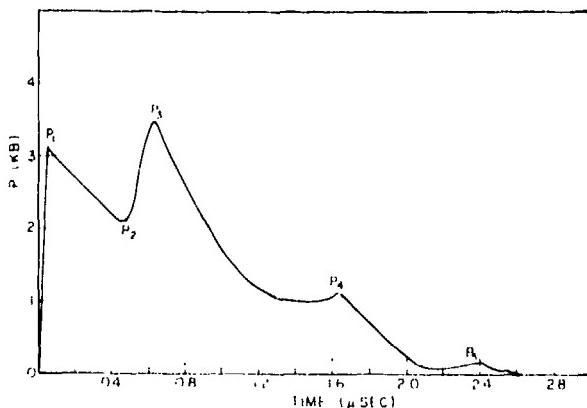

Figure 20 - Pressure-time curve for a massive astrolite impact (25.4 cm from impact point)

NAVAL RESEARCH LABORATORY

Three regimes of ablative hole damage exist: low energy, transition, and excess energy. In the transition regime there is a separate curve for each ablative thickness, and the ablative hole size varies as the energy-thickness ratio to the 0.7 power. Inappropriate extension of this curve beyond the point where high energy transition occurs can lead to large errors in hole size prediction. The excess energy regime is of greatest interest because of the impact damage potential to components located behind the target. The curve for $90°$ impacts into astrolite with steel back-up show that the hole size is proportional to the energy-thickness ratio to the 0.41 power in the thickness range where $2.8 > T_a/D_o > 1.4$. Values of hole size in the 25 to 125 kilojoules/cm range are very close to those presented in Reference 2 for impacts into ablatives in the excess energy regime.

The experimental shots made at $45°$ have shown that hole size is proportional to energy-thickness ratio to the 0.54 power. This increase in power could be due to a change from the normal wave interaction between back-up and projectile which occurs in $90°$ impacts. Hole sizes from shots made with aluminum projectiles at $T_a/D_o < 0.7$ fell below the curve for ratios greater than 1.4, indicating a thin plate effect.

REFERENCES

1. Hypervelocity Kill Mechanisms Program, Project Defender:

   a. Progress Report No. 7; NRL Report 5813, Semiannual Technical Progress Report for Period Ending June 1962 (S-RD)

   b. Progress Report No. 9; NRL Report 5913, Semiannual Technical Progress Report for Period Ending 30 September 1962, Vols. I & II (S-RD)

   c. Progress Report No. 11; NRL Report 5990, Semiannual Technical Progress Report for Period Ending 20 March 1963 (S)

   d. Progress Report No. 13; NRL Report 6077, Semiannual Technical Progress Report for Period Ending 30 September 1963 (S)

2. Persechino, M.A.; "Hypervelocity Impacts into Ablative Materials," Proceedings of the Sixth Symposium on Hypervelocity Impact, Vol. IV; Cleveland, Ohio; August 1963 (S)

3. Rockowitz, M., Carey, C.A.; "Impact Damage Phase-Hypervelocity Kill Mechanisms Program," Progress Report 13; NRL Report 6077; Section C Semiannual Technical Progress Report for Period Ending 30 September 1963 (S)

4. Schultz, G.F.; "Nichtstationäre Ein Dimensionale Gasbewegang" Forsch; Geb. Ing; Wes 13, PP. 125-134; 1942

5. Rudinger, G.; "Wave Diagrams for Non-Steady Flow in Ducts"; D. Van Nostrand Company, Inc., New York 1955

6. Kinsler, E.R., Frey, A.R.; "Fundamentals of Acoustics"; John W. Leg and Sons, Inc.; New York, 2nd Edition, 1962

7. Wagner, M.H., Louie, N.A.; "Determination of Hugoniot Equations-Of-State for Polymers and Re-entry Vehicle Materials and Investigations of Fracture Phenomena"; AFSWC-TDR-6266, Vol. II; Albuquerque, New Mexico, August 1962

8. Olshaker, A.E., Bjork, R.L.; "Scaling Laws for Dissimilar Materials"; Proceedings of the Fifth Symposium on Hypervelocity Impact, Vol. I, Part I; Denver, Colorado, 1961

9. Watson, R.W., Becker, K.R., Hay, J.E., Gibson, F.C.; "Hypervelocity Impact Phenomena"; Quarterly Report, Bureau of Mines; Pittsburgh, Penna., June 1963

10. Watson, W.W., Becker, K.R., Gibson, F.C.; "Hypervelocity Impact Phenomena"; Bureau of Mines; Pittsburgh, Penna., December 1963 - February 1964

11. Balchan, A.S.; "A Radiographic Study of Shock Loaded Iron"; Journal of Applied Physics, Vol. 34, No. 2, pp. 241-245; February 1963

LIST OF SYMBOLS

A	KB	empirical constant
a'	km/sec	empirical constant
a_o	km/sec	dilational wave velocity (other than shock)
b'		empirical constant
D_a	cm	diameter of hole in ablative
D_e	cm	diameter of hole in back-up
D_o	cm	diameter of projectile
E_o	kj	energy in impacting projectile
F	kg	force
g	km/sec	acceleration of gravity
K_1	gm-cm/joules	constant dependent upon target and projectile material, $\lambda = 3\gamma - 2$
K, K_2		constants empirically determined
K_3	cm (cm/kj)^a	constant empirically determined (dependent upon target and projectile material) $\alpha = 1/3\gamma - 1$
K_4	cm (cm/kj)$^\beta$	constant empirically determined (low energy transition) $\beta = 1/2\gamma - 1$
M_o	gm-km/sec	momentum of impacting projectiles
M_i	gm-km/sec	axial momentum of ith ring of particles
M_{ir}	gm-km/sec	radial momentum of ith ring of particles
n		number of waves passed at chosen time and place
P	KB	pressure in material at given location and time
P_o	KB	initial pressure in material
P_g	KB	pressure of gas in ablative cavity
ΔP_i	KB	incremental change in pressure due to ith wave
t	μsec	time
U	km/sec	shock wave velocity (reference to undisturbed region)

u	km/sec	particle velocity in material at given location and time
u_o	km/sec	initial velocity of material or projectile
u_e	km/sec	velocity of projectile and target ejecta
u_L	km/sec	axial particle velocity of ith region
u_r	km/sec	radial particle velocity of ith region
Δu_i	km/sec	incremental change in particle velocity due to ith wave
V_g	cm^3	volume of contained ablative gas
$\dot{W}$	gm/sec	rate of material ejection
W_i	gm	weight in ith wave region
		ratio of specific heat (decomposed ablative gas)
		ratio of densities, $\cdot$ $\cdot_o$
		$\cdots_o - 1$
		incremental change in $\cdots$
	gm/cm^3	density of shocked material under pressure
		distance projectile advances into target divided by D_o diameter (assuming u_o constant)
	cm	thickness (depends on scale factors of the experiment)

*   *   *

DOCUMENT NO. 64SD5162

This document contains 40 numbered pages.

Copy number 125 of 196 copies.

HYPERVELOCITY KILL MECHANISMS PROGRAM (U)

Aerothermal Phase

Semi-Annual Progress Report

For Period Ending

30 September 1964

SPONSORED BY

Advanced Research Projects Agency
Ballistic Missile Defense Systems Branch
ARPA Order No. 149-60
Program Code No. 3730

CONTRACTOR, GENERAL ELECTRIC COMPANY
RE-ENTRY SYSTEMS DEPARTMENT

D. E. Nestler, Technical Director
E. Richardson, Program Manager

GENERAL ⬤ ELECTRIC

LAN: 5731-40-2

CONTENTS

ILLUSTRATIONS

TABLES

SUMMARY

Work has continued under the Aerothermal Phase of the program with emphasis on the thermal performance of foam-filled axisymmetric models having simulated hypervelocity impact perforations.

The Malta Rocket Exhaust Internal Heating Test Program was concluded with the completion of Tests Number 6 and 7. The principal achievements of this program were the establishment of a correlation for the rate of energy influx through a heat shield perforation and the determination of the thermal performance of rigid urethane foam within perforated models. Detailed results of Tests Number 6 and 7 are presented herein, together with a summary of the overall program and principal results. The application of the correlation to a high performance ICBM re-entry vehicle indicates that an internal heating load of about 200 btu per square inch of perforation area is accumulated by 50,000 feet altitude for a perforation occurring at 100,000 feet altitude. The particular foams tested showed an energy absorbing capability of about 2000 and 3000 btu/lb for densities of 3.0 and 7.8 lb/ft^3, respectively.

Two new tasks were added to the program in August. Under the first task, an extensive investigation of the thermal performance of lightweight foams having simulated hypervelocity impact damage will be conducted. Axisymmetric foamed-filled models will be tested in the GE-RSD 5 - Megawatt Air Arc and Malta Rocket Exhaust facilities. The choice of foams will be based on screening tests performed in a blowtorch stream. Calorimeter models have been fabricated, and the arc shroud model configuration is being designed. A tentative list of promising foam candidates has been formulated.

Under the second new task, a thermostructural kill study is being conducted, with the objectives of (1) formulating a simplified computational model for thermostructural kill of ICBM re-entry vehicles due to hypervelocity impact perforations and (2) applying the computational model to selected advanced re-entry vehicle designs of two general classes: (a) hardened and (b) unhardened. Initial study under this task has resulted in the selection of seven vehicle configurations having ballistic coefficients from 1700 to 4400 lb/ft^2.

H-1

I. MALTA ROCKET EXHAUST INTERNAL HEATING TEST PROGRAM

A. General

The Malta Rocket Exhaust Internal Heating Test Program was completed with the performance of Tests Number 6 and 7. The general objectives of the program and detailed results of Tests Number 1 through 5 were presented in the preceding semiannual progress report (Ref. 1). A condensed summary report of the entire program was also published (Ref. 2).

The test agenda and objectives of the program are summarized in Table 1. The tests were conducted on identical sphere-cone models of 9.8 inches base diameter consisting of a laminated phenolic nylon heat shield hard-bonded to an Inconel structure. A single perforation was located on the conical skirt of each model. Tests Number 1 through 4 featured open internal compartments, while Tests Number 5 through 7 featured foam-filled internal compartments. In Tests Number 1 through 5, 30 thermocouples were used to measure heat flux distribution to the structure. For Tests 6 and 7, instrumentation was modified to include 10 thermocouple probes positioned within the foam to indicate the foam surface recession history.

TABLE 1. MALTA ROCKET EXHAUST INTERNAL HEATING TEST SUMMARY

Test No.	$A \sqrt{2}$ ^{3}	D (in.)	Internal Foam	Foam Density (lb/ft³)	Run Time (sec)	Test Objective
1	0.11	2.5	None	–	5	Internal heating data
2	0.27	4.0	None	–	5	Internal heating data
3	0.18	3.25	None	–	5	Effect of actual impact
4	0.07	2.0	None	–	–	Effect of simulated spall
5	–	4.0	Urethane	7.8	10	Foam response
6	–	4.0	Urethane	5.0	15	Foam response
7	–	4.0	Urethane	3.0	15	Foam response

A   initial perforation cross-section throat area
V   initial internal volume
D   initial perforation throat diameter

Tests 1, 2
Machined cylindrical perforations

Test 3
Actual impact perforation by NRL

Test 4
Machined bevelled perforation to simulate spall

Tests 5, 6

Test 7
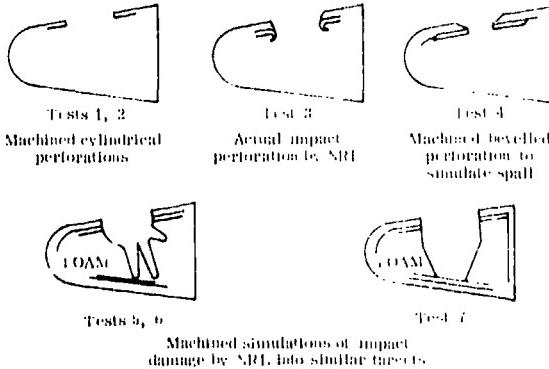
Machined simulations of impact damage by NRL into similar targets.

Nominal test conditions for all tests are shown in Table 2.

TABLE 2. MALTA PIT FOUR TEST CONDITIONS

Free-stream Mach number	3.0
Model stagnation conditions:	
Pressure	170 psia
Enthalpy	3250 btu/lb
Temperature	5650 °R
Cone static pressure	22 psia
Test medium	Exhaust gases (γ = 1.2, mol. wt. = 25)

The model for Test Number 7 is shown mounted on the pit number four test stand in Figure 1, prior to gimbaling the rocket exhaust nozzle into position for test.

Figure 1. Model on Test Stand (Malta Test No. 7)

H-4

B. Results of Tests Number 6 and 7

1. General

The principal objective of Tests No. 6 and 7 was to determine the heat protection characteristics of a lightweight urethane foam within axisymmetric models containing simulated hypervelocity impact damage. In each test, the foam used was a 3 lb/ft^3 rigid urethane foam (Hetrofoam 368) made by the Hooker Chemical Co.

To accomplish this objective, thermocouple beads were mounted at the end of 0.25-inch diameter probes made of GE Series 100 ablation material which were installed within the foam at ten locations as shown in Figures 2 and 3. The probes were threaded into the Inconel structure and were arranged to minimize interference between adjacent probes.

Cross-sections of the simulated impact cavity for each test are also shown in Figures 2 and 3. These cavities were idealized representations of hypervelocity impact damage into phenolic nylon-steel targets backed by urethane foam (Hetrofoam 368). The impact tests were performed by the Naval Research Laboratory.

The tests were intentionally run for a long enough time (15 seconds) to completely remove the foam during the test, thereby causing heating of the Inconel structure following foam removal by ablation. Structure temperatures were monitored by 20 thermocouples located on the structure at the shield-structure interface. Four static pressure taps were used to measure pressure within each model. Thermocouple and pressure tap locations are shown in Figures 2 and 3.

Pre-test and post-test photographs of the models for Tests No. 6 and 7 are given in Figures 4 through 7.

Figure 7 shows a longitudinal crack 0.25 inch in width that developed downstream of the perforation in Test No. 7. Fastex movies showed that the crack occurred at 12 seconds during the run. A similar crack developed during Test No. 2 (see Ref. 1). In Figure 5, scale deposits can be seen on the backplate within the model. Similar deposits were present in Model No. 7.

Typical probe thermocouple temperature histories for Tests No. 6 and 7 are shown in Figures 8 and 9. Due to the low thermal conductivity of the foam, no significant temperature response occurred until the foam surface receded to the thermocouple location. The thermocouples thus functioned as ablation sensors by locating the foam surface at various times during the test. After the foam surface receded past the thermocouples, their readings appear to level off in approximate equilibrium with the local gas recovery temperature at 1500 to 2200°F.

Plots of foam surface recession vs. time as determined from probe thermocouple records are given in Figures 10 and 11 for Tests No. 6 and 7. In several cases, the final surface location for a given thermocouple ray was obtained from the response of thermocouples mounted on the structure in line with the probe thermocouples.

H-5

ALL DIMENSIONS IN INCHES

□ PRESSURE TAP
⊙ THERMOCOUPLE ON BACKFACE OF STRUCTURE
+ THERMOCOUPLE WITHIN FOAM
• ATTACHMENT POINT OF FOAM THERMOCOUPLE SUPPORT ROD
— — CENTERLINE OF FOAM THERMOCOUPLE SUPPORT ROD
— — — ORIGINAL CAVITY CONTOUR
——— FOAM THERMOCOUPLE RAYS
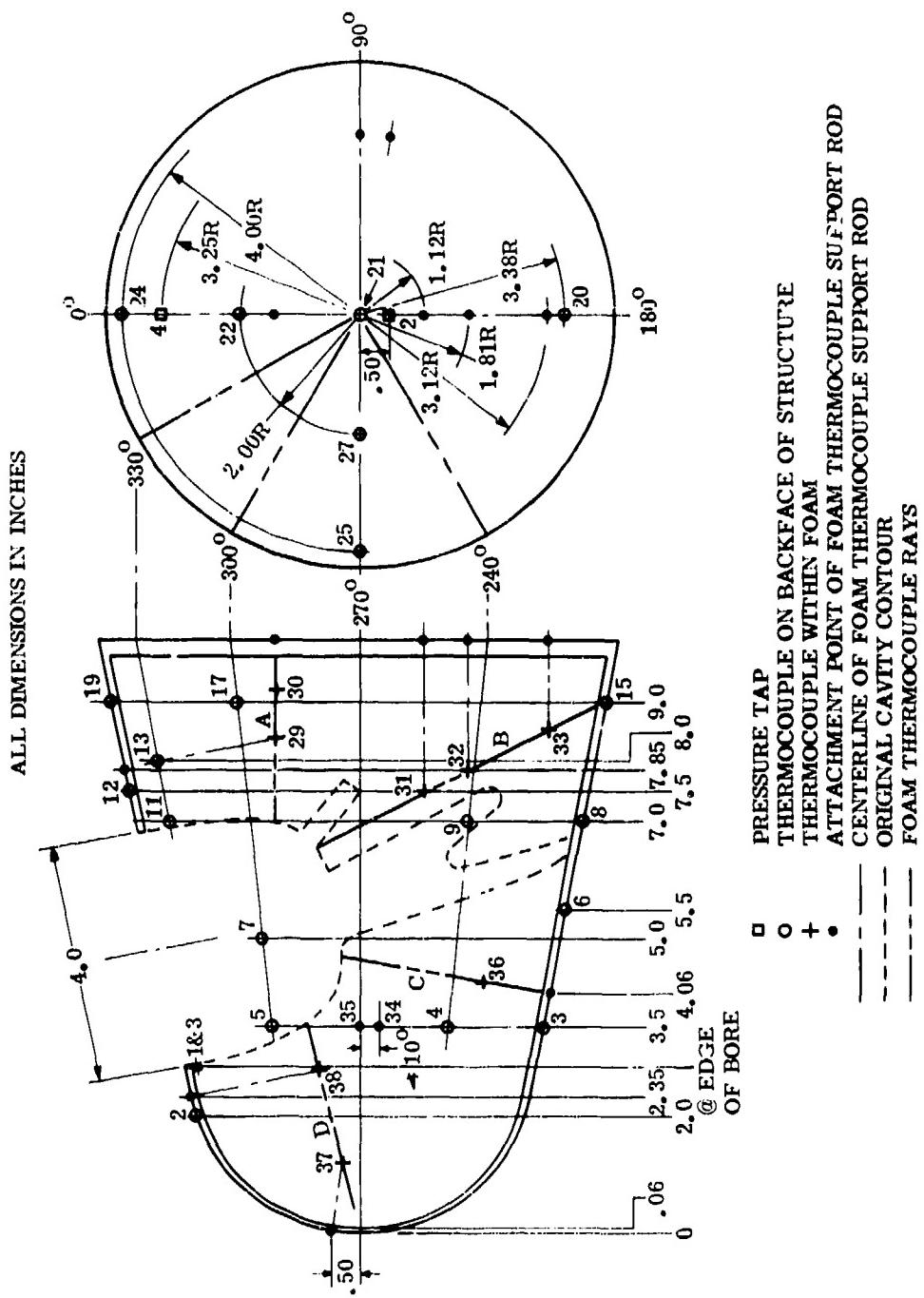
Figure 2. Cross-Section of Test Model No. 6

H-6

STRUCTURE THERMOCOUPLE INSTRUMENTATION SAME AS MODEL #6

◻ PRESSURE TAP
○ THERMOCOUPLE ON BACKFACE OF STRUCTURE
+ THERMOCOUPLE WITHIN FOAM
● ATTACHMENT POINT OF FOAM THERMOCOUPLE SUPPORT ROD
—·— CENTERLINE OF FOAM THERMOCOUPLE SUPPORT ROD
—·— ORIGINAL CAVITY CONTOUR
——— FOAM THERMOCOUPLE RAYS
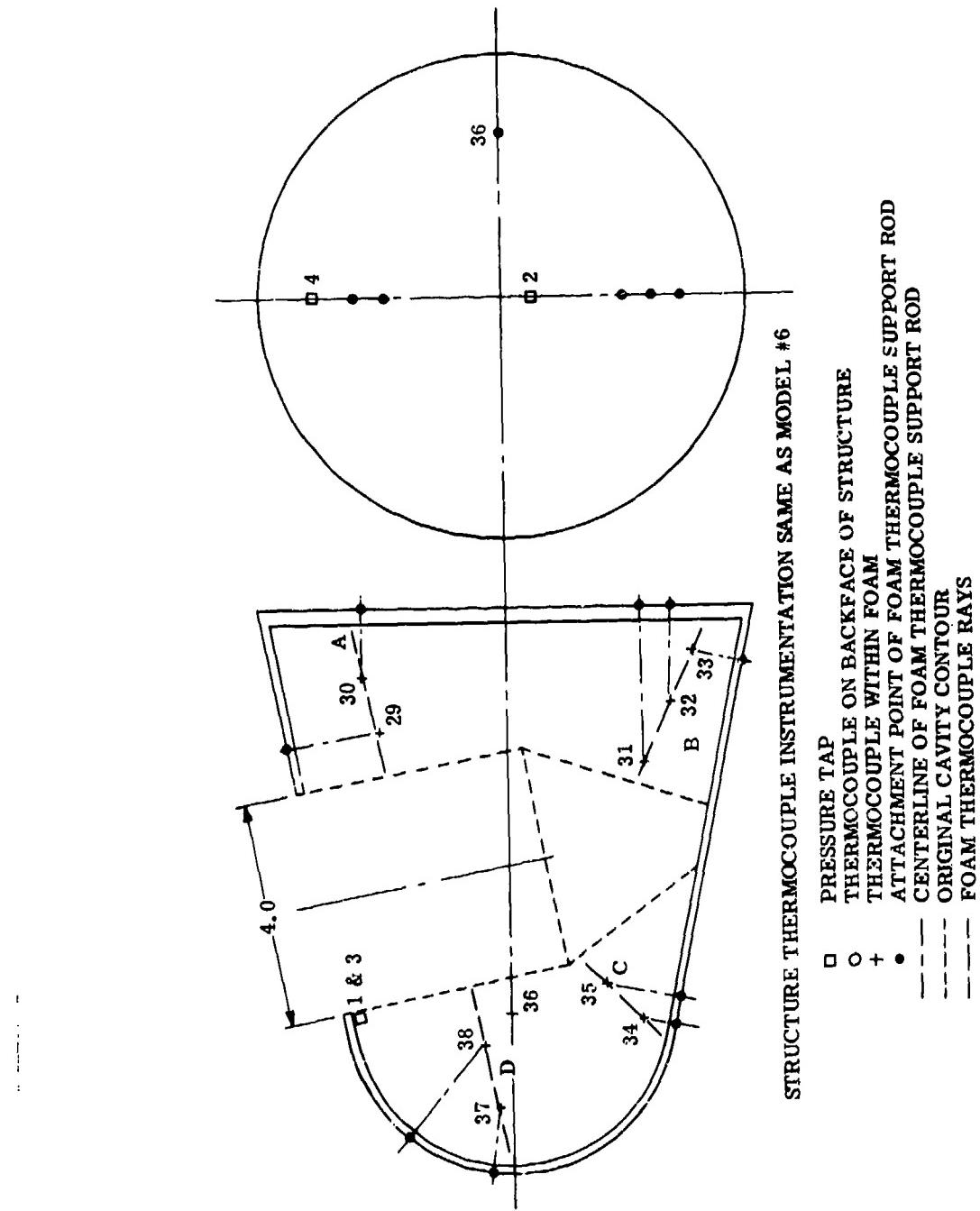
Figure 3.   Cross-Section of Test Model No. 7

H-7
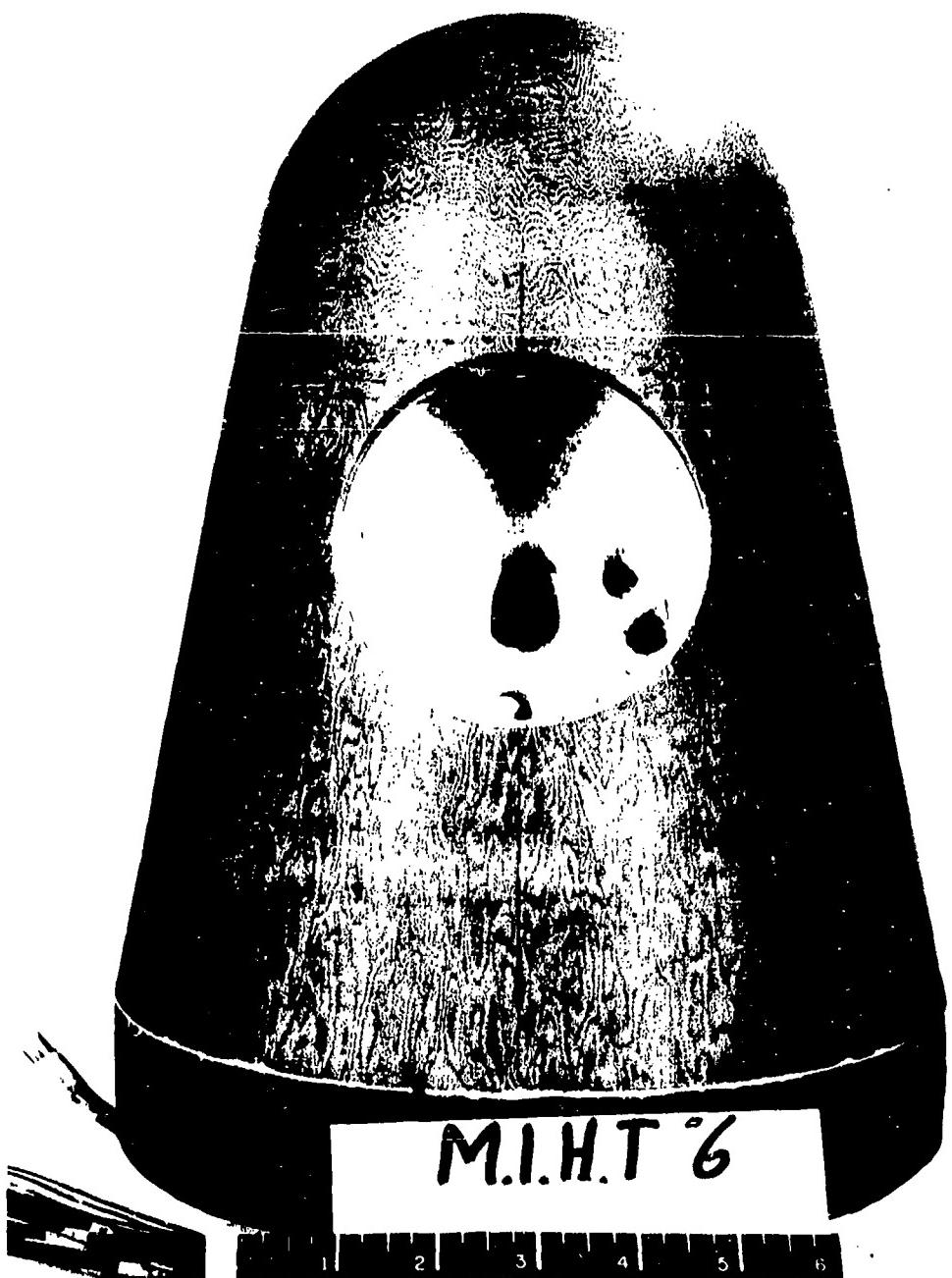
Figure 4. Malta Test No. 6 - Pre-Test View

H-8

Figure 5. Malta Test No. 6 - Post-Test View

H-9

Figure 6. Malta Test No. 7 – Pre-Test View

H-10

Figure 7. Malta Test No. 7 Post-Test View
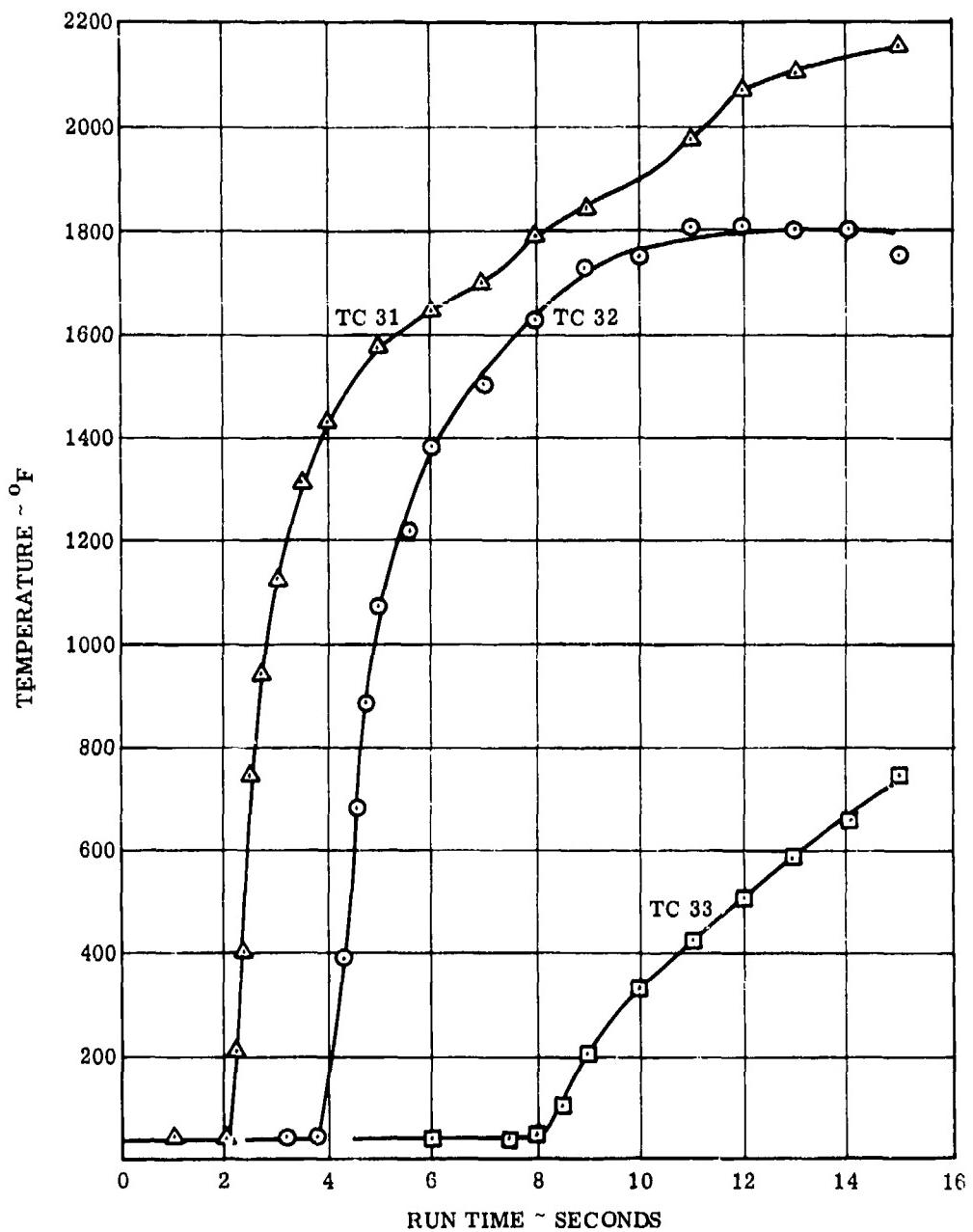
Figure 8. Typical Temperature Histories - Malta Test No. 6, Ray B

H-12
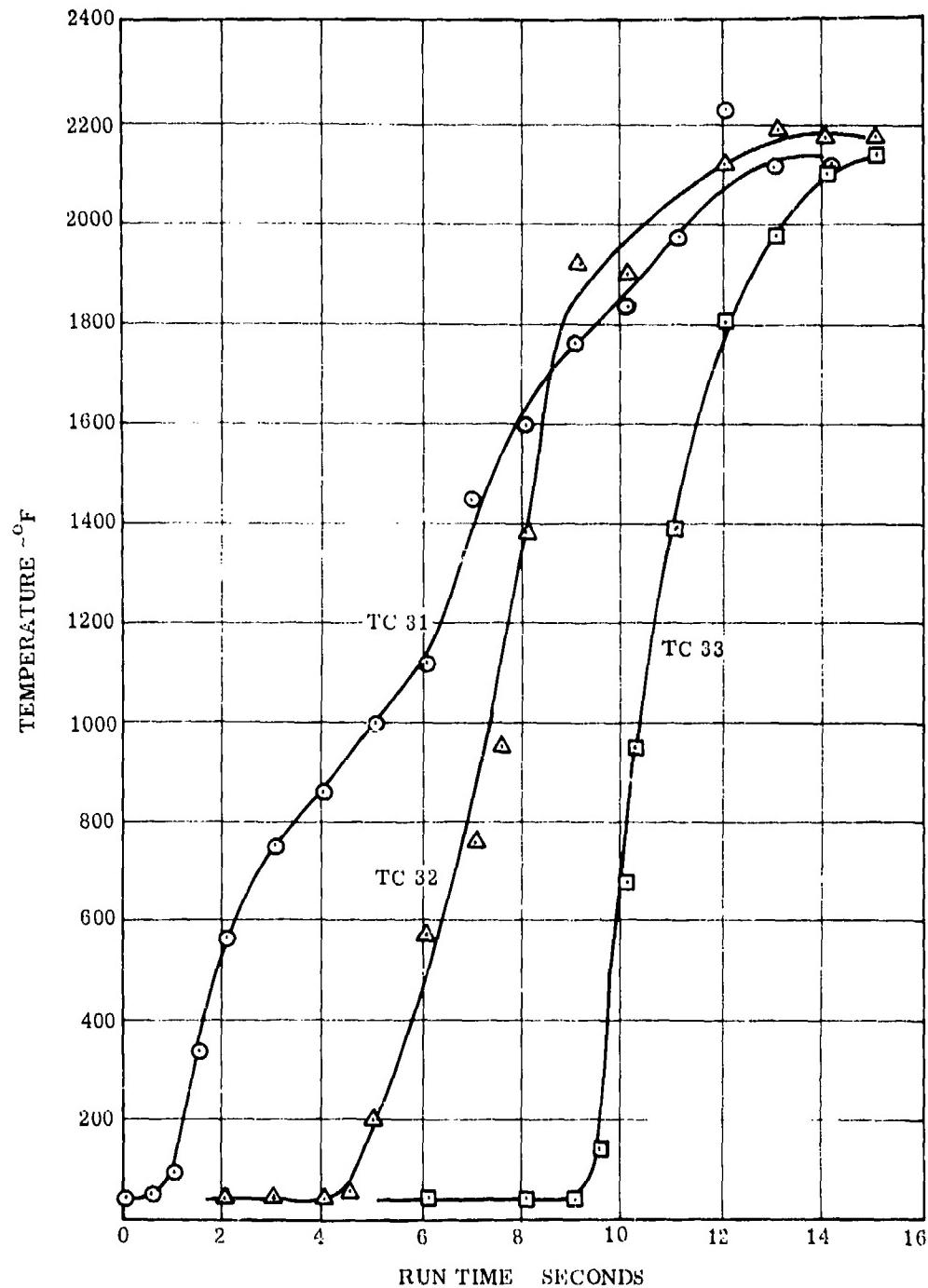
Figure 9. Typical Temperature Histories - Malta Test No. 7, Ray B

H-13
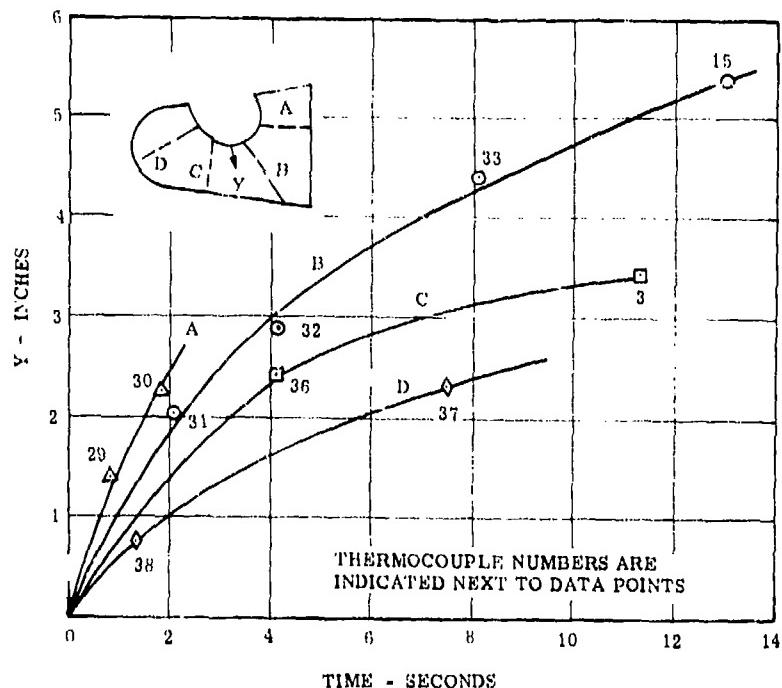
Figure 10. Foam Surface Recession Histories - Malta Test No. 6
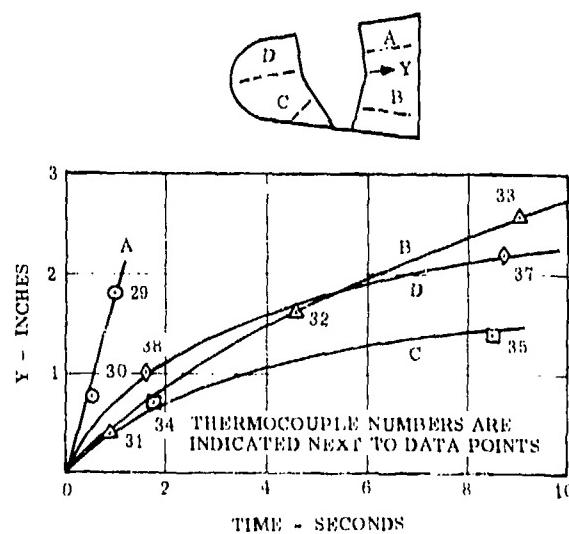
Figure 11. Foam Surface Recession Histories - Malta Test No. 7

H-14

2. Thermal Performance of Hetrofoam 368

Figures 10 and 11 were used to construct approximate foam surface recession contours as shown in Figure 12 and 13. These contours were used to approximate the weight of foam removed at various times during the test. The foam cavity cross-section in a plane perpendicular to the cavity axis was assumed to be elliptical, with a variation of b/a (b — major axis, a — minor axis) corresponding to the final foam cavity shape of Test No. 5.

The thermal performance of the foam was characterized by an effective heat of ablation Q^* defined as:

$$Q^* = \frac{\Delta E}{\Delta M} \tag{1}$$

in which ΔE — total energy entering perforation cavity and
ΔM — weight of foam removed by ablation.

Values of ΔM at various times during the run were determined as described in the preceding paragraph. Values of ΔE were determined by assuming a constant rate of energy addition of 135 btu/sec to the cavity, based on the result obtained in Test No. 2 for the same size perforation. Therefore equation (1) is an arbitrary definition for Q^* in which the effects of perforation area enlargement and foam decomposition gases generated during the test are included in the definition.

The results of the analysis described above are given in Table 3. The result given for Q^* for Test No. 5 supersedes the value given in Ref. 1, which was incorrect due to an error in the calculation of ablated foam volume. Consistent results were obtained from computations performed for times of 2 and 4 seconds, using the contours of Figures 12 and 13.

TABLE 3. VALUES OF FOAM HEAT OF ABLATION Q^* FOR HETROFOAM 368

TEST NO.	5	6	7
Foam density (lb/ft^3)	7.8	3.0	3.0
Q^* (btu/lb)	2900	2300	1800

These values of Q^* are subject to uncertainties on the order of ±25 percent due to uncertainties in the exact values of ΔE and ΔM.

In Tests No. 6 and 7, the structure heat flux distribution following ablation of the foam indicated that the maximum heating occurred downstream of the perforation, rather than opposite the perforation as in Tests 1 through 4. This shift in internal heat flux distribution is attributed to the thinner downstream edge caused by ablation during the longer runs. Exact heat fluxes and rate of energy absorption could not be determined following foam ablation due to the deposition of scale formed from the melted Inconel structure adjacent to the perforation.
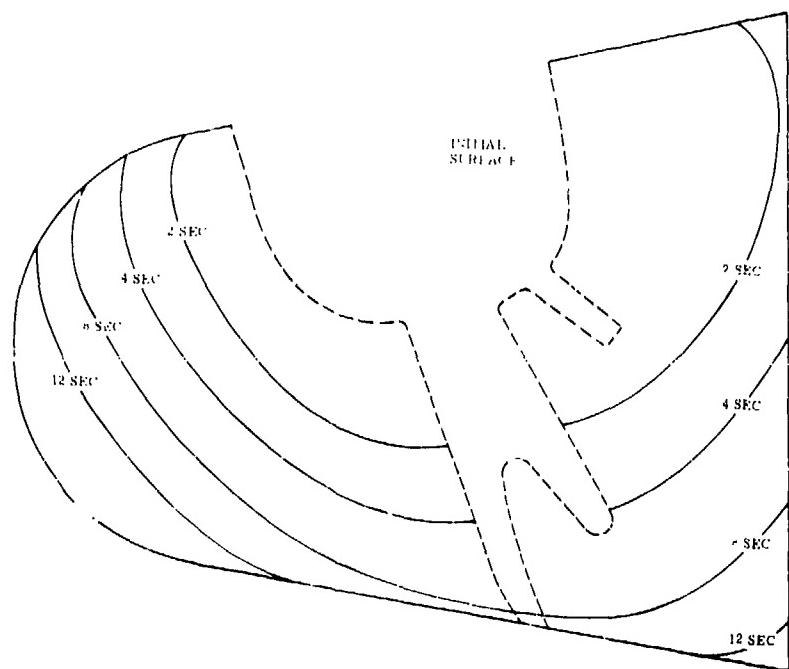
Figure 12. Foam Surface Recession Contours - Malta Test No. 6
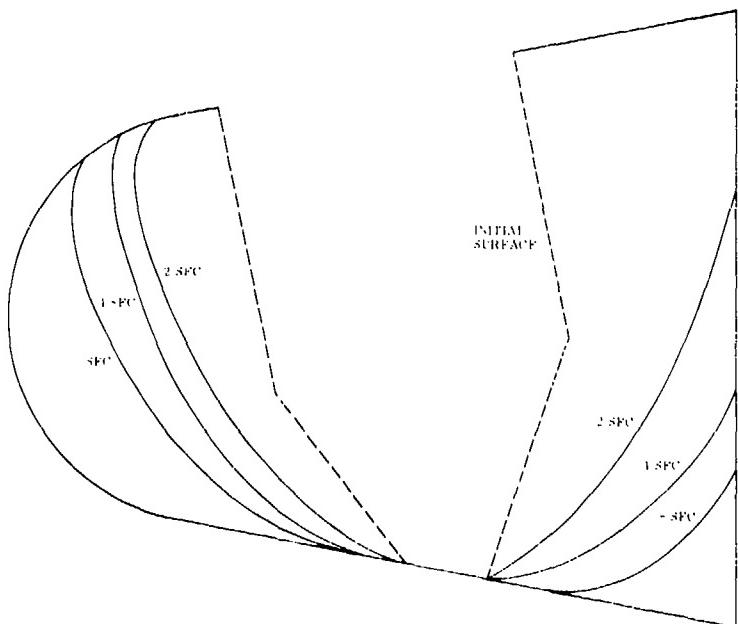
Figure 13. Foam Surface Recession Contours - Malta Test No. 7

H-16

(See Figure 5.) The scale had a relatively thick, crusty appearance, and constituted a significant added thermal resistance which reduced the local heat flux due to increased surface temperatures. This effect was verified experimentally by subjecting scaled and unscaled areas of the backplate to identical heating conditions from a blowtorch. The temperature response of a thermocouple on the back-face of the scaled area indicated a heat flux of approximately half that for the unscaled area.

3. Perforation Enlargement Due to Ablation

Tracings and measurements of the perforation contours were made directly from the models after testing for Models No. 4 through 7. Pre-test and post-test contours of the perforations in the heat shield and structure are shown in Figure 14. More heat shield material was removed than metal structure, despite the greater heat of ablation of phenolic nylon relative to that of Inconel. This effect is due partly to the higher heat flux near the upper corner, but may also be the result of poorer ablation performance due to high vorticity in the re-attachment region of the separated shear layer which develops over the perforation. The steep gradient in ablation of the downstream edge of the perforation is shown in the sketch, which is typical of results for Tests No. 5 through 7.
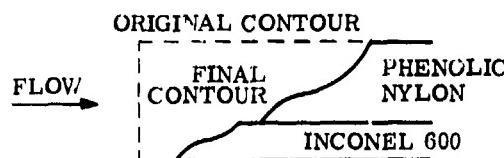
It is seen from Figure 14 that significant perforation enlargement due to ablation occurred for the longer test durations of Tests No. 6 and 7. Computations for these cases yielded the results shown in Table 4.

TABLE 4. PERFORATION ENLARGEMENT DUE TO ABLATION

TEST NO.	6	7
Percent increase in heat shield perforation area	43	37
Percent increase in Inconel liner perforation area	19	18

4. Pressure Measurements

The pressure measurements for Test No. 7 are plotted in Figure 15. Little pressure rise was observed for tap locations on the backplate, due to clogging by pieces of foam. The taps located directly beneath the upstream edge of the perforation recorded a pressure history quite similar to that which was obtained for Test No. 2. Thus, it appears that the presence of foam decomposition gases within the model has no significant effect on the pressure history.
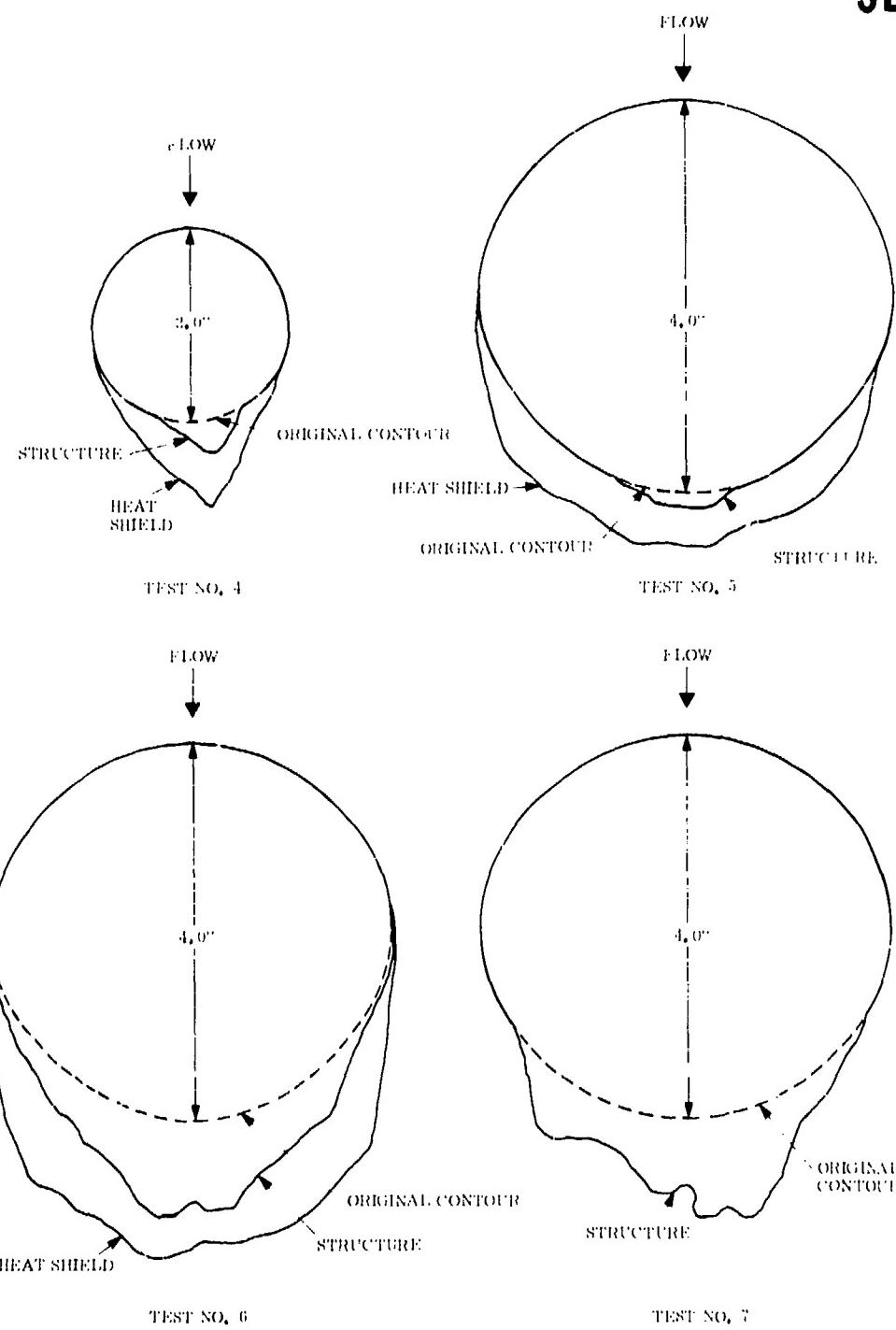
Figure 14. Perforation Enlargement Contours

H-18
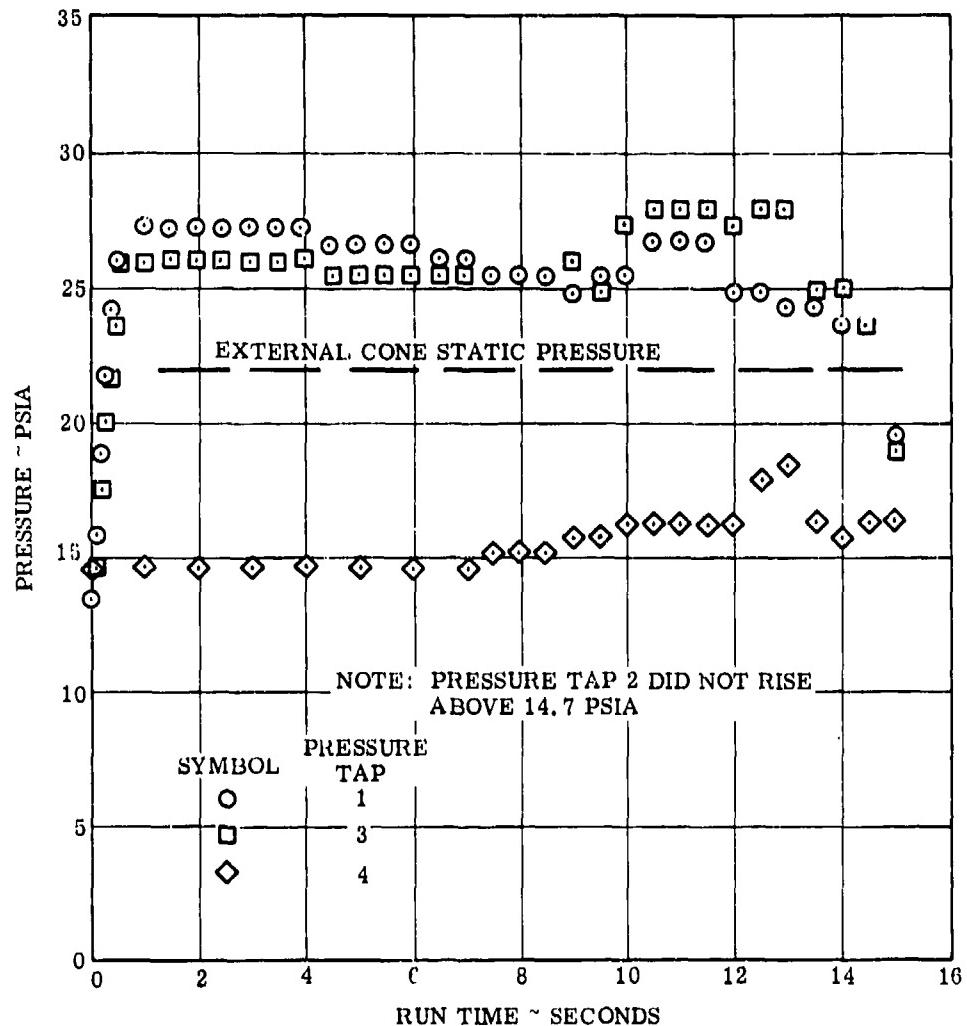
Figure 15. Internal Pressure Histories - Malta Test No. 7

5. Foam Characteristics

The results of Tests No. 5, 6, and 7 shown in Table 3 indicated relatively good performance of Hetrofoam 368 for the Malta rocket exhaust environment. This observation prompted additional laboratory investigations of the structural and thermal degradation characteristics of this foam.

Compressive tests of 1 inch cubes were performed on an Instron universal testing machine to determine the modulus of elasticity and ultimate stress in the

H-19

foam-rise direction and perpendicular to it. The test results are shown in Table 5, and indicate higher strength in the foaming direction, as well as increased strength with increased density.

TABLE 5. COMPRESSIVE TEST RESULTS FOR HETROFOAM 368

Density (lb/ft^3)	Modulus of Elasticity (psi)	Ultimate Strength (psi)	Loading Condition
3.0	1800	60	Direction of foaming
3.0	700	52	Perpendicular to direction of foaming
7.3	4900	152	Direction of foaming
7.3	3300	115	Perpendicular to direction of foaming

Thermal degradation tests were performed by heating rectangular samples to 1000°F by means of a Nichrome wire connected to a Variac. In the first test, the temperature was increased slowly (from room temperature to 1000°F took 2 hours); in the second test, a more rapid heating rate was used to reach 1000°F in a few minutes. Samples of both densities (3.0 and 7.3 lb/ft^3) reacted similarly; they warped, discolored, charred, and finally broke due to spring tension induced by the heater wire. Charring began at a temperature of approximately 500°F. The foam smoked considerably in the higher heating rate test, but no sign of combustion was observed. It was noted that the foam burned in the flame of a match, but was self-extinguishing upon the formation of a char layer on its surface.

C. Final Correlation of Internal Heating to Open Volumes

In Ref. 1, a semi-empirical correlation of wind tunnel and rocket exhaust test results was developed for the rate of energy absorption by the walls of axisymmetric models having single perforations. The correlating parameter was based on the compressible turbulent shear layer analysis of Chow and Korst (Ref. 3), and included the Crocco number C and a mixing similarity parameter σ.

Further study of the results showed that the effect of C and σ can be incorporated into the empirical proportionality constant with little loss in accuracy, due to the compensating effect of Mach number on these terms. The resulting correlation is shown in Figure 16, and is considerably simpler to evaluate than the previous correlation. The correlating parameter used in Figure 16 is equivalent to the simple result obtained by Donaldson (Ref. 4) by means of a turbulent shear layer mixing analysis, with the constant adjusted to agree with the experimental results. The success of this method of correlation over a range of 3 decades in the correlating parameter and for two widely different test environments lends credence to the shear layer model for the case of a single perforation.

The resultant correlation equation for the rate of energy absorption by the structure is:

$$dE/d\theta = .0105 \frac{\gamma}{\gamma - 1} \frac{pUA}{J} \qquad (2)$$

with symbols being defined in Figure 16. The scatter of the bevelled and impact perforation results about the mean correlation line for cylindrical perforations indicates that the correlation is a reasonable representation for actual impact perforations.

D. Application of Results to ICBM Re-entry

Equation (2) was applied to the C-1 Advanced Target Vehicle design of Ref. 5. This hypothetical re-entry vehicle is a slightly blunted cone with the following characteristics:

Ballistic coefficient:	3000 lb/ft^2
Semi-vertex angle:	11 degrees
Re-entry velocity:	25,000 feet/second
Re-entry path angle:	23 degrees
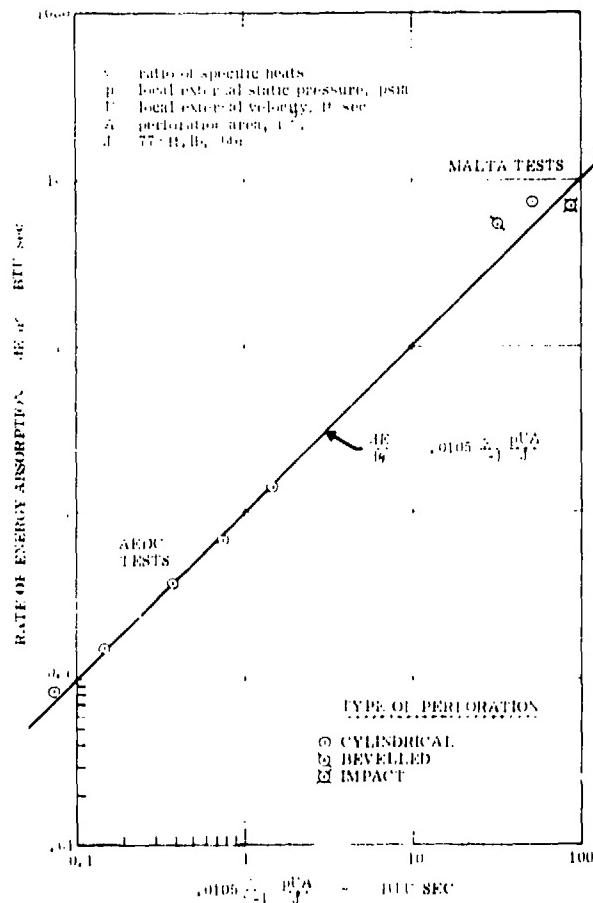
Figure 16. Correlation of Internal Heating Results

H-21

The results are shown in Table 6, and apply for a single perforation anywhere on the cone, assuming intercept to occur at an attitude of 100,000 feet.

TABLE 6. ENERGY INFLUX THROUGH PERFORATION FOR C-1 VEHICLE

Z-Altitude(ft.)	70,000	50,000	30,000
E/A integrated energy per unit perforation area, (btu/in^2) from 100,000 ft. to Z ft.	50	170	375

These results neglect the effect of perforation enlargement during re-entry. From calculations of this type, lethal perforation areas were presented in Ref. 1 for various structural designs of the C-1 class of vehicle as a function of vehicle size, intercept altitude, and kill altitude.

Estimates of weight penalties to a given vehicle design by the use of internal foam for hardening against thermal effects can be obtained by use of a foam heat of ablation on the order of 2000 to 3000 btu/lb, as obtained in Tests 5 through 7. * However, choice of foam density must be related to foam compressive strength considerations. Cone pressures for high ballistic coefficient vehicles will be several times higher than that of the Malta environment, such that compressive collapse of the lighter foams may occur.

This result is strictly applicable only for conditions simulated by the Malta test environment. Higher values of Q would be expected for higher enthalpy levels of flight. This effect will be pursued in a new phase of the program, as discussed in Section II which follows.

II. THERMAL PERFORMANCE OF FOAMS

A one-year study was begun in August 1964 with the objective of developing an understanding of the heat protection characteristics of lightweight foam having simulated hypervelocity impact damage.

The use of lightweight foams has been proposed as a means of heat protection for the interior of a re-entry vehicle whose shield/structure may be perforated by hypervelocity impact. Since impact tests have demonstrated that foam fillers placed behind outer shells are effective in absorbing the impact energy, the use of internal foam would appear to have a dual purpose.

In order to avoid excessive weight penalties, foam densities of less than 15 lb/ft^3 are desirable. Essentially, no thermal performance data for this class of material exist at present.

The study is being conducted under two separate but related phases:

Phase 1. Study of Fundamental Ablation Process for Cavity Heating

Phase 2. Response of Selected Foams

In Phase 1, effort will be concentrated on the understanding of the basic ablation phenomena associated with cavity heating. In Phase 2, the response of selected foams having simulated impact cavities will be determined in GE-RSD's 5-Megawatt Air Arc Facility. A detailed description of each phase of the program is given below.

A. Program Plan

1. Phase 1. Study of Fundamental Ablation Process for Cavity Heating

In this phase of the program, experimental studies will be conducted according to the test program shown in Table 7, using the model configurations shown in Figure 17. Emphasis will be placed on developing an understanding of the basic ablation process for lightweight foams having simulated impact cavities. A discussion of each group of tests follows:

Tests 1 and 2: Calorimeter models will be tested to determine the calorimeter heat flux distribution within various shapes of cavities. External pressure measurements will be made from which local flow conditions approaching the cavity will be determined.

Tests 3 through 8: Foam response for two densities of urethane foam will be determined in three different facilities in order to determine the effects of widely varying test environments. The characteristics of these facilities are shown in Table 8.

Tests 9 and 10: The effect of simulated impact cavity size and shape on foam performance will be determined for a given foam in a given test environment. The foam degradation will be correlated with the calorimeter heat flux distribution of Test 1 for each cavity shape.
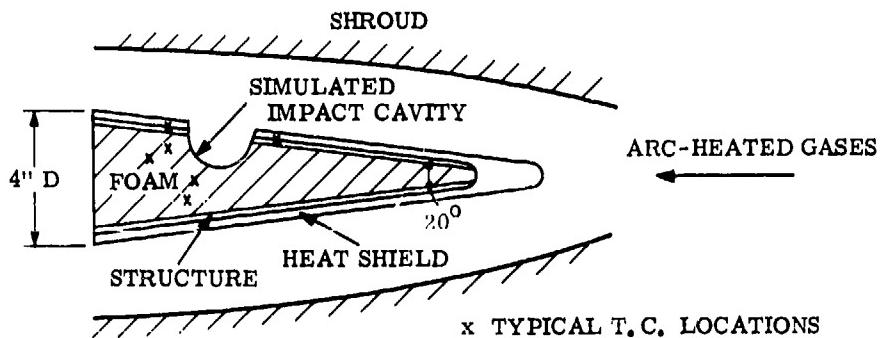
(a) ARC SHROUD CONFIGURATION
(SAME MODEL WILL BE USED FOR MALTA PIT ONE TESTS)
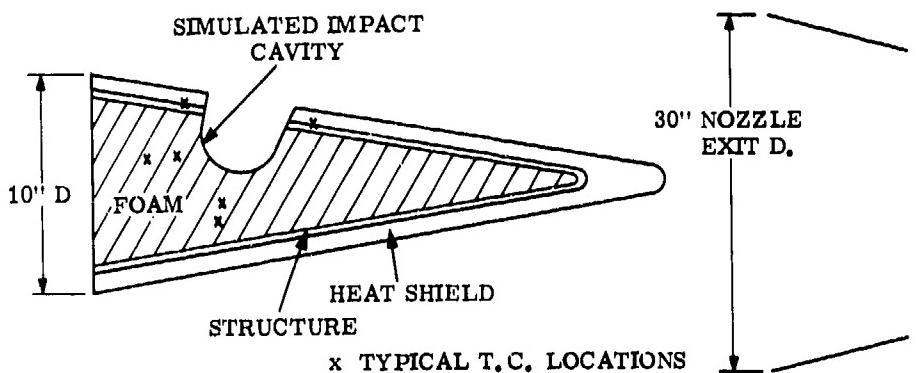
(b) ARC TUNNEL CONFIGURATION

Figure 17. Thermal Test Model Configurations

H-24

TABLE 7. THERMAL TEST PROGRAM - PHASE ONE

Test No.	Foam	Density (lb/ft^3)	Impact Cavity No.	Test Facility	Test Objective
1			1, 2, 3	Arc Shroud	Model Calibration (Calorimeter heat flux pressures).
2			1, 2, 3	Arc Tunnel	
3	Urethane	7.5		Arc Shroud	Determine effect of test environment on foam response for two densities of urethane foam having a given impact cavity.
4				Arc Tunnel	
5				Malta Pit One	
6		3.0		Arc Shroud	
7				Arc Tunnel	
8				Malta Pit One	
9			2	Arc Shroud	Determine effect of impact cavity size and shape on foam response (comparison includes Test No. 6).
10			3		
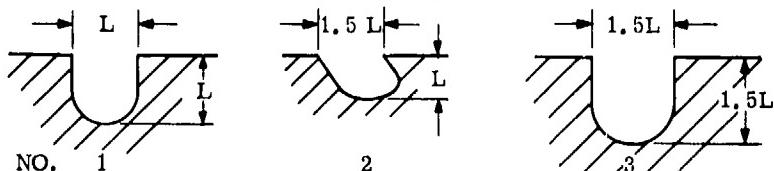
EXAMPLES OF IMPACT CAVITIES

TABLE 8. THERMAL TEST FACILITY CHARACTERISTICS

Facility	GE-RSD 5 MW Arc Tunnel	GE-RSD 5 MW Arc Shroud	Malta Rocket Pit One
Stagnation enthalpy (btu/lb)	6000 - 20,000	6000 - 20,000	3250
Model Stag. press. (atm)	0.1 - 1.0	1 - 5	8
Free Stream Mach No.	5 - 7	Subsonic	2.5

H-25

2. Phase 2. Response of Selected Foams

A review of available foams will be made to select several possible materials suitable for this application. Based on present knowledge, it is expected that foams of the following classes will be considered: (a) epoxy, (b) silicone, (c) urethane, (d) phenolic, (e) ceramic, and (f) composites such as ceramic backed with urethane. In addition, consideration will be given to lightweight materials such as balsawood (fire-retardant impregnated) and Insulcork.

The capacity of a foamed solid to serve as a thermal barrier is a function of a number of interrelated variables, including: (a) composition of material, (b) wall size, (c) pore size, (d) pore size distribution, and (e) flammability of the foam. The materials chosen for thermal evaluation will provide a broad spectrum in anticipated structure and potential thermal performance. As an example, one or more specific formulations will be varied to produce a range of densities, with corresponding variations in structural, mechanical and thermal properties.

Promising foam candidates will be evaluated in a thermal test program as outlined in Table 9. An initial screening phase will be conducted in which flat samples will be subjected to a blowtorch test to determine relative performance. The more promising foams will be tested in axisymmetric model configurations (Figure 17) according to the test schedule of Table 9. Simulated impact cavities will be provided in the foam. A discussion of each group of tests follows:

Tests 1 - 20: Flat circular disk specimens of foam will be screened for thermal response in a blowtorch stream.

Tests 21 - 26: The relative performance of several foams will be determined for a given simulated impact cavity in a given test environment.

TABLE 9. THERMAL TEST PROGRAM - PHASE TWO

Test No.	Foam (Choices are for illustrative purpose only)	Density lb/ft^3	Impact Cavity No.	Test Facility	Test Objective
1 - 20	Miscellaneous	3 - 15	None	Blowtorch $\dot{q}$ = 20 btu/ft^2 sec P = 1 atm.	Screen candidate foams for further testing. Flat test samples.
21	Epoxy	3	1	Arc Shroud	Determine relative performance of several foams having a given impact cavity --- (comparison includes Tests No. 3 and 6 of Table 7).
22	Epoxy	7			
23	Silicone	10			
24	Ceramic	10			
25	Composite	10			
26	Phenolic	3			

H-26

SECRET

In all tests, thermocouples will be placed at selected locations to monitor the heat flux reaching the metal substructure due to internal heating. Final foam degradation will be measured and correlated with the measured calorimeter heat flux distribution for the given cavity shape to determine the effective heat of ablation for the foam. In addition, arrays of thermocouples will be embedded within the foam on selected tests to obtain approximate recession rate histories.

B. Progress to Date

1. Phase I

The arc shroud calorimeter model has been designed and fabricated and is shown in Figure 18. This model will be used to determine the convective heat flux distribution to three simulated impact cavities. In Figure 18, cavities number 1 and 2 are geometrically similar to check scale effects, while cavity number 3 represents the anticipated effect of an oblique impact. The cavities have been located fairly far back on the model in order to facilitate transition to a turbulent boundary layer upstream of the cavities. The heat flux distributions obtained in the calorimeter model test will be used in the analysis of the ablation performance of foams having the same initial impact cavity shapes.

The basic arc shroud foam test models have been designed. The external configuration for the models will be the same as the calorimeter model of Figure 18, including a simulated impact cavity; however, the internal portion of the models will be hollow to contain various foams for thermal evaluation. The model shell will consist of a one-piece phenolic nylon heat shield of 0.25 inch thickness bonded to an 0.080 inch aluminum structure. A graphite shroud will channel the arc flow over the model as shown schematically in Figure 17. The shroud is being designed to provide a sonic flow at the location of the base of the model, with a high subsonic flow at the cavity location. An analysis is underway to determine the effect of heat loss from the flow to the model and shroud surfaces. The mold design for the foams for these models is in preparation. The tests will be run for from 5 to 10 seconds to obtain approximately one inch of recession of the foam surface.

2. Phase II

A review of available high-temperature lightweight foams is in progress. The seminar on Cellular Plastics was attended at the University of Michigan (August 3-7). As a result of this and other contacts, additional new foams have been added to the list of promising candidates. Samples of a thermally stable 2 lb/ft^3 high-temperature urethane foam have been received from the Amoco Chemical Corporation. A list of foam candidates for the screening tests is given in Table 10.

The fabrication procedures for producing urethane foams of CPR-18 have been determined, and density variations have been established. By removing the outer one inch areas of a foamed block, the variations in density are held to within 0.5 lb/ft^3. This foam will be supplied to the Naval Research Laboratory in 12-inch cubes for hypervelocity impact testing.

The Linde torch equipment is being readied for the screening phase of the program. Agreement was reached on the design of the sample holder and temperature monitoring. Design of a fixture for installing thermocouples in the foam samples prior to exposure to the Linde torch is being pursued so that the resultant data may be meaningful and consistent. This fixture should be able to double as a device capable of measuring recession rates in future testing. Tests will be performed to characterize promising foams by determining significant temperature ranges for mass loss and phase transitions.

TABLE 10. FOAM CANDIDATES FOR SCREENING TESTS

| Class	Specific Material	Density lb/ft^3	Max. Temp. $^\circ$F
1. Epoxy	Ecco-foam EFB	10, 15	300
2. Epoxy	Ecco-foam EFF	10, 15	300
3. Silicone	DCR-7002	14	~500
4. Ceramic	Ecco-foam LM-43A	15	1000
5. Ceramic	Ecco-foam Q (or equivalent)	12	2500
6. Ceramic	Foamglass	9	1000
7. Urethane	CPR 18	8-15	350
8. Urethane	CPR 18 + Fire Retard.	8-15	350
9. Urethane	CPR 18 + Fire Retard. + Hollow Glass Fibers	10-15	350
10. Urethane	CPR 18 + Fire Retard. + Flake Glass	10-15	350
11. Urethane	CPR 18 + Fire Retard. + Ecco-spheres SI	10-15	350
12. Urethane	Hetrofoam 368/269	4-15	350
13. Urethane	Balsawood (Fire Retardant Impregnant, as is and as plywood)	6-8	---
14. Composite	4 or 5 backed up with 15	10-15	>350
15. Urethane	Hetrofoam HLR-250 + PAPI	4-15	>350
16. Composite	Glass Phenolic Honeycomb + Glass backing, all backed with Urethane foam 15 or 7.		·350
17. Urethane	Hetrofoam HLR-250 (or equivalent) + PAPI + Hollow Glass Fibers	10-15	>350
18. Phenolic	Tetrafoam	10	~350
19. Urethane	Amoco Chemical Corp.	2	500

H-28
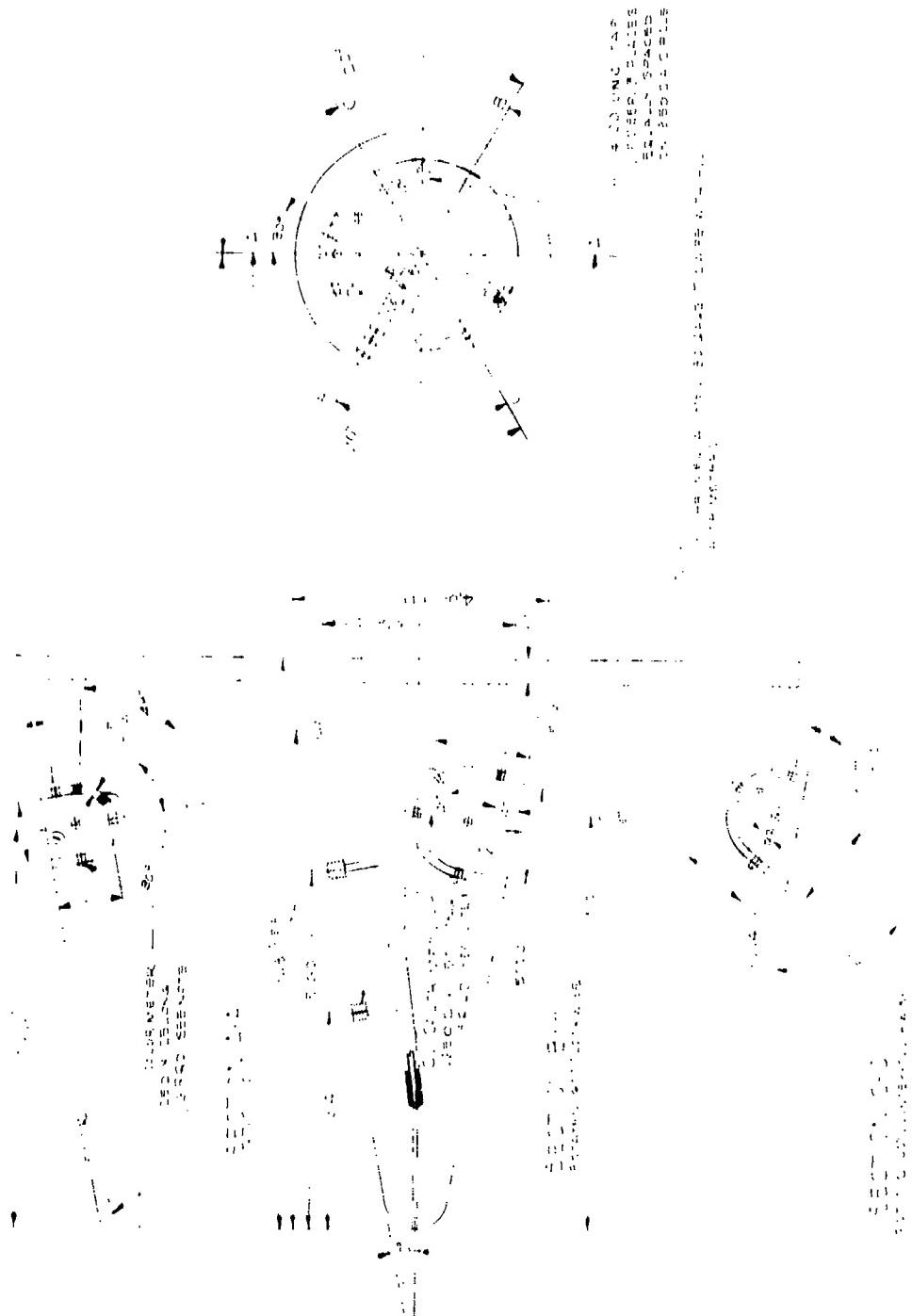
SECRET

Figure 18. Arc Shroud Calorimeter Model

III. THERMOSTRUCTURAL KILL STUDY

A one-year study was begun in August with the objectives of:

1. the formulation of a simplified computational model for the determination of thermostructural vehicle kill due to hypervelocity impact perforations; and

2. the application of the computational model to selected advanced ICBM re-entry vehicle designs of two general classes: (a) unhardened; and (b) hardened.

A. Program Plan

This aspect of the continuing work under the HKM program comprises the following subtasks.

Subtask 1: Approximate heat shield and structure designs will be prepared for several advanced ICBM re-entry vehicle configurations having ballistic co-efficients greater than 1500 psf. Cone angle and length will be varied over representative ranges of interest. Three types of structure design (e.g., monocoque, ring-stiffened, and honeycomb-sandwich) and two materials (e.g., steel and aluminum) will be considered for each configuration. The designs will be "un-hardened" per the following definition: no foam within the internal compartments of the vehicle, standard aft cover design, and no nuclear blast loading requirement.

Subtask 2: Approximate structure designs will be prepared for selected configurations of Subtask 1 which are "hardened" per the following definition: foam within the internal compartments of the vehicle for shell stiffening, aft cover designed to withstand cone pressure, and various levels of nuclear blast loading requirement.

Subtask 3: Structural failure criteria will be formulated for forecone and aftcone regions which have been perforated, for unhardened and hardened designs. These criteria will be based primarily on existing analytical techniques, with a minimum of additional cylinder buckling tests similar to those reported on in Reference 1 being performed if required.

Subtask 4: An approximate model will be formulated for computing structure temperature rises and foam ablation rates due to internal heating of perforated compartments. The model will include the effects of perforation growth during re-entry and non-uniform internal heating distribution. Simplified relations will be employed in order to express the internal heating rates as functions of free-stream quantities. Approximate trajectories and pressure distributions will be used in an attempt to obtain closed form solutions for internal pressure and structural temperature rise as functions of ballistic coefficient, re-entry velocity and path angle, and altitude at which perforation occurs.

Subtask 5: Parametric computations will be made for the vehicle designs of Subtasks 1 and 2 to determine perforation size required for thermostructural kill as a function of altitude at which perforation occurs and altitude of kill. The

H-30

computations will assume a single perforation in either the forecone or aftcone region. Approximate heating loads to exposed payload and components following thermostructural kill will also be determined. Results for the "unhardened" class of vehicle will include the effect of 5 and 10 percent weight additions in the form of foam for thermal hardening only.

B. Progress to Date

Subtask 1

Initial study under this task has resulted in the selection of seven vehicle configurations having ballistic coefficients from 1700 to 4400 psf, with cone half-angles from 8 to 12 degrees and lengths from 100 to 267 inches. A summary of these configurations is given in Table 11.

TABLE 11. SUMMARY OF VEHICLE CONFIGURATIONS

Configuration Number	Cone Half-Angle (degrees)	Length (inches)	W/C_DA (psf)
1	8	125.0	2470
2	8	153.5	4375
3	8	267.3	3410
4	10	99.7	1720
5	10	133.7	2675
6	10	213.2	2335
7	12	176.9	1690

Subtask 4

A review of calorimeter heat transfer and perforation ablation measurements obtained during the AEDC Tunnel C and the Malta Rocket Exhaust Internal Heating Test Programs is in progress. Turbulent shear layer theory will be applied to this data to formulate a correlating parameter for the rate of perforation enlargement due to re-entry heating.

REFERENCES

1. GE-RSD, "Hypervelocity Kill Mechanisms Program, Aerothermal Phase, Semi-Annual Progress Report for Period Ending 30 September 1964", GE-RSD Document No. 64SD629, March 31, 1964 (Secret).

2. Nestler, D. E., "Summary Report, Malta Rocket Exhaust Internal Heating Tests, Hypervelocity Kill Mechanisms Program", GE-RSD Document No. 64SD891, July 17, 1964 (Secret).

3. Chow, W. L., and Korst, H. H., "On the Flow Structure Within a Constant Pressure Compressible Turbulent Jet Mixing Region", NASA TN D-1894, April 1963.

4. Donaldson, C. duP., "A Short Review of the Status of the Aerothermal Phase of the Hypervelocity Kill Mechanisms Program", Proc. of Sixth Hypervelocity Impact Symposium, Cleveland, Ohio, April 1963 (Secret). Also included in "Hypervelocity Kill Mechanisms Program, Progress Report No. 11", NRL Report 5990, June 1963 (SRD).

5. GE-RSD, "Hypervelocity Kill Mechanisms Program, Aerothermal Phase, Annual Progress Report for Period Ending 20 Sept. 1962", GE-RSD Document No. 62SD837 (Secret); Included as Section II of "Progress Report No. 9, Hypervelocity Kill Mechanisms Program", NRL Report 5913, Jan. 1963 (SRD).

HYPERVELOCITY KILL MECHANISMS PROGRAM

ARPA ORDER 149-60

Aerothermal Phase

Semi-Annual Progress Report

For Period Ending

1 September 1964

Research and Advanced Development Division

AVCO CORPORATION

Wilmington, Massachusetts

K

Project Code No. 7300

Contract NOnr 3307 (00)

APPROVED
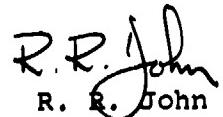
R. R. John
Project Director

-ii-

ABSTRACT

This report discusses work performed on contract NONR 3307(00) in the period March to September 1964. The major portion of the effort expended to date has been in the area of instrumentation and investigation of arc instabilities. Descriptions are presented of the apparatus constructed for measurement of gas enthalpy, composition, velocity and density of a free compressible, turbulent, high enthalpy jet.

NOMENCLATURE

The list below defines the principal notations used in the report. Those symbols that were used infrequently, are defined in the text.

Symbols

c_p	Specific heat at constant pressure
E	Voltage applied to arc
h	Enthalpy
1	Current
K	Turbulent Exchange Parameter for Velocity
K_T	Turbulent Exchange Parameter for Temperature
M	Mach number
P	Pressure
r	Radial distance
R	Jet nozzle radius
T	Temperature
U	Velocity
$\dot{W}$	Weight flow rate
X	Axial distance
δ	Specific heat ratio
ρ	Density

Subscripts

A	Ambient conditions	S	Stagnation conditions
C	Coolant	O	Jet exit conditions
CL	Jet centerline	1	Probe entrance
g	Gas sample	2	Probe exit

CONTENTS

ILLUSTRATIONS

ILLUSTRATIONS (Con t)

I. INTRODUCTION

The work to be accomplished at Avco/RAD under this program consists of an extensive experimental study of the characteristics of a high enthalpy jet mixing with a stationary ambient atmosphere. Velocity, enthalpy, and density distributions obtained under a variety of jet operating conditions, along with pressure and heat flux distributions measured on a flat plate held normal to the jet, will be correlated with existing theories in order that a capability for the prediction of heat transfer may result.

A high enthalpy jet is produced by an electric arc heater. This jet is probed with an enthalpy probe, which, together with an assumption that the gas in the jet is in thermal equilibrium, results in sufficient information to deduce the desired enthalpy, velocity, and density values. The resulting data on turbulent jet mixing is intended to produce values of the turbulent exchange coefficient (related to the eddy viscosity) in a regime of temperature and Mach Number for which such information is not presently available.

In addition to the determination of the aerodynamic properties of the flow and our ability to predict them, the heat transfer to a flat plate placed normal to the flow will be investigated. Pressure distribution on a flat plate in the jet will be measured and used to determine the stagnation point velocity gradients, which will in turn be used to calculate the expected heat flux. These calculated values of heat flux will be compared with measured values.

Ultimately this effort is intended to result in a procedure whereby the heat transfer from a jet of specified properties to a flat plate held normal to the jet axis may be predicted. The program being undertaken is thus primarily experimental, including an attempt to correlate data with prediction.

II.   EXPERIMENTAL APPARATUS AND PROCEDURE

   A.   1.5 Megawatt Facility

       1)   General

            The facility employed in producing the high enthalpy,
compressible jet to be investigated is the 1.5 Megawatt Plasma Generator
shown in Figures 1 & 2. Basically the arc heater consists of an exit
nozzle anode assembly, an arc chamber, and a cathode assembly. Although
the arc can be modified to give three different configurations (1), the
system to be used in this study is the gas stabilized arc configuration
(with the option of magnetically driven arc roots) shown schematically
in Figure 3. The facility has the capability of being operated over a
large range of chamber pressures (1) thus making it possible to produce
both subsonic and sonic jets with various degrees of underexpansion. At
pressure levels to be considered in this program it is not necessary to
drive the arc roots with magnetic fields, hence for its present appli-
cation the facility may be considered to be gas stabilized.

            Gas enters the plasma generator through a series of inlet
holes in the arc chamber and is heated to a high enthalpy by flowing
through the discharge which passes across the gap between the cathode
and anode. The heated gas then exhausts to the atmosphere through the
exit nozzle.

            The working fluid to be employed in all experiments con-
ducted in the program is nitrogen. The use of air was not considered
since it would result in erosion of the cathode assembly thus contamiat-
ing the exhaust jet. Simulated air (i.e., using nitrogen as the primary
fluid, passing it through the arc column, and then adding oxygen to the
hot gas in a plenum chamber between the anode and exit nozzle to produce
simulated air) was not considered since the amount of mixing using this
technique has not been established; hence it would not be possible to
insure that the exhaust jet would be homogeneous in nature. Nitrogen as
a working fluid has several advantages in that the arc may be run for
extended periods of time, the amount of contamination is kept to a mini-
mum, and it simulates air to a reasonable degree.

            A major portion of the investigations in this program, i.e.,
measurement of axial and radial profiles of jet density velocity, com-
position and enthalpy, are to be conducted with an 0 75-inch diameter
exit nozzle. Hence, the jet will be considerably larger than the diag-
nostic probes (described below) required to obtain these quantities.
Operation of the arc facility takes place in a region of mass flow rates
and gas enthalpies such that the jet Reynolds Number is well above the
value of approximately 1500 (2) required for production of a turbulent
jet.

            Operating conditions for the facility are tabulated
below.
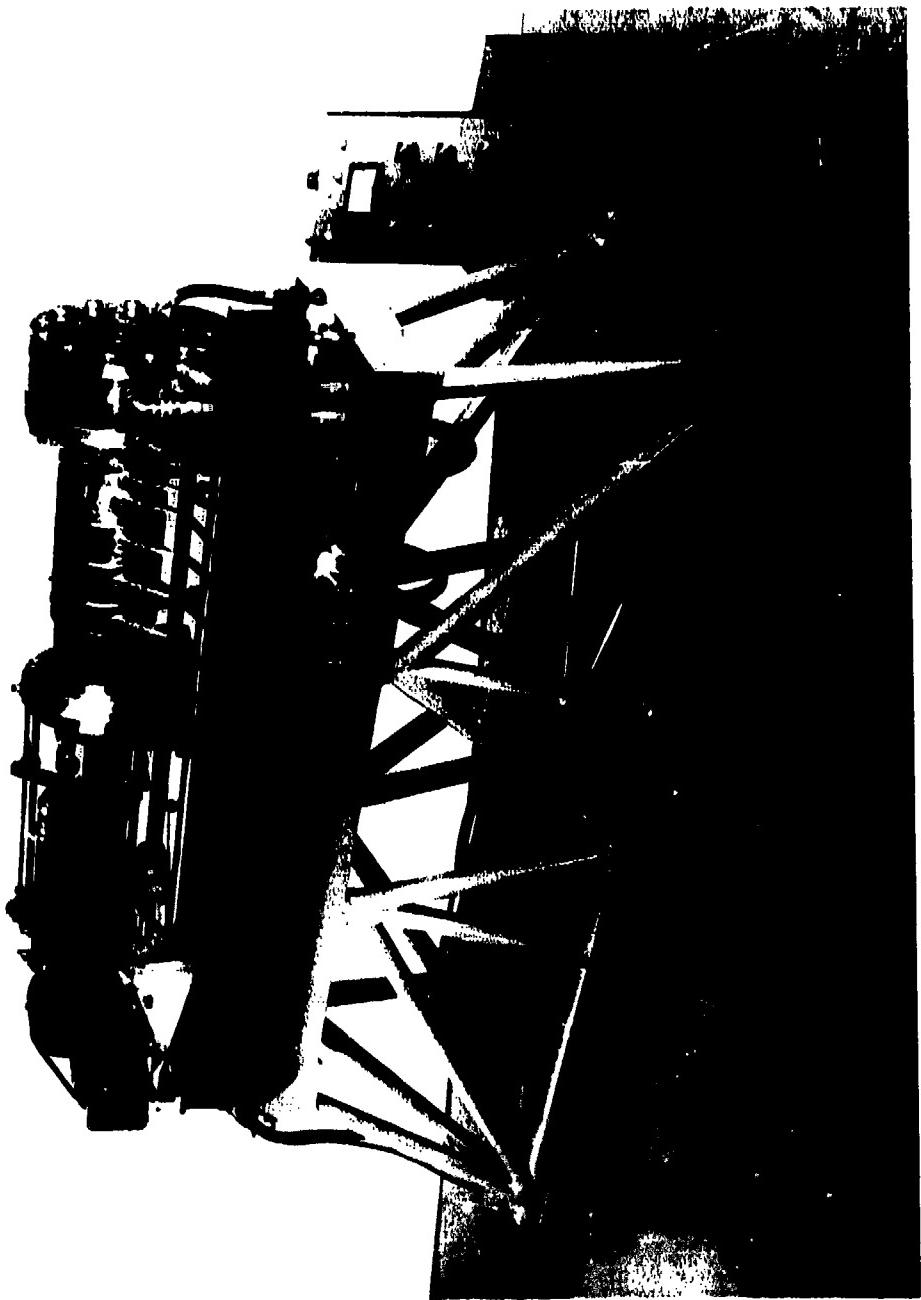
Figure 1--Overall View of 1.5 Megawatt Plasma Generator

Figure 2--Closeup View of 1.5 Megawatt Plasma Generator Electrodes
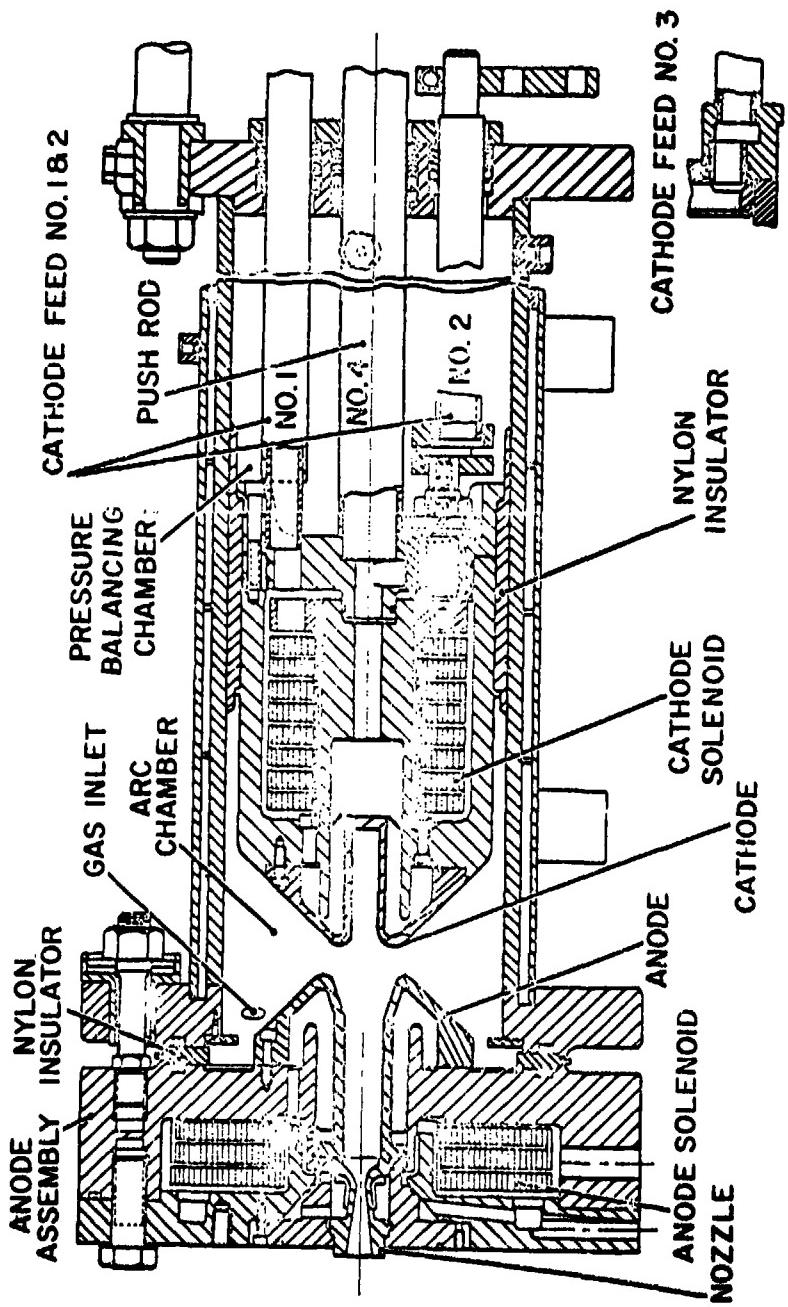
Figure 3--1.5 Megawatt Plasma Generator--Gas Stabilized Arc Configuration with Magnetically Driven Arc Roots

TABLE I

1.5 MEGAWATT PLASMA GENERATOR OPERATING CHARACTERISTICS

Voltage, volts	500-750
Current, amperes	500-1500
Power, kilowatts	250-1125
Efficiency, %	45-60

EXIT NOZZLE DIAMETER, 0.75-INCH

Gas Enthalpy, H/RT_O	75-165
Gas Temperature, $^\circ K$	4000-7000
Gas Density, lb/ft^3	5×10^{-3}-2.5×10^{-3}
Mach No.	.9 - 1.0
Gas Velocity, ft/sec.	3750-5000
Reynolds Number	18,000-8,000
Exit Pressure Ratio	1-2

2.) Jet Stability Studies

In the determination of mixing parameters which would allow one to predict jet decay it is extremely important that mixing of the jet and ambient fluid should be the result of turbulent shear mechanisms and not caused by jet instabilities peculiar to the particular device employed. Relatively large scale jet fluctuations such as flapping and/or "on-off" instabilities may cause a probe mounted in the stream to be periodically immersed in the jet and ambient fluids. Due to the response time of the probes, the measured quantities, such as impact pressure, gas enthalpy, and composition, would be time averages of the jet and ambient fluid variables. Data of this nature would indicate that the axial decay, and radial spread of the jet would be more rapid than that of its steady counterpart. Hence, mixing parameters obtained with an unsteady jet would be extremely difficult to interpret. Therefore, it is essential that the jet have a high Strouhal number, i.e., any instabilities in the flow should have a low amplitude and a high frequency.

An investigation of the time dependent characteristics of the 1.5 Megawatt Plasma Generator exhaust jet has been initiated. Stability of the high enthalpy jet was examined by high speed, motion picture photographs (2,000, 4,000, and 8,000 frames/second). The initial studies were performed with the arc having the configuration shown in Figure 3. A typical sequence of film (8,000 frames/second) from this test series is presented in Figure 4. The films demonstrated that the jet had both flapping and on-off instabilities, both of which were believed to be associated with the location of the anode arc roots. A significant portion of the arc discharge was occurring within the nozzle throat and in the vicinity of the downstream face of the exit nozzle. This phenomena was responsible for the bright region immediately downstream of the nozzle (see Figure 4).

Subsequent to these experiments, the arc configuration (as shown in Figure 3.) was modified by the addition of a plenum chamber between the anode and nozzle. In addition, the length of the exit nozzle was increased. Both alterations made it possible to eliminate the discharge occurring within the throat and to move the anode arc roots upstream of the plenum chamber. The location of the plenum between the arc discharge and exit nozzle made it possible to reduce the jet instability. A typical sequence of high speed motion picture film (8,000 frames/second) for the modified generator is included in Figure 4. Although there are some fluctuations still present in the jet the flapping instability has been essentially eliminated and "on-off" instabilities have been considerably reduced.

At present the arc is being further modified by addition of a weak magnetic field. It is expected that the field will help to produce a more diffuse arc column and hence increase the jet stability.

Further information on the mechanism of jet decay and stability can be obtained by measurement of the jet acoustic power spectrum. Jet mixing caused by turbulent shear mechanism produces a "white" noise, i.e., the sound pressure level (SPL) would be constant over a wide range of frequencies, whereas mixing produced by jet
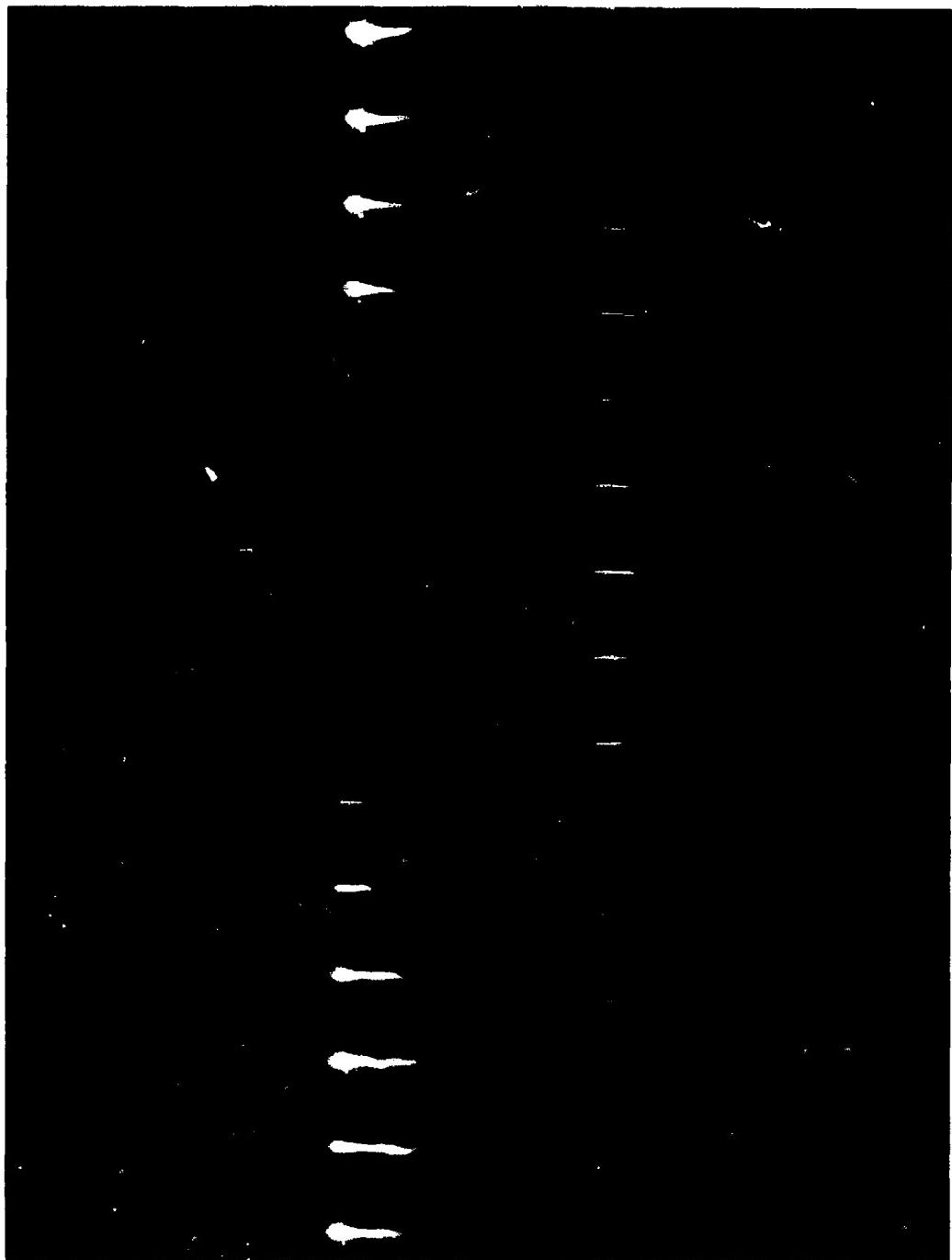
Figure 4--High Speed Film Sequence of 1.5 MW Plasma Generator Exhaust Jet,
Without Plenum (left), With Plenum (right); Camera Speed (8,000 fps)

instability results in a peak in the SPL at various frequencies associated with the particular apparatus.

Measurements were made to determine the SPL of the jet produced by the 1.5 MW Arc facility (with plenum chamber). In addition to the alterations described above the arc was modified further by addition of a large diameter plate in the exit plane of the nozzle so as to simulate a jet issuing from a hole in an infinite wall. Measurements were made at arc operating conditions identical to those employed in the last series of high speed motion picture tests (see Figure 4.). Data obtained were limited to tape recordings of the jet noise which could then be analyzed in the laboratory. The following equipment was employed in these experiments:

Ampex Tape Recorder,	Model 601
Massa Microphone,	Model M-213, S/N 33
Massa Amplifier and Power Supply,	Model M-185
Massa Pre-Amplifier.	Model M-114B, S/N 572
Massa Microphone Base,	Model M-218

The microphone was oriented for normal incidence with respect to the jet nozzle and in the plane of the baffle plate. The microphone was clamped on a stand which rested on the concrete floor. Sheets of rubberized horse-hair packing material, approximately two inches thick, were placed on the floor in the vicinity of the microphone so as to reduce sound reflection from the floor to the sensor. Facing upstream, the microphone was located in the third quadrant.

Recordings obtained in each test were analyzed with a 1/3 octave frequency analyzer by running a continuous loop of the tape through the spectrum analyzer and examining the noise level obtained with each filter separately. Two loops were analyzed for each experiment and the results were corrected to that which would be obtained with constant bandwidth filters. The output of a General Radio Noise Generator Model 1390B was recorded and analyzed to determine the deviation of the tape recorder from flat response. Noise level of all equipment associated with the arc facility (without the arc running) was also measured and analyzed.

The results of these experiments in the form of SPL or db with reference to 0.002 dyne/cm^2 as a function of frequency are presented in figures 5 through 7. Comparison of the data obtained on the noise level of the auxilliary arc equipment and that produced by the jet indicate that the rise in the SPL of the jet at frequencies below 100 cps and above 8000 cps may be the result of ambient noise. The results indicate that the jet audio output was relatively flat over a wide range of frequency. No single bandwidth had noise levels greatly different from the mean SPL indicating that no resonant characteristic of the arc showed up significantly in the exhaust jet.

-9-

SOUND PRESSURE LEVEL (db)

FREQUENCY CYCLES/SECOND

AMBIENT NOISE IN ABC TEST CELL

= 15

90

80

70

60

50

40

FIGURE 6.

JET SOUND PRESSURE LEVEL
MICROPHONE DISTANCE 33 IN

○ — LOOP 1
□ — LOOP 2

FIGURE 7

JET SOUND PRESSURE LEVEL
MICROPHONE DISTANCE 28 IN

◯ LOOP 1

◻ LOOP 2

SOUND PRESSURE LEVEL, db

FREQUENCY, CYCLES/SECOND

- 12 -
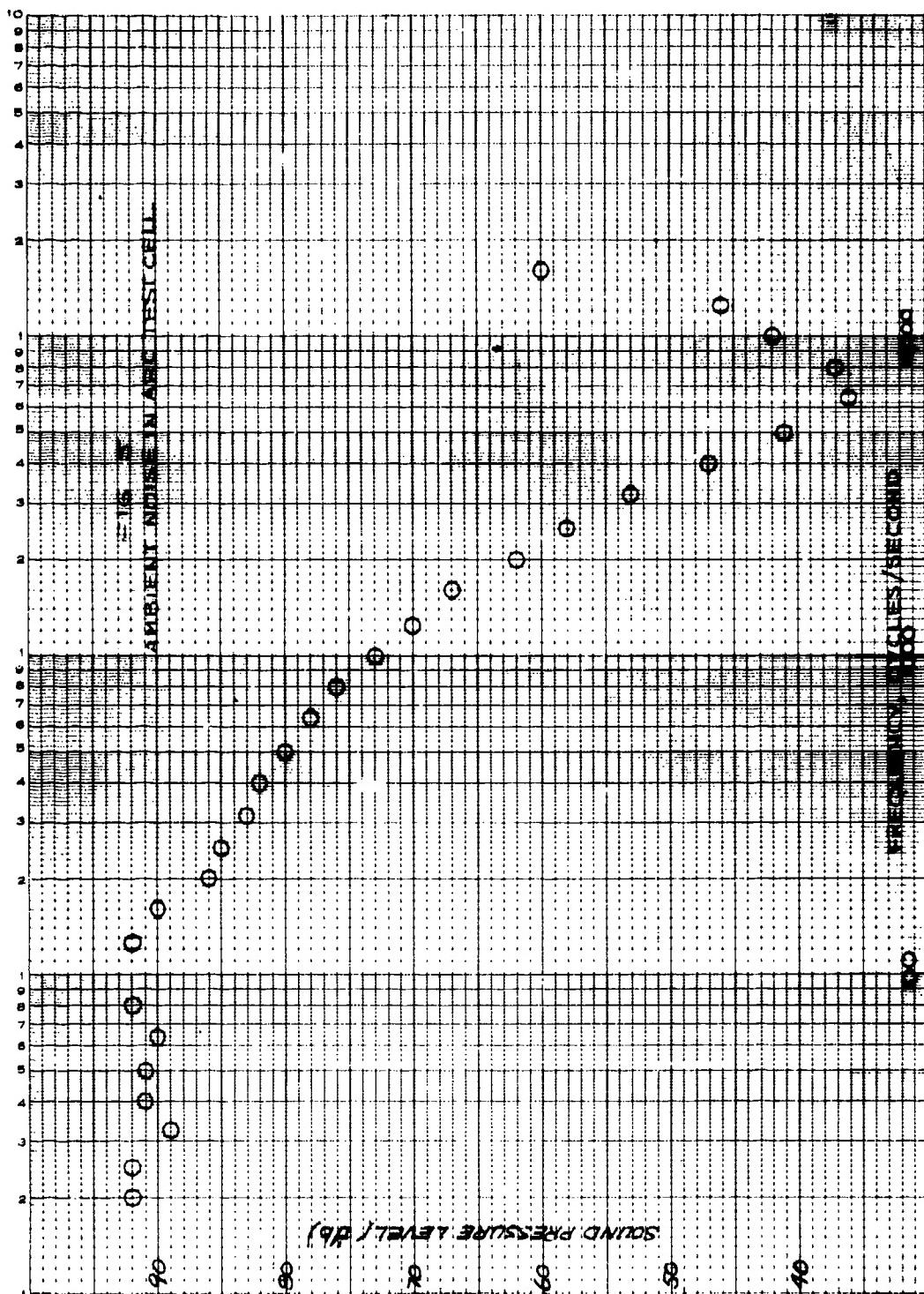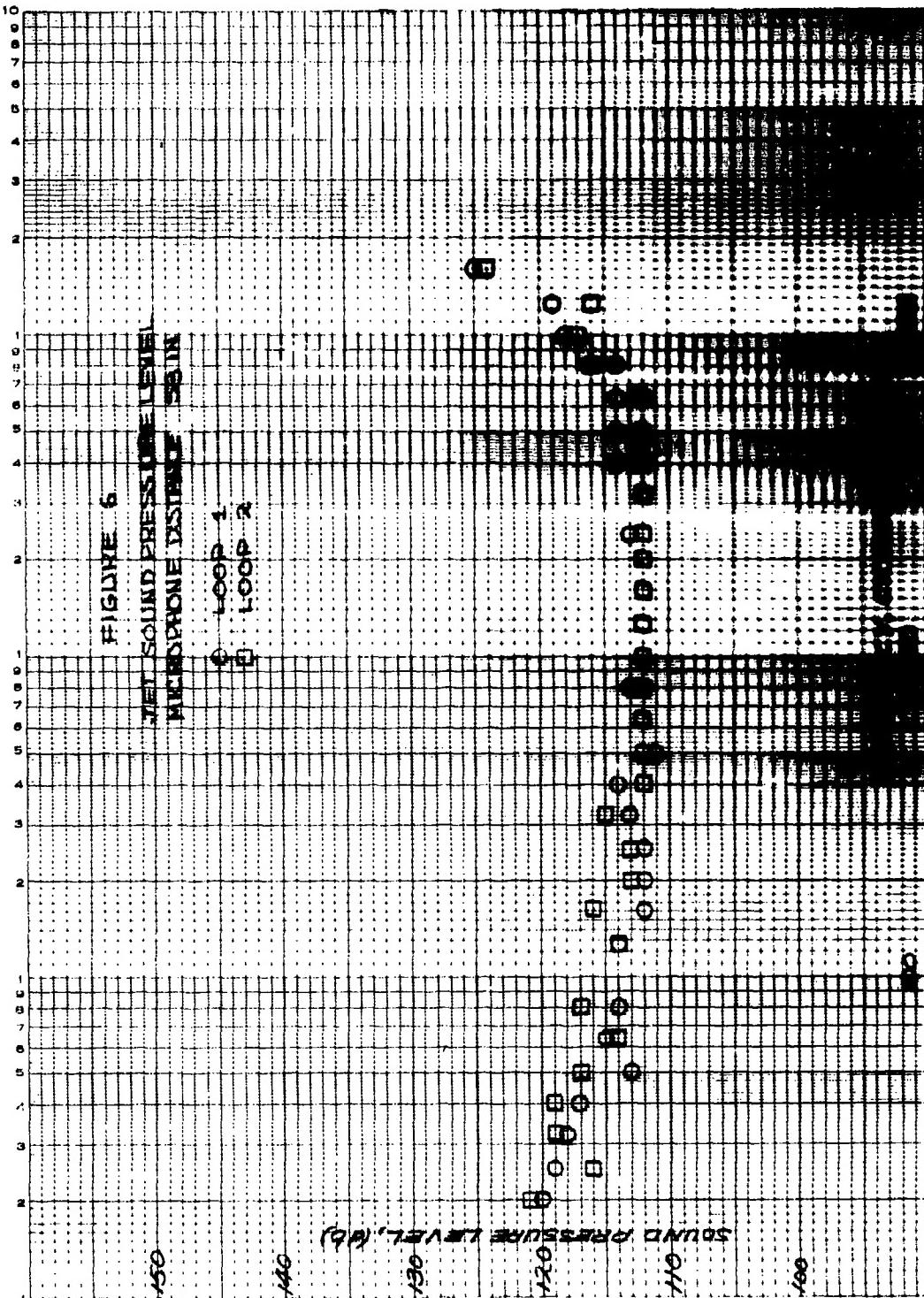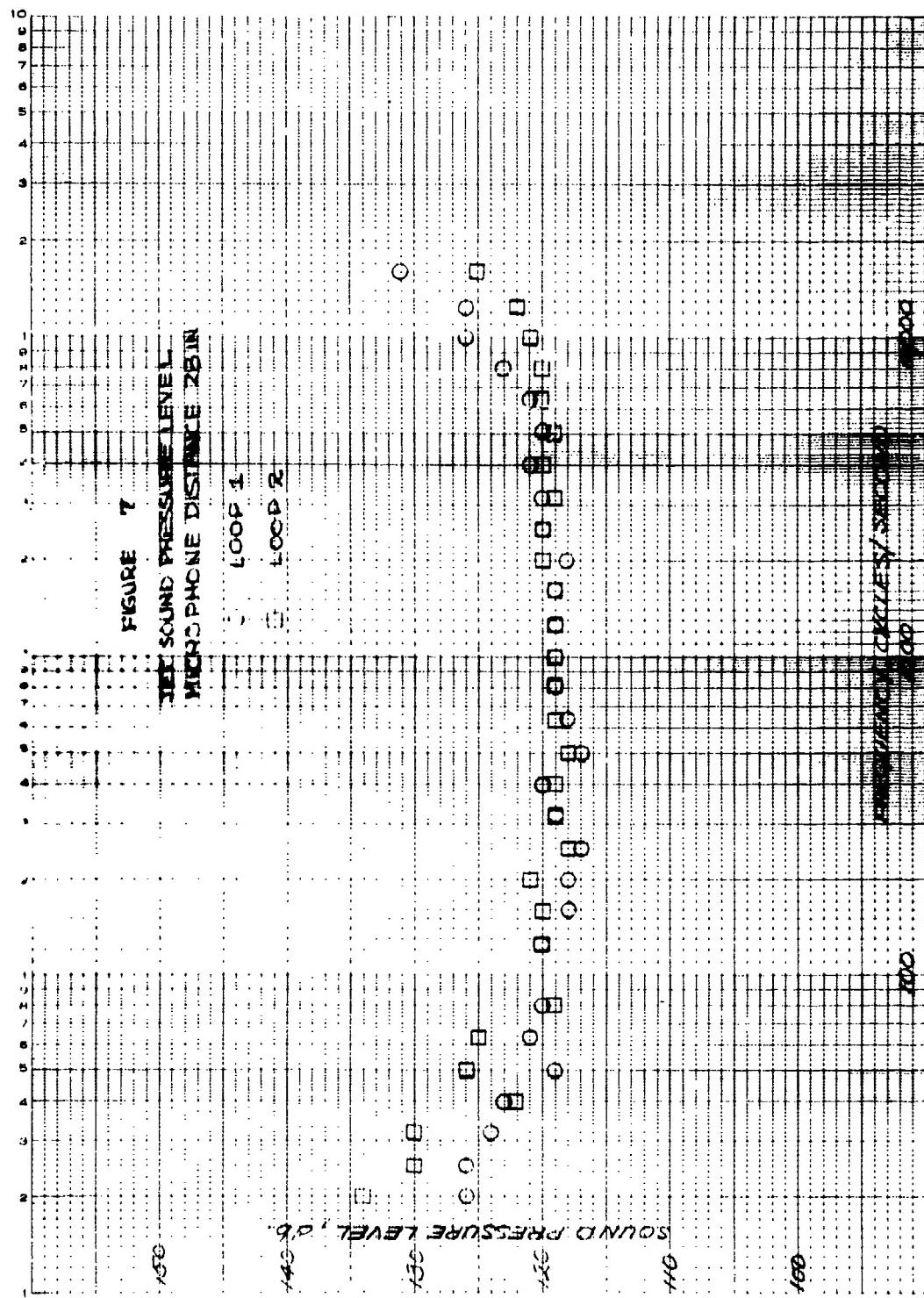
B   GAS PROBES

For a considerable period of time a company sponsored probe develop-
ment program has been underway at Avco/RAD. The purpose of this program
has been to develop thermodynamic and calorimetric probes for diagnostic
studies in all facilities which provide high enthalpy gases for laboratory
use. Probes have been developed to determine local enthalpies, gas com-
positions, mass flow rates, heat fluxes, and both static and impact
pressures.

Of the facilities available for test purposes, the most severe conditions
are encountered in the 10 Megawatt Arc(3). For that reason it was felt
that, if the probes could withstand the high heat flux at the 10 Megawatt
Arc without melting, then there would be no questions about their ability
to withstand the environments produced by other plasma generators.

Early in the probe development program it was decided to use copper
for all surfaces that are in a contact with the hot gases. Despite the
fact that copper has a relatively low melting point, it was felt that
with a proper design of a water-cooling system, advantage could be taken
of the high thermal conductivity of this metal.

1.) Prototype Water Cooled Probe

In the initial phase of this probe development program a proto-
type probe (Figures 8 & 9)was constructed and placed in the 10 Megawatt
Arc exhaust jet.Experiments performed with an 0.25-inch diameter probe
proved successful in that the device could withstand estimated heat
fluxes of 18 X 10^{6} Btu/ft^{2}hr with a water coolant pressure of 280 psig.

In view of the favorable experience in the 10 Megawatt facility
a series of watercooled calorimeters for measuring heat flux have been
designed and are in operation. The calorimeters vary in size from ¼ in.
diameter and larger, depending on the requirement. Emphasis is being
placed in future design on miniaturization, fast response and reduction
of error due to heat losses

2.) Mass Flow Probes

Probes designed to measure the local mass flux in a supersonic
gas stream have been, constructed and tested in the exhaust of a 30
kilowatt arcjet engine. The mass-flux probes were 0.250 inch in outer
diameter and had various diameter (0.042-0.062 inch) gas sampling tubes
located on the probe axis. In contrast with the prototype calorimetric
probe, the mass flux probes have a conical front face which comes to a
sharp edge at the junction with the gas sampling tube. Cone half angles
used in these probes were 20° and 45°. A typical mass flux probe is
shown in Figure 10.

Experiments conducted with the mass flux probe (20° nose angle)
were performed in the 30 kilowatt arcjet engine. The probe was placed
as close as possible to the exit plane of the engine and operated success-
fully to within 0.10 inch of the jet's axis of symmetry. Experience with
this probe indicated that when a reasonable pressure difference was main-
tained across the probe sampling tube, all shocks in the stream tube
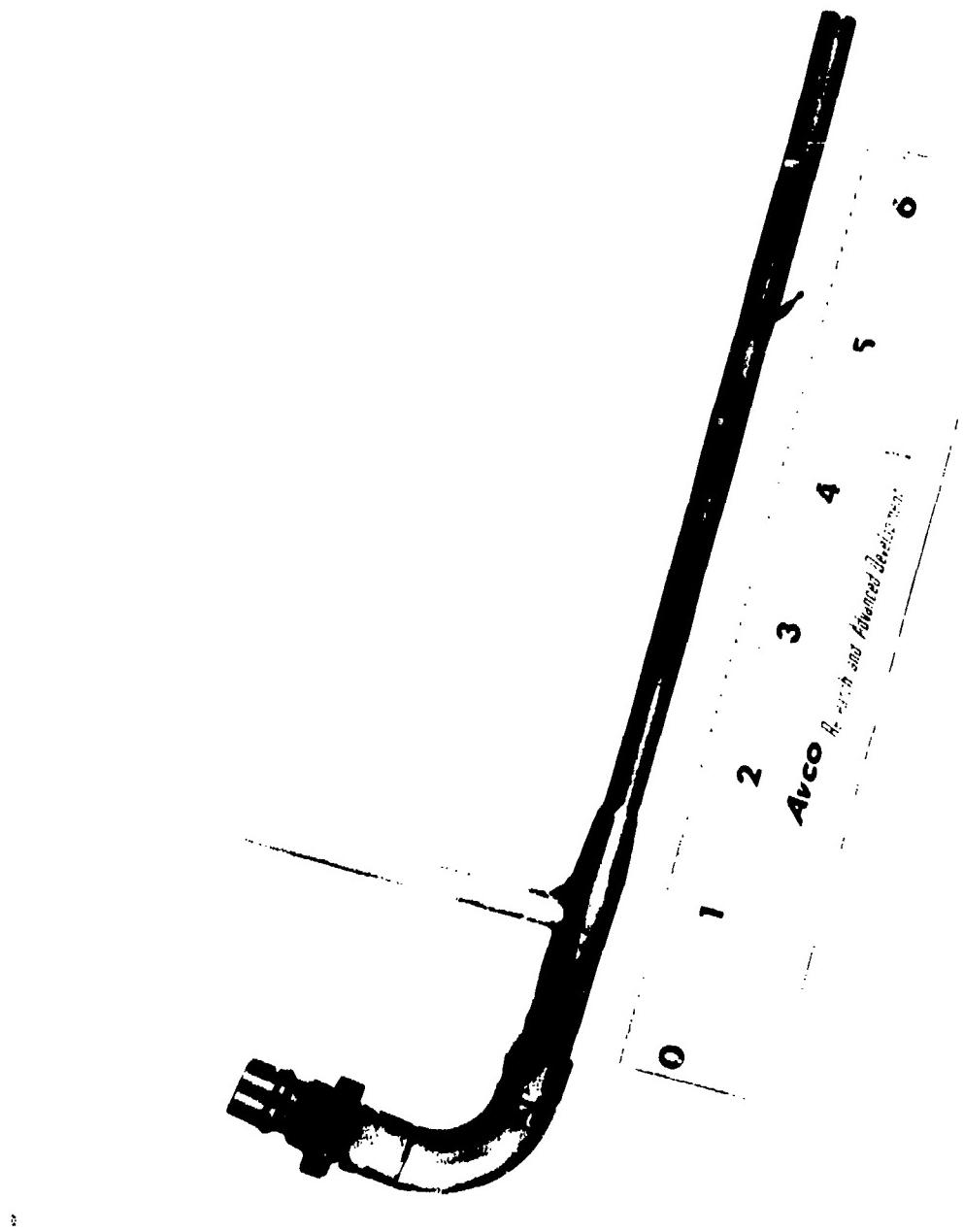
Figure 9.--Prototype Water Cooled Probe
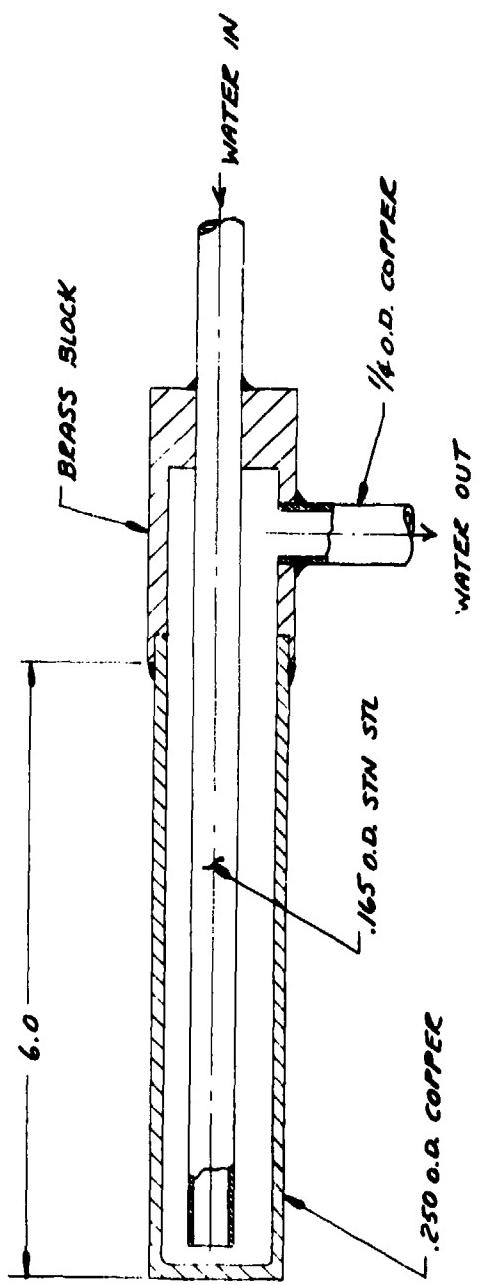
FIGURE 9 SCHEMATIC DIAGRAM OF PROTOTYPE WATER-COOLED PROBE
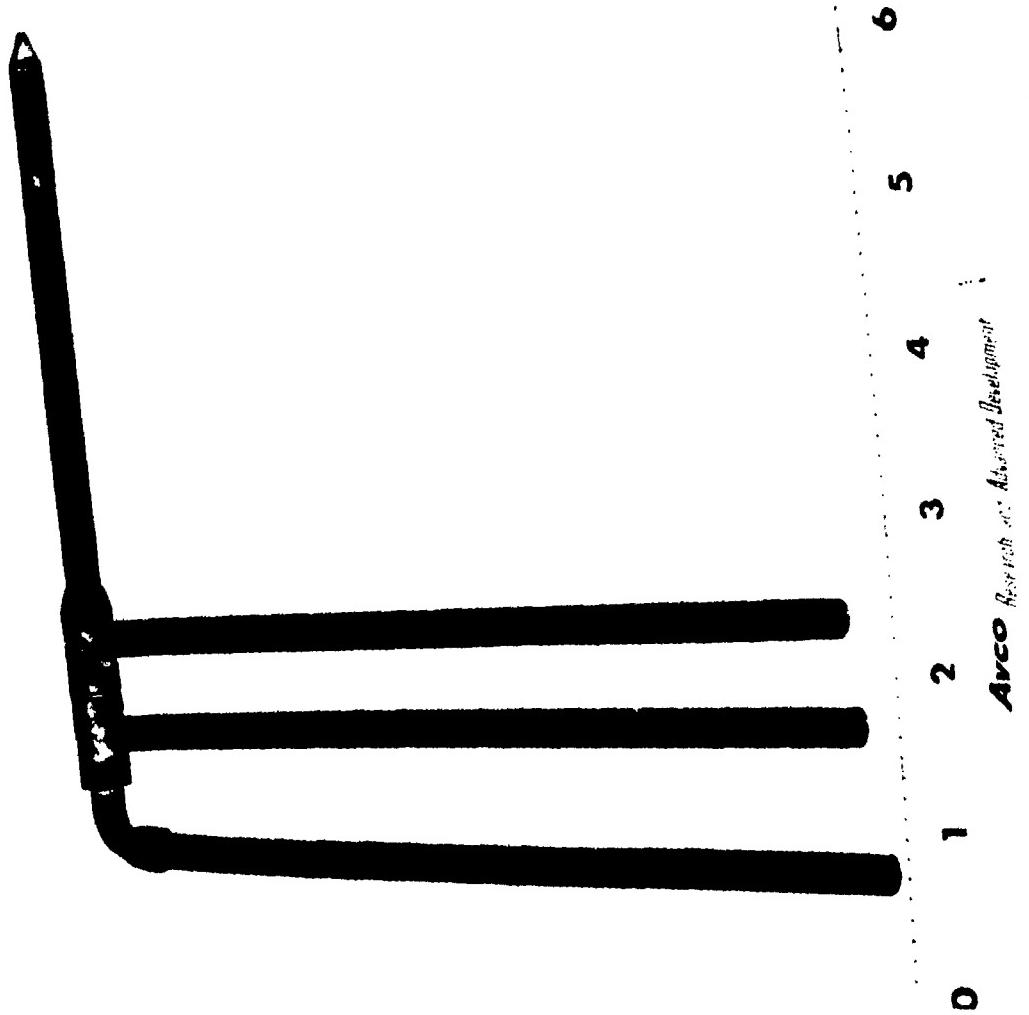
Figure 10--Typical Mass Flux Probe, Supersonic Flow

being sampled occur within the probe. i.e., the probe shock was "swallowed".

A typical mass flux profile obtained in the arcjet engine exhaust by using water cooled and carbon mass flux probes in a plane 0.0625 inch from the nozzle exit is presented in Figure 11. The nature of the mass flux profile was in agreement with prediction and the total integrated mass flux was within 17% of the flow to the engine.

Future experiments to be conducted with the supersonic mass flux probes are to investigate the effects of probe nose angle and sampling tube diameter on the ability to swallow the probe bow shock.

3.) Pressure Probes

Flat nosed impact pressure probes were fabricated and tested in the 10 Megawatt facility exit jet. In general the pressure probe was of the same shape as the prototype water-cooled probe (Figures 8 & 9). The pressure probe operated satisfactorily at heat flux levels up to 18×10^6 Btu/ft^2 hr.

In addition a water cooled probe (Figure 12) designed to measure static pressure within a high enthalpy, high velocity, gas stream has been developed. In brief, the probe has four pressure ports on the side of the instrument to measure static pressure within a plane perpendicular to the direction of gas flow. The openings are equally spaced around the surface of the probe. Pressure lines leading from each pressure port open into a common plenum within the probe body, hence the static pressure measured with this device will be an average value.

4) Enthalpy Probes

The measurement of gas properties at atmospheric pressures and very high temperatures has long been a difficult problem. Recently, water cooled probes capable of steady state operation in such environments have been developed (5) These probes have the capability of determining total pressure, composition and, in some cases, mass flux as well as enthalpy. A diagram of such a probe is given in Figure 13 Such probes are based on the principle that the rate of heat loss by the gas flowing through the probe is equal to the rate of heat input to the cooling water. Errors due to heat i t from gas which does not flow through the probe are effectively eliminated by performing a "tare" measurement, that is, by recording the coolant temperature rise when no gas flows through the probe and subtracting it from the temperature rise of the coolant when the sample is allowed to pass.

Two types of enthalpy probe have received primary consideration for use in this program. The first is termed the "single-jacketed" enthalpy probe. A probe of this type was developed by J Grey at Princeton and is described in detail in Reference 5 One of these probes was purchased from the Greyrad Corp In addition a probe of this type was constructed at Avco in order to allow the use of lower water pressure than are required for operation of the Greyrad probe.

-17-
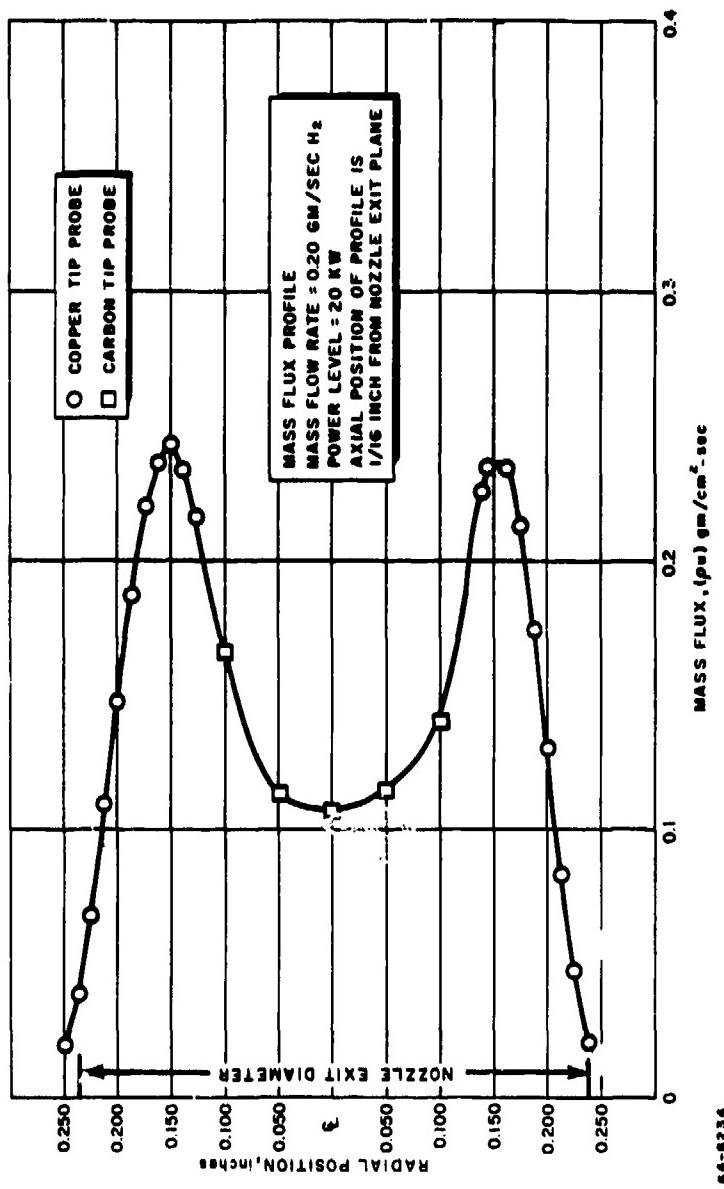
Figure 11--Mass Flux Profile, Avco Plasma Ergine

64-8234
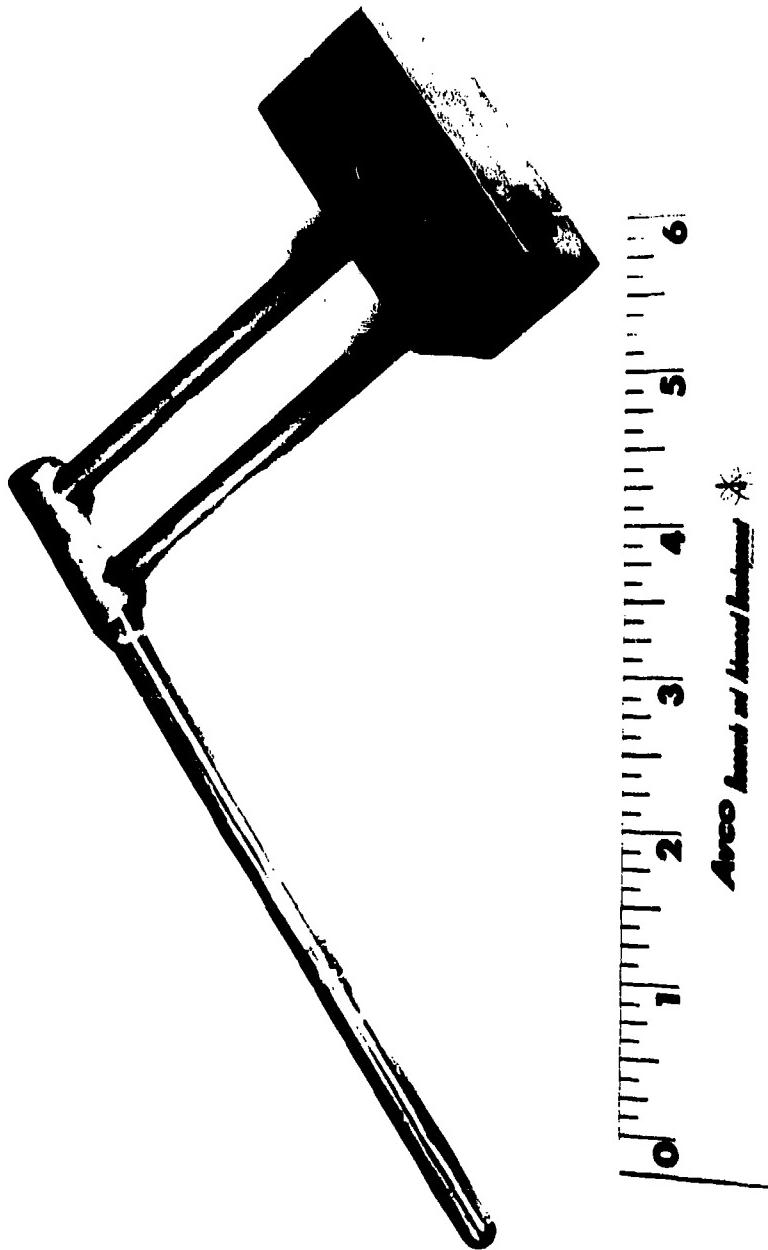
Figure 12--Static Pressure Probe

SHUT-OFF VALVE

GAS SAMPLE EXHAUST

THERMOCOUPLE: COOLED GAS SAMPLE

BAFFLE(NC INSULATION OR HEAT-TRANSFER CAGE REQUIRED)

COOLANT IN

COOLANT OUT

THERMOCOUPLES: COOLANT TEMPERATURE RISE

HOT GAS

64-7108
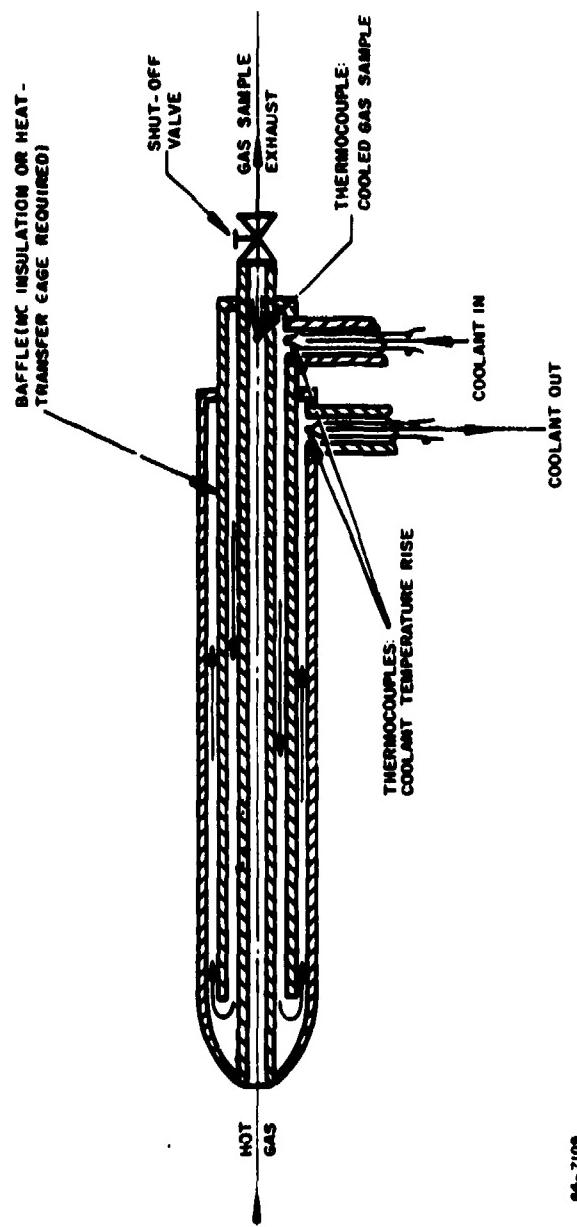
Figure 13--Schematic of Single Jacketed Enthalpy Probe

The Avco single jacketed enthalpy, Figure 14, 0.187 inch o.d., was tested in the exhaust of the 30 kilowatt arcjet engine. The probe was initially tested six inches downstream from the engine orifice and then moved gradually to three inches. The impact pressure at the probe tip was sensed without difficulty, and the coolant temperature rise was also measured with sufficient accuracy once the coolant flow rate was reduced to a low enough value. This initial experiment with the single-jacketed enthalpy probe proved that reasonable values of stagnation enthalpy may be determined with this device.

Nevertheless, in all runs made with this probe, the tare reading, or coolant temperature rise with no flow through the probe, was a minimum of 80% of the coolant temperature rise with the probe opened. Because of the necessity of subtracting large numbers during the enthalpy calculation, it is difficult to visualize the possibility of accurate determinations of the total enthalpy with this device. It is obvious that a small error in measuring the tare will cause a relatively large error in computing the enthalpy. Such small errors in determining the tare may be inherent in the technique since the tare which is measured when there is no gas flow through the tube is not the same "tare" that exists when there is flow. The difference between these two tares, however, may be so small that for practical purposes it may be ignored.

In order to reduce these difficulties as much as possible and to gain the greatest accuracy possible in the enthalpy determination, a double-jacketed probe termed a "split-flow" enthalpy probe was designed and constructed. This probe is shown in Figure 15. This probe is 0.218 inch o.d. and is believed to incorporate a significant improvement over the single-jacketed probe. In this probe the tare values can be reduced to an insignificant portion of the total heat gain by the water and thus greater accuracies may be expected in determining the enthalpy of the gas. A schematic drawing of this Avco probe is shown in Figure 16.

The probe consists of four concentric tubes. The innermost tube is open to permit gas flow through it. The annulus between the second and third tubes is used to admit the water coolant. At the tip of the probe the water flow is split, hence the designation "split-flow". The outer water is used to cool the outer probe surface while the inner water is utilized to cool the gas which is tested. With this design the tare is proportional only to the temperature rise of the test-gas water coolant when there is no gas flow through the center of the probe. Since the outer water flow rate can be adjusted so that its temperature rise is equal to that of the inner water, there should be no heat transferred between the outer water colant and the test-gas coolant.

For mass-flow measurements, the tip of the probe can be made knife-edged to "swallow" the bow shock when the flow is supersonic. It is expected that the same probe can be used to determine impact pressures, mass flow rates and enthalpies.

Before an enthalpy probe is used, it should be calibrated. When an arc facility is employed, the arc itself may be utlized as the standard calorimeter. In a instrumented arc generator the total energy to the plasma may be determined by subtracting the losses from the total

-21-
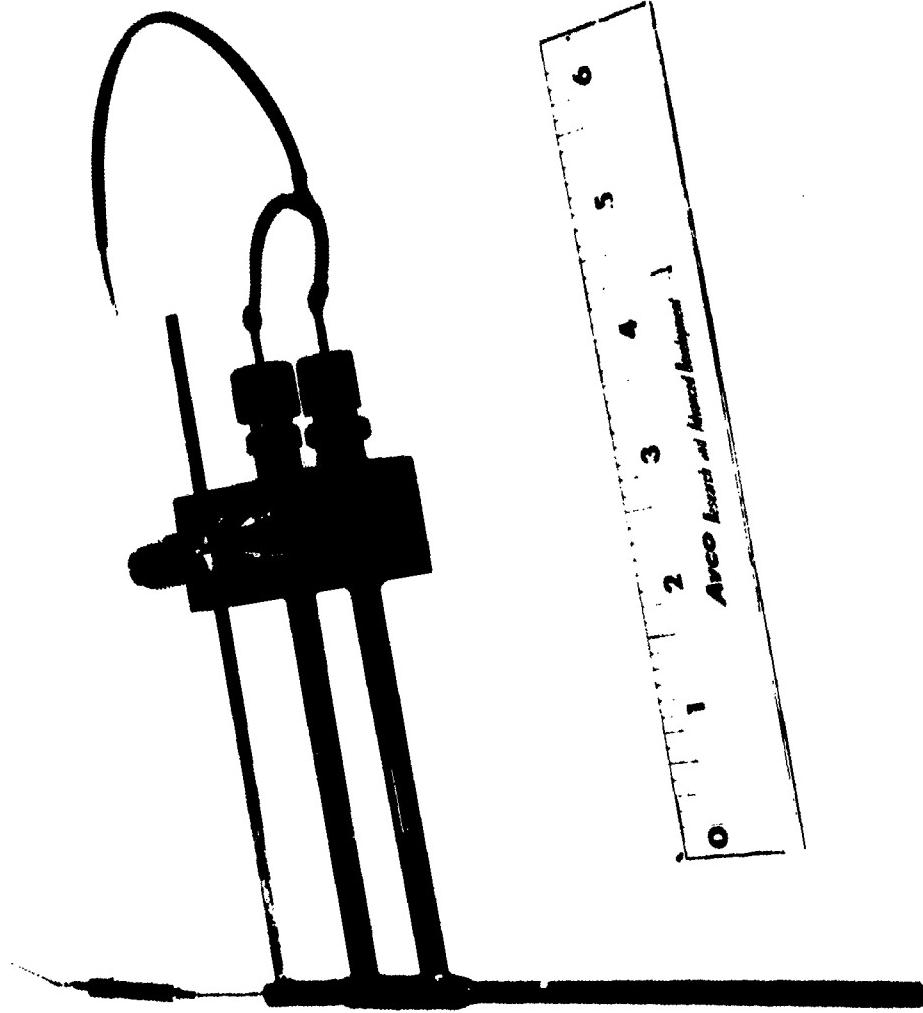
Figure 14--Single Jacketed Enthalpy Probe
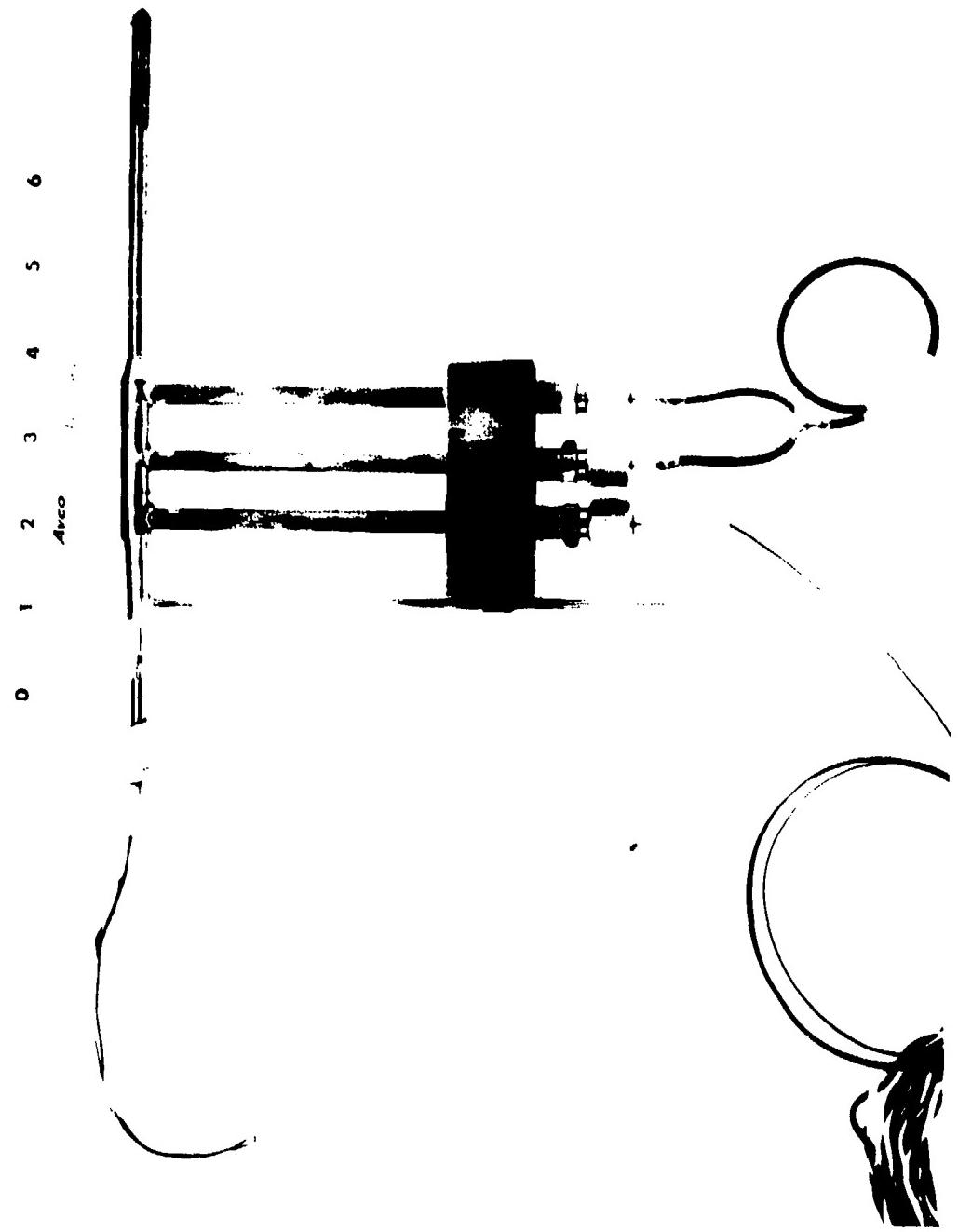
Figure 16.--Split Flow Enthalpy Probe

-23-
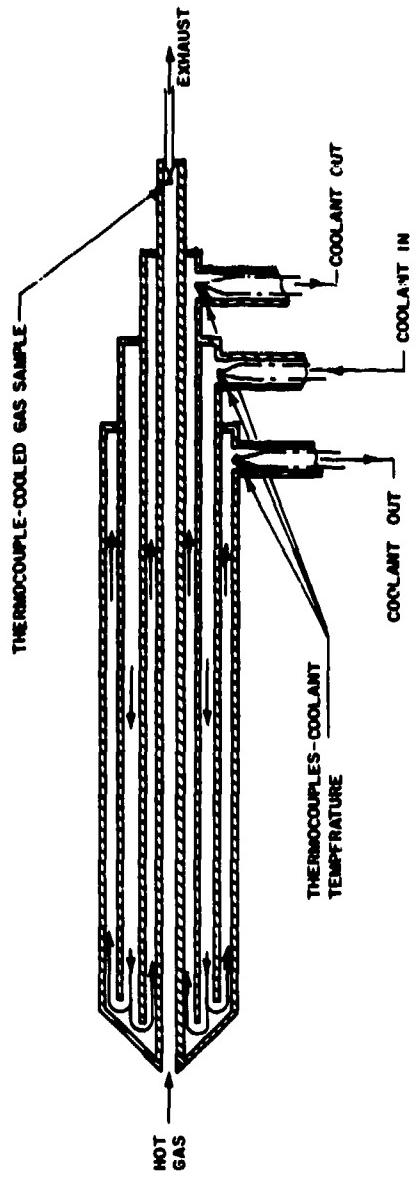
Figure 16--Schematic of Split Flow Enthalpy Probe

84-782

-24-

electrical input. This value is then compared to the integrated value of the individual points indicated by the probe when the plasma jet is traversed radially. The difference between the integrated value and the computed input to the plasma is assumed to be the probe error. The mathematical relationshi for determining the percent error is as follows:

$$\text{Error} = \frac{\left[\left(\int_0^r 2\pi r \rho u h \, dr\right) - \left(EI - \dot{W}_c C_p \Delta T_c\right)\right] 100}{EI - \dot{W}_c C_p \Delta T_c} \quad (1)$$

The relative merit of the "split-flow" probe as compared to the "tare" instrument was determined by testing the "split-flow" device in the Model 500 ARC facility (6). This facility produces a subsonic exhaust jet at gas enthalpies ranging from 3,000 to 11,000 Btu/lb. with stagnation point heat transfer rates of 2,000-4,000 Btu/ft^2 second to conical bodies having a spherical nose radius of 0.125 inch. The energy balance technique used to determine the exhaust gas enthalpy has been found to be accurate for this facility,(6) hence the Model 500 is believed to be an excellent device for probe calibration.

A "split-flow" probe (0.218 in outside diameter) was placed in the Model 500 exhaust jet. In this particular series of tests, nitrogen was employed as the working fluid. The arc heated gases exhausted to the atmosphere through a nozzle having an exit diameter of ½ inch as a subsonic jet with a Mach number of 0.70. A series of enthalpy measurements were made at axial distances between 9 and 24 nozzle radii (Figures 17 and 18). The probe was not moved closer to the exit nozzle since the measured temperature rise of the probe coolant indicated that boiling was imminent at the smaller axial distance. This heat transfer limitation of the probe was a result of the low water pressure available at the facility (200 psig) and the restriction of the coolant flow by a 0.006 inch outer water passage within the probe. The "split-flow" probe has been redesigned to provide greater coolant flow through the outer water channel. Two probes of this type have been constructed and will be used in conjunction with a high pressure water supply system (200-1,000 psia) for the remainder of this program. These probes are to be calibrated using the Model 500 Arc as a reference.

It is significant that tare values considerably less than the minimum of 80% found with the single-jacketed probe were recorded during these tests. A facsimile of a typical recorder trace obtained during operation of the split-flow probe in the arc facility is shown in Figure 19. Tare measurements were reduced to values between 30 and 60% of the final gas coolant temperature rise. This was so even though no effort was made at that time to minimize the tare by adjustment of the inner and outer flow rates. Since this feature is expected to provide a greater increase in the accuracy of the enthalpy determinations at the expense of very little added probe complexity, the Avco "split-flow" enthalpy probe has been chosen as the primary experimental tool to be employed in this program.

Although the positioning of the probe within the arc exhaust jet was not to the accuracy required for the measurements to be made in this program, jet mixing parameters were determined using the method

-25-

FIG. 17

BRIDGE ROD MOMENTUM AT
ABS CATAPULT - VELOCITY

CL = 13600 LBS

WARREN, K = .078 (1)

FIG. 18
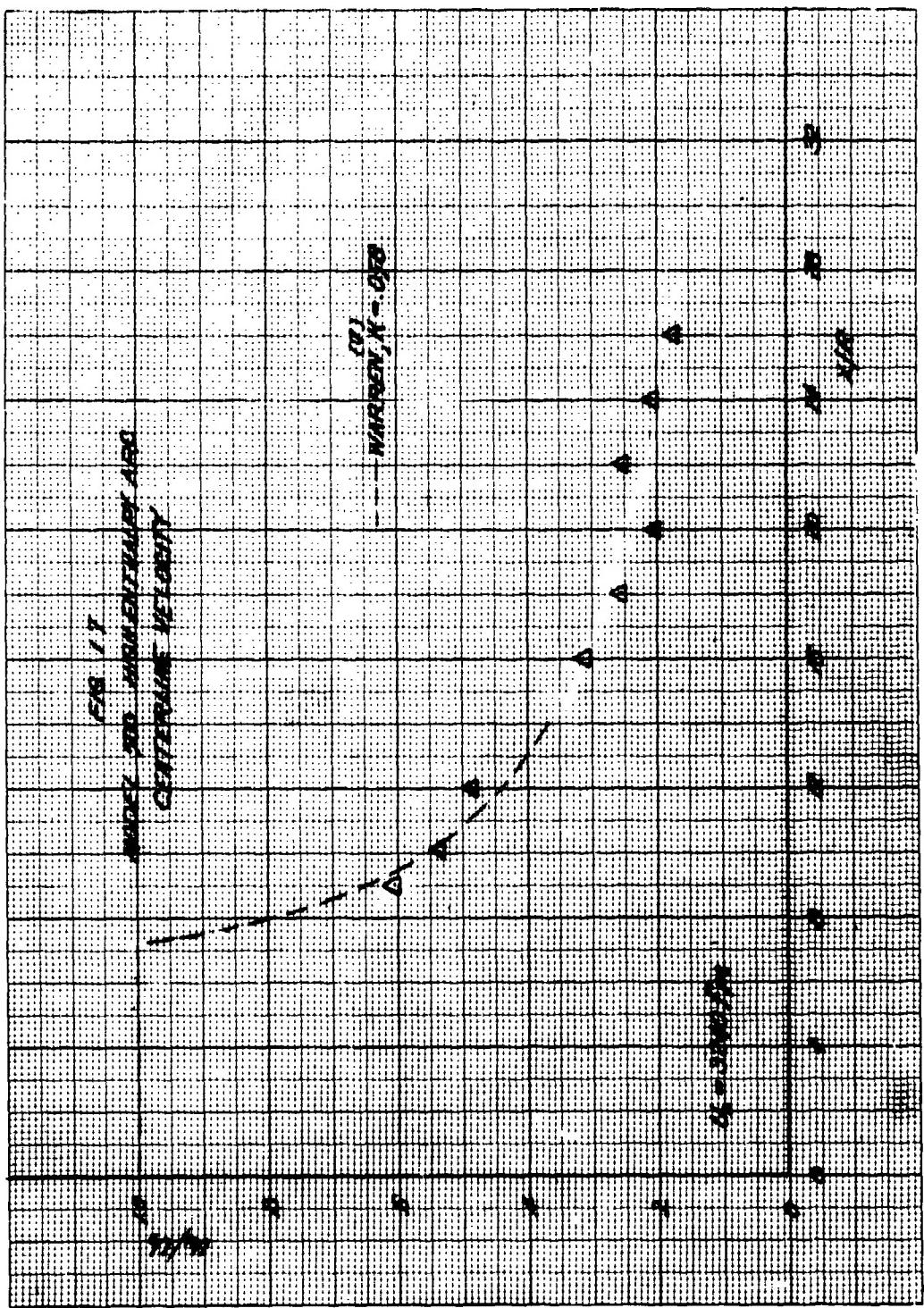
MODEL 500 HIGH ENTHALPY ARC
CENTERLINE TEMPERATURE

--- WARREN; $K_3 = .062$

$T_0 = 5450 °K$

$\dfrac{T_0 - T}{T_0 - T_A}$

GAS TEMPERATURE
CONSTANT VOLUME TANK

TEMPERATURE RISE
INNER CHANNEL COOLANT

ARC OFF

PROBE OPENED

ΔT_G FLOW

ARC ON

ΔT_G
NO FLOW

GAS TEMPERATURE
PROBE EXIT THERMOCOUPLE

COOLING WATER TEMPERATURE
OUTER CHANNEL

TIME
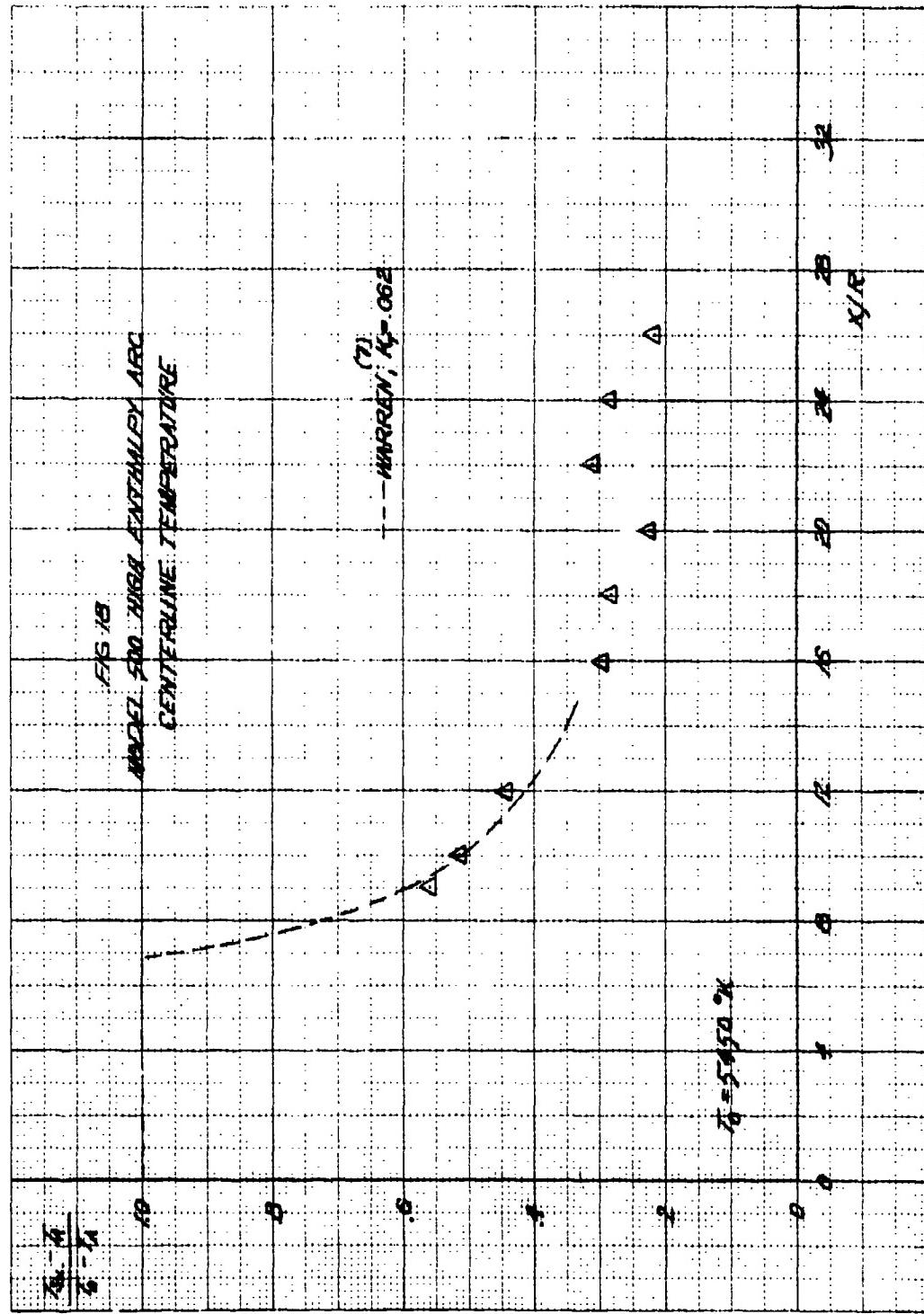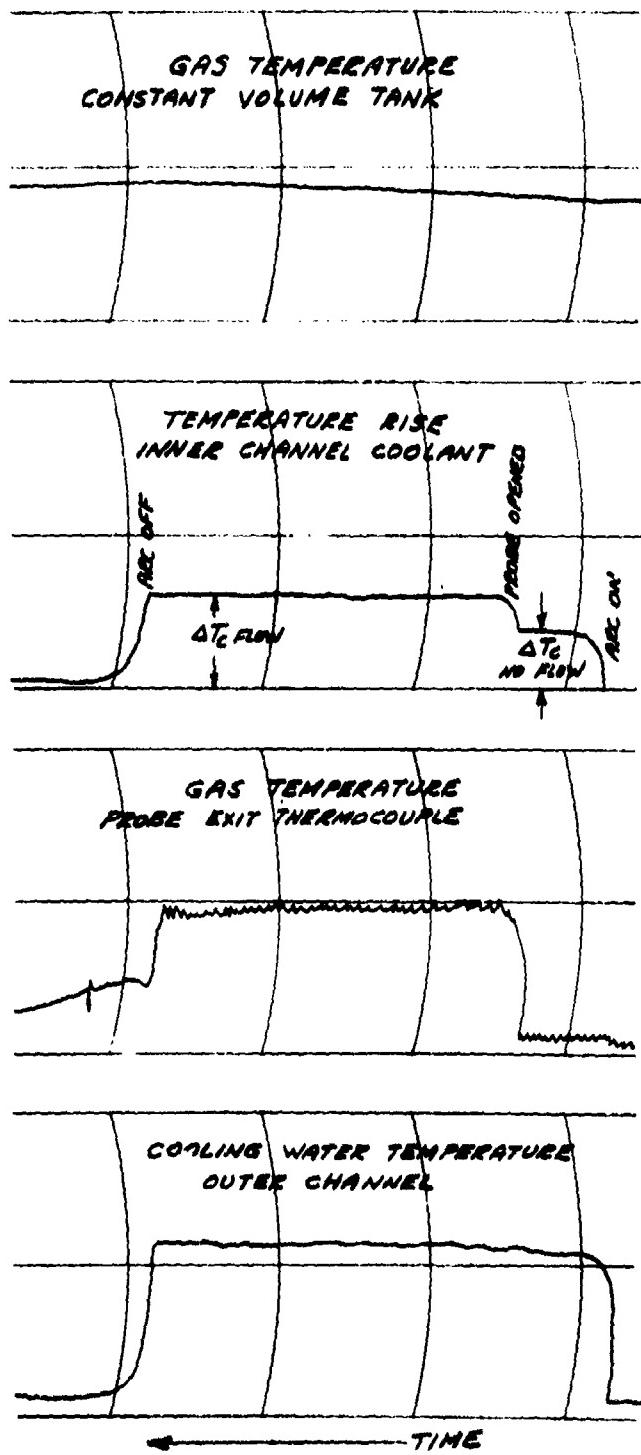
FIGURE 19   TYPICAL RECORDER TRACES - MODEL 500 A.E.C.

-28-

by Warren(7). The analytical curves (Figures 17 and 18) were found by extrapolating and interpolating between Warren's results for the appropriate temperature ratio and Mach number. Values of the mixing parameters K and K_T were determined to provide the best fit to the Model 500 data. Calculated mixing parameters found were a factor of two larger than predicted with Warren's correlation. It should be noted that since the accuracy of the positioning device used in these tests is an unknown factor, and that it was not possible to use the enthalpy probe close to the jet exit plane the results obtained in the Model 500 experiments should be viewed with caution.

4.) Calorimetric Probes

The calorimetric probes are used to determine the heat flux from a hot-jet which comes in contact with the calorimeter surface. From equationd derived from theoretical heat transfer analysis(8) it is also possible to compute the enthalpy of the gas when the pressure and heat flux are known. It is to be noted that whenever these calorimetric probes are used in a reacting gas, the catalytic activity of the wall surface must be considered (reference 9). Some experimenters believe that the the discrepancies in certain reported data are due to the differences in the catalytic activity of the surfaces of the calorimetric devices used in the various experiments.

It is convenient to divide these calorimeters into two main groups: (a) Steady state calorimeters and (b) transient state calorimeters.

(a) Steady State Calorimeters

The steady state calorimeters are usually made of copper and are water cooled. They are generally designed so that only the surface normal to the jet is exposed to the gas. To insure this condition, a water cooled copper guard is used. As shown in Figure 20, the calorimeter and guard are in the form of two concentric tubes closed at the ends.

The heat flux is determined from measurements of the water flow rate, temperature difference between water in and water out of the calorimeter, and the area of the calorimeter surface exposed to the hot gas. (This method is sometimes called the "cold wall method" because f the relatively cool contact surface). The temperature of the water in the guard is measured and the flow rate is adjusted to minimize the temperature difference between the adjacent wall of the calorimeter and the guard ring.

Calorimeters of this type have been used at this laboratory for several years with relatively good results. However, it is believed that they must be re-designed to reduce heat loss errors and also miniaturized so that local values may be determined. The re-design of this calorimeter is in progress at the present time.

Another type of steady state calorimeter is now being developed. In this calorimeter, as shown in Figure 20, a resistor to heat transfer, in this case constantan, is sandwiched between two copper plates. One of the copper plates is water cooled while the other plate is in contact with the hot gas. The copper plates and the constantan are

-29-
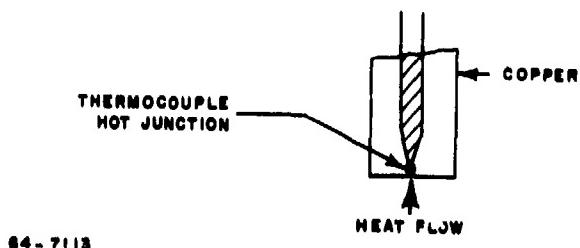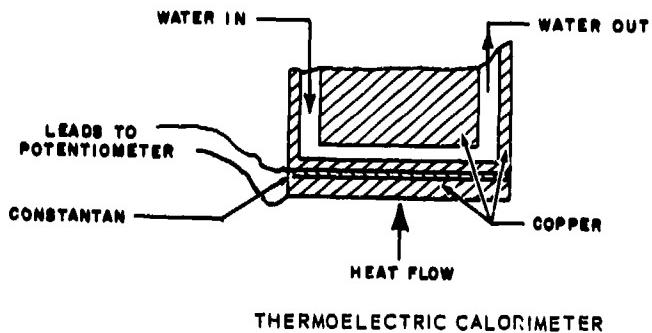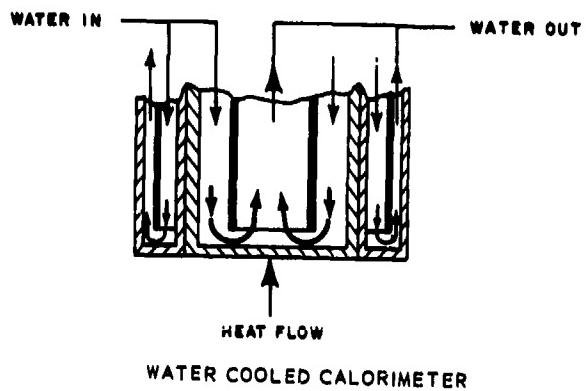
Figure 20--Calorimetric Probes

in effect a copper-constantan thermocouple with the "hot" junction on the gas side and the "cold" junction of the water side of the constantan. By connecting the two copper plates, through copper leads, to a potentiometer the emf developed due to the temperature difference at the junctions is measured. Since the emf is approximately proportional to the heat flux, the calorimeter can be calibrated to indicate the heat flux supplied to it.

(b) Transient Calorimeters

Transient calorimeters have been used successfully, at this laboratory for quite some time (Reference 10). The heat flux is measured by determining the rate of temperature rise of the surface of the solid exposed to the hot gas. In general, the calorimeter consists of a copper cylinder of known mass and dimensions. One end surface of the cylinder is exposed to the hot gas while the other surfaces are insulated. It is assumed that the heat flow is unidirectional and that all unexposed surfaces are adiabatic. The disadvantage of this calorimeter is that it can be used only for a brief period of time (up to several seconds) before corrections must be made, in some cases, for heat losses at the calorimeter rear face. Its important advantage is that it can be readily used, because of its simple design, on various shapes to measure local heat transfer rates.

Based on the above described calorimeters, the determination of heat fluxes can be readily made and cross-checked using the steady state and transient state calorimetric techniques.

Probes to be employed specifically on this program include the following:

a.) Split Flow Enthalpy Probes to determine the axial and radial variations in jet properties, i.e., enthalpy, velocity, composition, and density.

b.) Static Pressure Probes to measure the jet static pressure which will be used in conjunction with the impact pressure measurements to determine local jet velocity.

c.) Calorimetric probes (transient device) to measure the heat flux distribution obtained from high enthalpy gas jet impinging upon a plate. In addition, the heat flux as determined by steady water cooled probes on the jet axis of symmetry can be employed with standard heat flux correlations(8) to determine gas enthalpy. The latter measurements would be used to provide a check on enthalpy determinations made with the split flow enthalpy probes.

C. Probe Support Equipment

In order to use the probes described previously to their full advantage various pieces of support equipment such as a probe positioning mechanism, a high pressure water collant system, and a gas collecting system have been constructed. A brief description of these items is given below.

-31-

A.) Probe Positioning Mechanism

In order to obtain reliable and reproducible probe measurements it is important to have a means of positioning the probe in some known location relative to certain convenient references such as the arc nozzle exit plane and nozzle axis. To accomplish this end a probe positioning table has been constructed;a photograph of the table is shown in figure 2. With this table the various probes can be moved in all three directions in a precise and controlled manner.

The bottom most plate consists of a hardwood table upon which all the structure above is either directly or indirectly fastened. This bottom plate can be moved vertically by means of four jack screws whose motion can be accomplished by means of a single drive shaft. This drive shaft can either be moved manually or turned by a motor. The motor employed is of the gear reduction type given a drive-shaft speed of 5.7 rpm. The gearing of the jack screws is such that eight turns of the motor shaft moves the table one inch. The vertical position of the bottom table can be varied over a range of some eleven inches.

At present it is envisioned that the vertical degree of freedom will be used to position the various probes at the correct height relative to the nozzle axis. The radial profiles are to be taken in the horizontal direction. If it proves to be desireable to make radial profiles using the vertical degree of freedom, a microswitch has been positioned relative to the drive-shaft which serves the function of automatically stopping the motor after a half-turn of the drive shaft or after any multiple thereof. A half-turn of the drive shaft changes the vertical position of the probe 0.0625 inches. Dynamic breaking is employed so that there is no coasting after the power to the motor is interrupted.

The next plate up is made of aluminum, ½ inch thick and is constrained to move in the axial direction, i.e., along the axial direction of the jet. This plate rides on four matching precision roller bearings along two ground case-hardened steel shafts having a nominal diameter of 1 inch. The tolerance between the shaft and the bearing is 0.001 inches. This plate is driven by a 25 rpm gear-reduction motor through a lead screw having a ~h of 10 threads per inch. The axial motion of the plate can be ·d over a range of 32 inches so that without moving the table, an profile can be obtained which starts from the nozzle exit plane and .ds some 43 nozzle diameters (0.75 inch diameter) downstream. The il lead screw is fitted with a microswitch so that the axial motion cι be made in units of 0.05 inches.

The next plate, also made of aluminum, is 3/8 inch thich and is constrained to move in the horizontal direction. The sliding apparatus is similar to that for the table below and differs .y in that shafts have nomir. l diame r of 3/4 inch. This plate moves relative to the plate below by means of a hydraulic piston which has an 8 inch stroke. The purpose of this piston is to have the capability of positioning the probe and the jet impignment plates (described below) in and out of the exhaust jet much more rapidly than can be obtained with the lead screws which are primarily used for controlled positioning. A displacement transducer is mounted in such a way as to monitor the piston travel to ensure that identically the same piston stroke occurs.   -32-

Figure 21--Probe Positioning Mechanism

-33-

The top plate upon which the various probes are to be fastened is made of aluminum, 3/8 inch thick, and is also constrained to move in the horizontal direction. The sliding arrangement for this plate is identical as for the plate below. This plate is driven with a 14 rpm motor and a lead screw having a pitch of 20 threads per inch. This lead screw is also fitted with a microswitch so that the horizontal motion can be made in units of 0.025 inches. The total travel is 10.5 inches.

A control panel has been built whichallows the probe positioning table to be operated from the control room of the arc facility. Through the use of counters on the control panel the position of the probe within the jet can be established from the control room. A subsidiary control panel is mounted on the end of the probe positioning table to facilitate probe alignment and other preparatory procedures.

B.) High Pressure Water Supply

A high pressure gas-driven water supply has been fabricated; a schematic is shown in figure 22. Basically it consists of a pressure tank, a heat exchanger, a collecting tank and a flow meter. The system as designed will provide chemically clean water, free of particles larger than 5 microns, at operating pressures up to 1000 psi. The pressure tank holds approximately 40 gallons which should provide a running time of an hour.

C.) Mobile Instrumentation Platform

A compact mobile instrumentation platform has been designed and built. All auxilliary equipment, with the exception of the probe positioning and coolant systems, required for operating of the probes to be used in the course of this program is provided for on the platform. It thus provided the capability of moving and setting up a probe experiment in the shortest possible time. The instrumentation platform is shown in Figure 23. Located on the lower shelf can be seen the constant volume tank, the vacuum pump, and array of six solenoid valves (two pair of which are arranged in series opposition), and a thermos bottle which provides the reference ice junction for the thermocouple which reads the temperature of the gas in the tank. Located on the top platform are gauges to read probe impact pressure and vacuum tank pressure (to be replaced by transducers), a micrometer needle valve to regulate the mass flow rate of gas through the probe and into the tank, an array of sample bottles, each of which disconnects for analysis of the composition of the gas collected therein, and, on the extreme right, the gas inlet to which the probe is connected. A schematic diagram of the lines and instrumentation located on the mobile platform is shown in Figure 24. Yet to be added to the assembly are a remote switch box for operation of the solenoid valves, a timer connected to solenoid #3, and an inert gas bottle for flushing probe lines and bringing gas sample bottles up to atmospheric pressure prior to disconnect.

In operation, vacuum is first established in the tank and the sample bottle (figure 24) with valves one, two, five and six open. The initial temperature and pressure in the tank are recorded. The
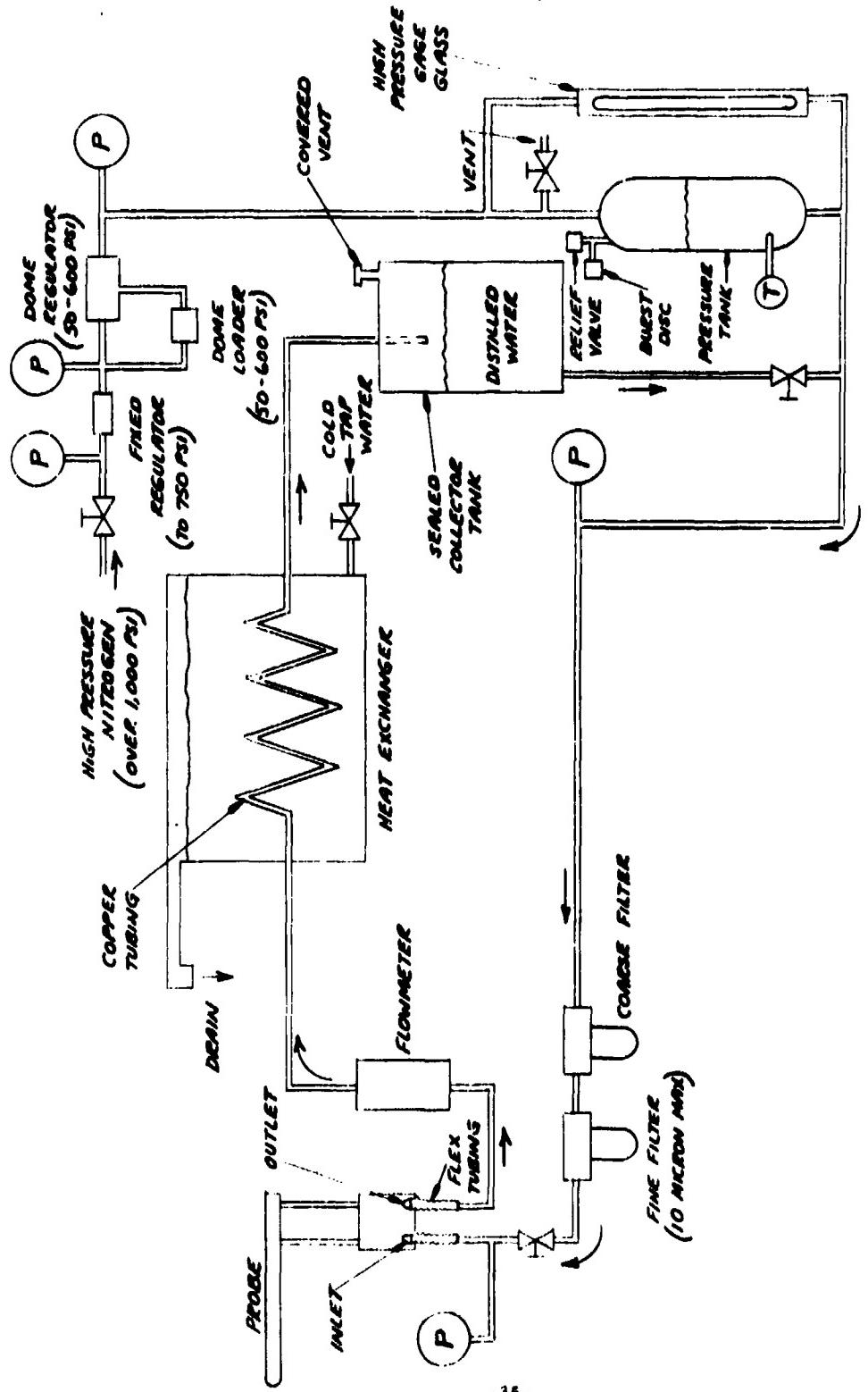
FIGURE 22 GAS - PRESSURIZED COOLANT SYSTEM (FROM REFERENCE 11)

-35-
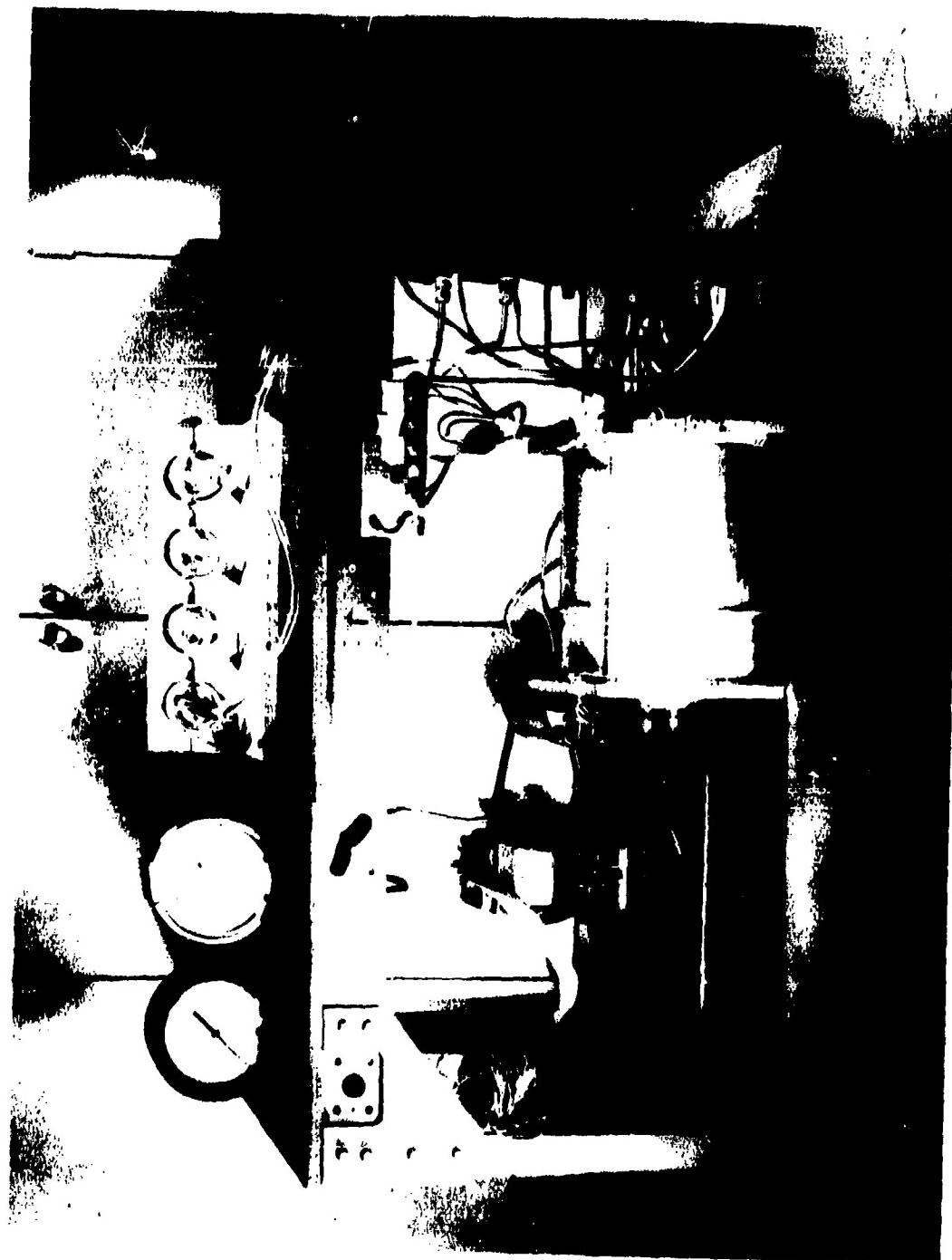
Figure 23--Probe Instrumentation Platform

valves are then shut and the probe is exposed to the jet to be investigated. The impact pressure and the temperature rise of the inner coolant with no gas flow (the "tare") are recorded at this time. Valve three is then opened, allowing a sample to flow through the probe (the needle valve having been preset). During this time, the temperature rise of the inner coolant, the temperature of the gas at the probe exit, and the temperature of the water leaving the outer probe cooling jacket (in order to prevent damage to the probe), are recorded. At the conclusion of the test, valve three is shut and the temperature and pressure of the gas collected in the vacuum tank are noted. Valves one and two are opened, thus filling the sample bottle. Valves three and four are opened to purge the lines with inertgas and to bring the sample bottle to atmospheric pressure, subsequent to which the bottle is disconnected and its contents analyzed for the ratio of O to N. This is done using the Abcor Model WB-7 Radio Frequency Mass Spectrometer shown in Figure 25.

The enthalpy of the gas being probed is found from the following formula:

$$h_{lg} = h_{2g} + \frac{\dot{W}_c}{\dot{W}_g} C_{p_c} \left(\Delta T_{c, flow} - \Delta T_{c, no\ flow} \right) \tag{2}$$

The known gas composition along with initial and final values of temperature and pressure in the tank and the time of the run allow a simple calculation of $\dot{W}g$ using the perfect gas law. The measured gas exit temperature, gas composition, and the known equation of state for nitrogen-air mixtures provides a value of h_{2g}. The other quantities are directly measured and h_{lg} is easily determined.

An Avco computer program for the thermochemical properties of nitrogen-air mixtures has been utilized for the preparation of Figures 26 through 30. These charts given dimensionless enthalpy vs entropy, temperature, density, specific heat ratios, and speed of sound. Pressure is one atmosphere in all cases. The atom ratio of oxygen to nitrogen is a parameter on all curves. Thus the known values of enthalpy and composition, along with the assumption that the gas in the jet is in equilibrium, provide values of temperature, density, speed of sound, and specific heat ratio. The measured values of stagnation pressure and the value of γ read from the charts, give the Mach No. from the isentropic flow relationship.

$$\frac{P_2}{P} = \left(1 + \frac{\gamma - 1}{2} M^2 \right)^{\gamma/\gamma - 1} \tag{3}$$

Finally, the Mach No. and the speed of sound give the local velocity. The assumption that the static pressure in the jet is everywhere equal to one atmosphere will be checked frequently with the static pressure probe described above.
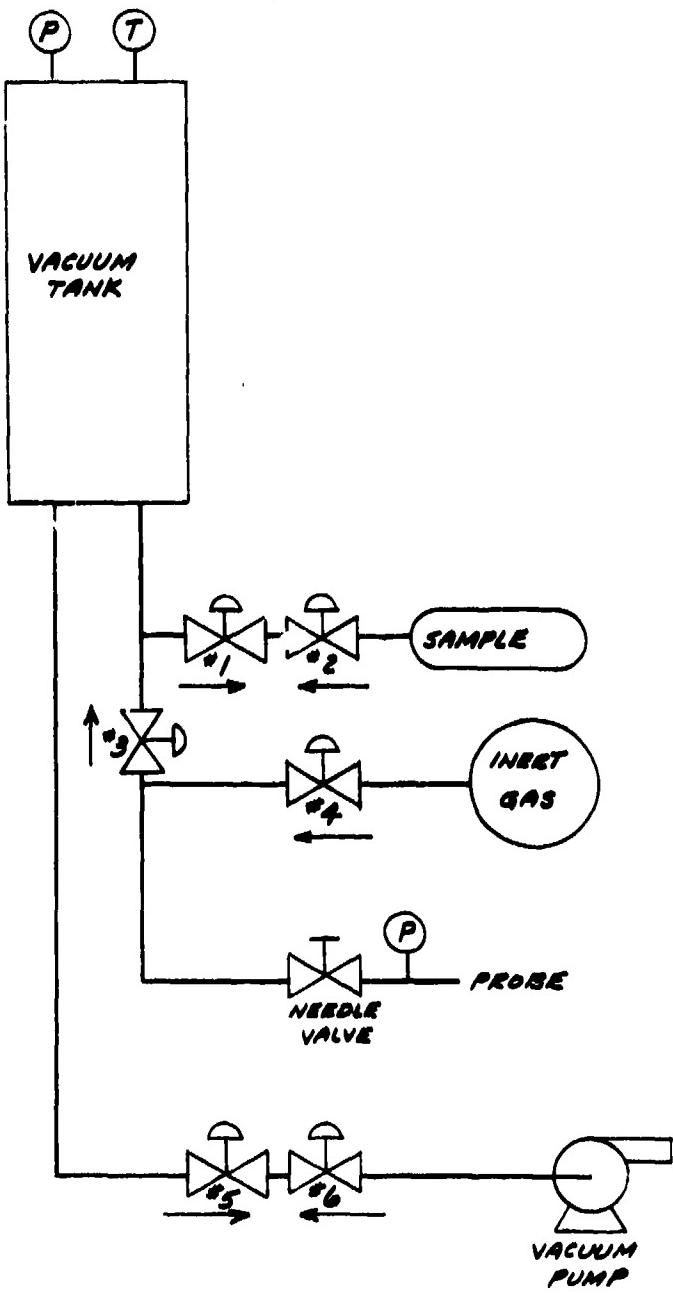
FIGURE 24   SCHEMATIC OF PROBE INSTRUMENTATION

Figure 25--Radio Frequency Mass Spectrometer

USEFUL CONSTANTS FOR NITROGEN

W = 28.016 (MOLECULAR WEIGHT OF UNDISSOCIATED NITROGEN)
P_0 = 1 ATM = 76 cm Hg = 1.013 x 10^6 dynes/cm^2 = 2117 lb/ft^2 = 14.70 lb/in^2
T_0 = 273.16 °K = 491.69 °R
ρ_0 = 1.250 x 10^3 gm/cm^3 = 4.518 x 10^{-5} lb/in^3
= 7.806 x 10^{-2} lb/ft^3 = 2.425 x 10^{-3} slugs/ft^3
R = 1.987 cal/mole °K = 7.093 x 10^{-2} cal/gm °K = 7093 Btu/lb°R
= 2.969 x 10^6 cm^2/sec^2 °K = 1.776 x 10^3 ft^2/sec^2 °R
RT_0 = 542.8 cal/mole = 19.38 cal/gm = 34.88 Btu/lb
= 8.111 x 10^8 cm^2/sec^2 = 87.30 x 10^4 ft^2/sec^2

ENTHALPY, H/RT_0

ENTROPY, S/R

64-7024

Figure 26--Nitrogen-Air Mixtures: Enthalpy vs Entropy

-40-
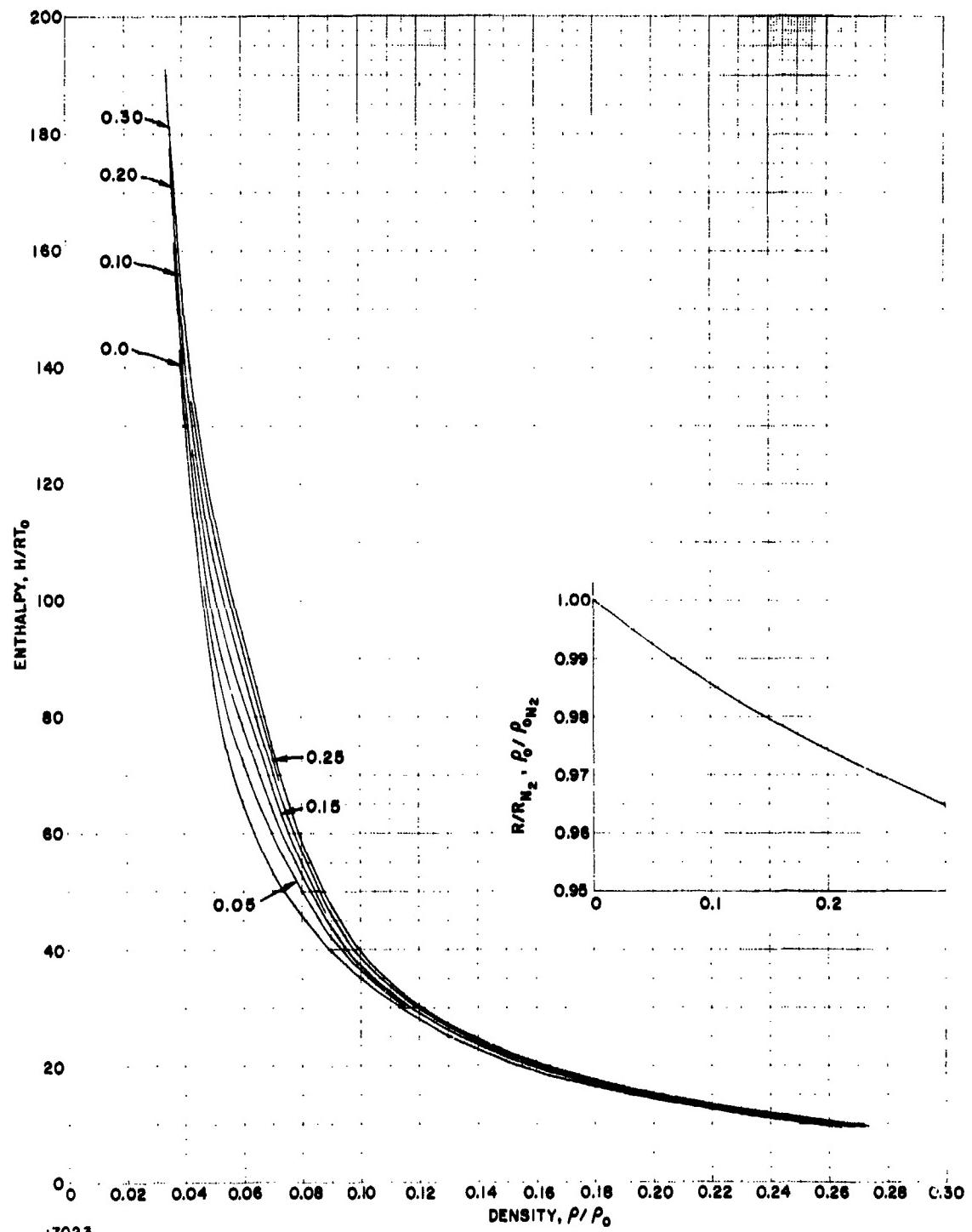
Figure 27--Nitrogen-Air Mixtures: Enthalpy vs Density

-41-
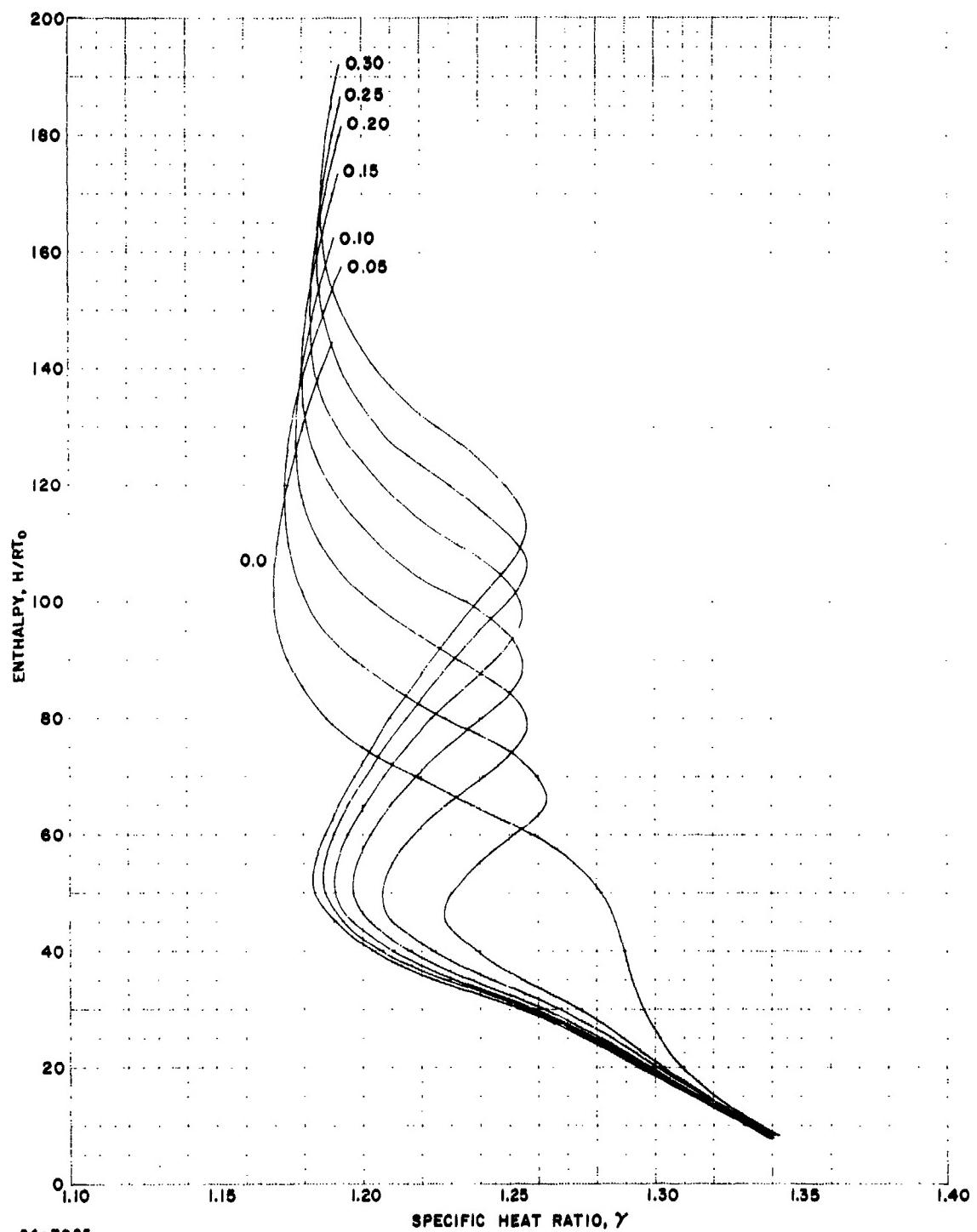
64·7025

Figure 28--Nitrogen-Air Mixtures: Enthalpy vs Specific Heat Ratio
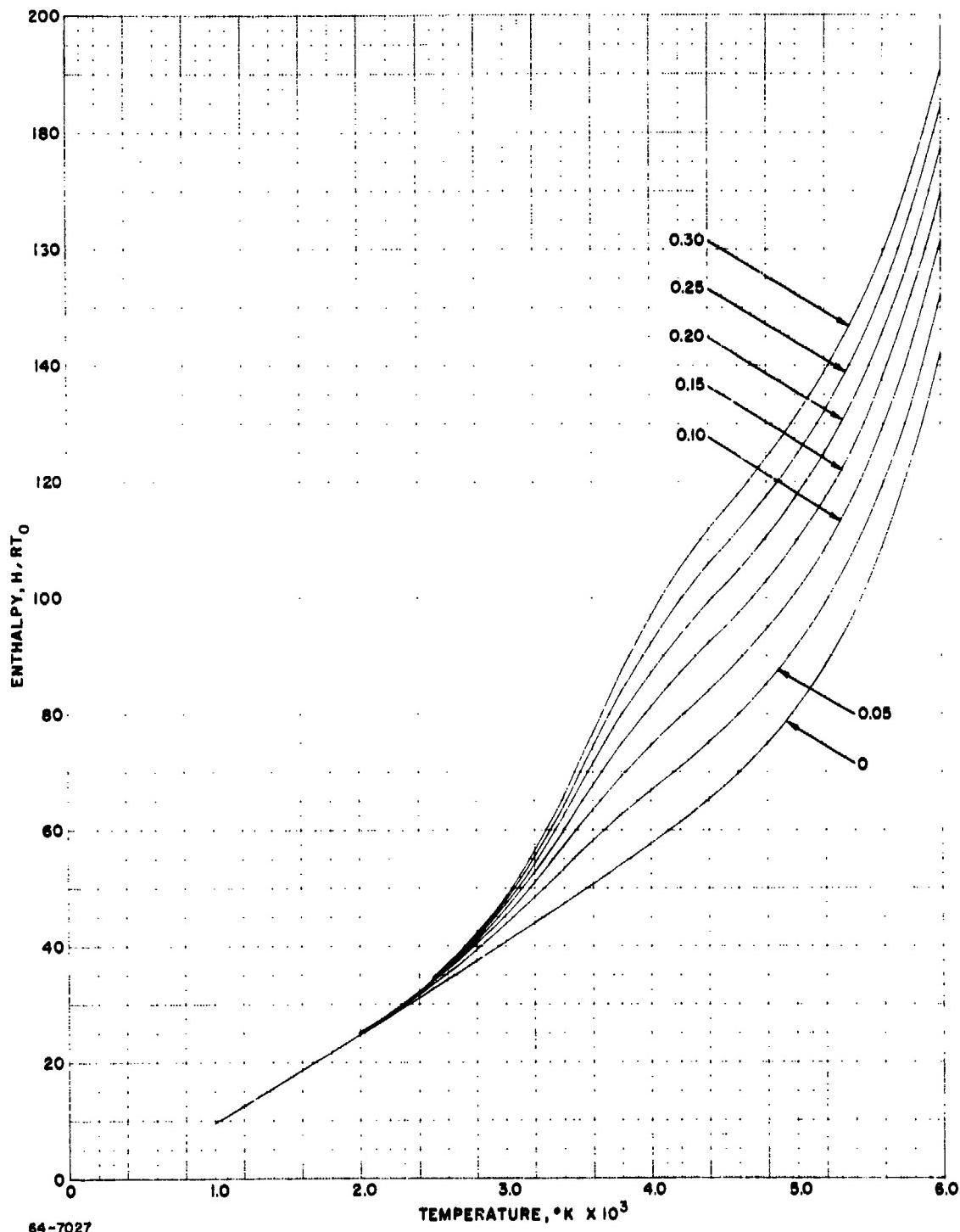
Figure 29--Nitrogen-Air Mixtures: Enthalpy vs Temperature

64-7027

-43-
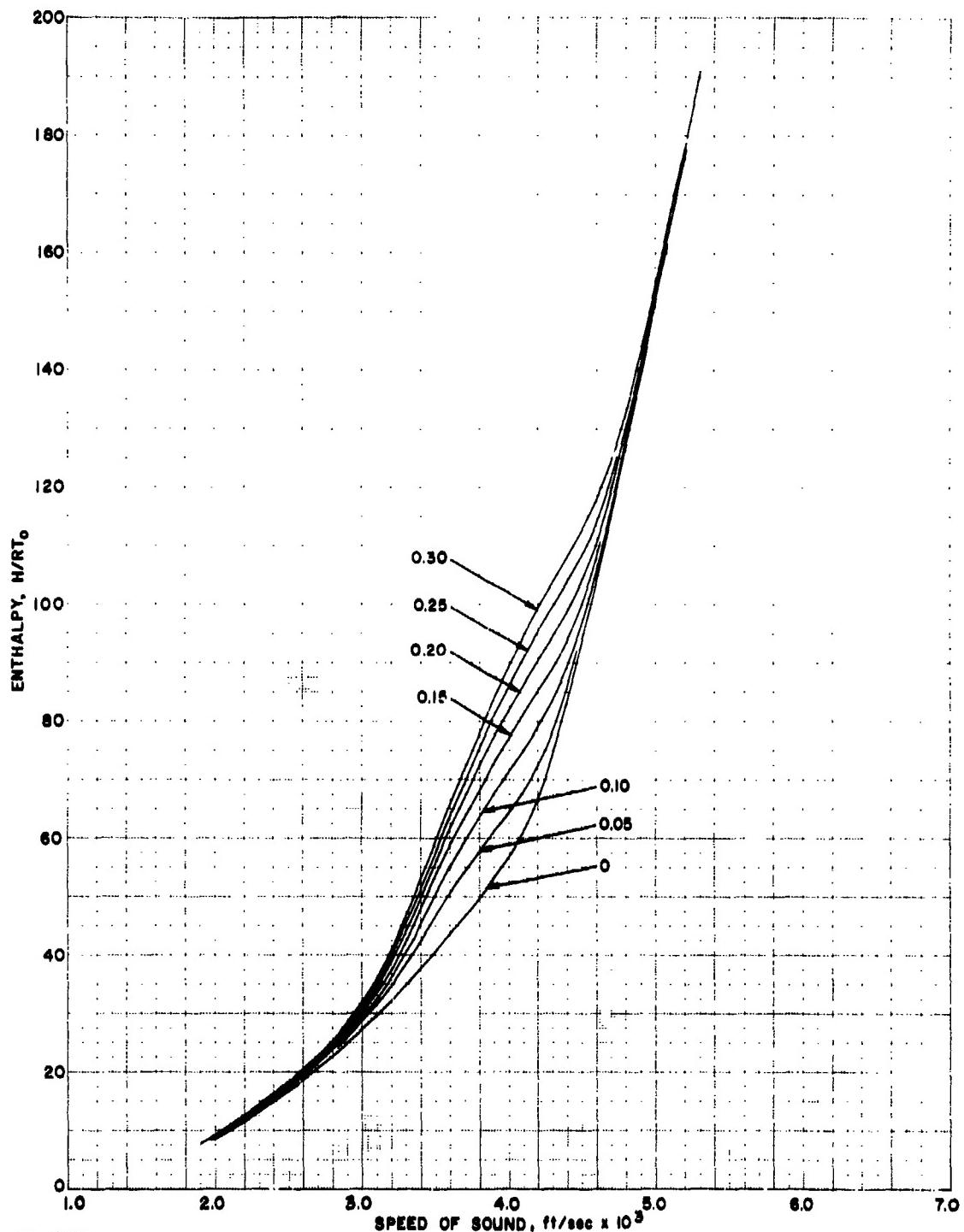
Figure 30--Nitrogen-Air Mixtures: Enthalpy vs Speed of Sound

D. Pressure and Heat Flux Distribution Plates

Flat copper plates, nine inches in diameter, have been constructed. One is designed to determine the heat flux distribution produced by the impinging jet; the other, the pressure distribution. The pressure distribution plate is water-cooled utilizing a number of concentric cooling passages. The heat flux plate is uncooled, and is instrumented with a number of transient calorimeters. The pressure distribution plate has undergone preliminary testing in the Avco Hydrogen-Oxygen Rocket Motor Facility in order to determine its ability to withstand the high heating environment. Pressure taps are now being added to the plate. A total of eleven taps are being provided, one in the center, seven on one radius, and three others to insure that the jet and plate axes of symmetry are coincedent.

The plate designed to determine heat flux distribution has also been completed. Eleven 3/16" transient copper calorimeters are located in such a manner that none disturbs the radial flow passing over another. Each calorimeter consists of 3/16 inch diameter and 1½ inch long copper cylinder into which a thermocouple has been brazed in place. The thermocouple consists of 10 mil chromel-alumel wire contained in a 2-hole alumina rod, all placed in a stainless steel sheath. The thermocouple has been brazed into the copper slug by means of a 20 KW vacuum induction heater. The location of the thermocouple is such that whatever temperature the thermocouple senses is the surface temperature of the copper slug without the presence of the thermocouple. Once the surface temperature-time history is determined for the one dimensional heating of the copper slug, an IBM program is employed to determine the heat flux to the copper calorimeter as a function of time. This calorimeter is mounted in a copper sleeve with an annular air gap between the calorimeter and the sleeve.

The flat plate pressure distribution will be utilized to find the radial velocity gradient at the stagnation point of the plates. Following Bade(12), the velocity distribution produced by normal impingement of a free jet upon a flat plate can be represented approximately by the analytical form

$$u = \beta r (1 + C_1 r) \tag{4}$$

in which u is the component of the velocity parallel to the surface at the edge of the boundary layer r is the radial distance from the stagnation point β is the stagnation point velocity gradient and C_1 is a coefficient with the dimensions of an inverse length. Using the measured pressure data and assuming isentropic flow, the ratio of local velocity to free stream jet velocity (u/u_∞), is calculated for each port location. The non-dimensional parameter $K(r) = (D_{jet}/r)(u/u_\infty)$ is computed for each experimental pressure reading. $K(r)$ is then plotted against r and the experimental points are fitted with a straight line equation of this line is

$$K(r) = (D_{jet}/u_\infty) \beta (1 + C_1 r) \tag{5}$$

-45-

The intercept K(o) of the fitted line at r=o therefore gives the coefficient in the velocity gradient relation

$$\beta = K(o) \left(U_\infty / D_{jet} \right) \qquad (6)$$

The stagnation point velocity gradient so determined will be used in the Fay-Riddell(8) equation for stagnation point heating in order to calculate the heat flux to the plate. Such calculations will be compared with the measured values of heat flux obtained as described above.

III. ANALYTICAL

During the technical information meeting of 21 July 1964, Aeronautical Research Associates of Princeton presented an analysis of turbulent mixing along a plane free jet boundary. Both incompressible and compressible cases were considered. The flow model and nomenclature used in the analysis are shown in Figure 31. In this manner it was possible to relate all of the flow properties of interest, including the turbulent exchange coefficient, to the spreading parameter $a = \delta/x$, a quantity which can be experimentally determined. An important assumption made in this analysis is that the particular form of the assumed velocity profile across the mixing region does not greatly affect the turbulent exchange coefficient determination. Thus, for simplicity, a linear profile, $u = U_o + y/\delta$ was chosen. In order to provide a single check on that assumption, an alternate sinusoidal velocity profile (which should be chosen to reality), was chosen: $\frac{2u}{U_e} = 1 + \sin(\frac{\pi}{2} + \pi \frac{y - y}{\delta})$ The incompressible results obtained under each assumption are shown in the table below.

VELOCITY PROFILE

	Straight Line	Sinusoidal
U_o/U_e	2/3	.692
η_1	a/3	3a/8
η_2	$\frac{-2a}{3}$	-5a/8
v_3/U_e	a/6	a/8
η^*	-.090a	-a/16
K	.063a	.067a

It can be seen that the expression for K is changed only slightly by the alternate velocity profile assumption, thus suggesting that the original assumptions of a straight line profile is sufficient and that K is not sensitive to the particular profile chosen.

IV. PLANS FOR THE NEXT QUARTERLY PERIOD

During the next quarterly reporting period it is intended that a good portion of the axial and radial surveying of the jet be completed.

ASSUMED PROFILE: $u = \frac{1}{2}u_e + \frac{1}{2}u_e \sin\left(\frac{\pi}{2} + \pi\frac{y-y}{\delta}\right)$
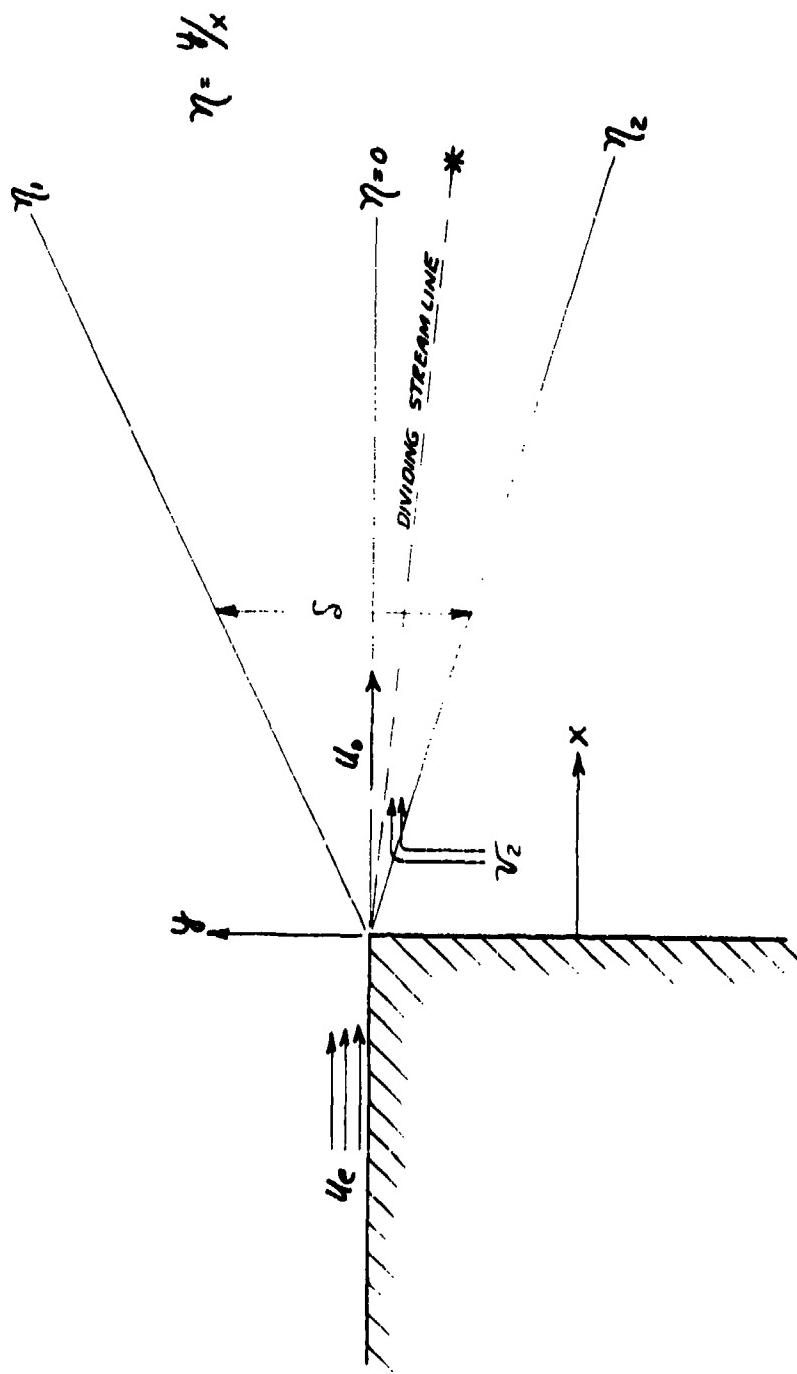
FIGURE 31 FLOW MODEL TURBULENT MIXING ANALYSIS

This will be preceded by completion and calibration of the probes to be used, and final construction of the instrumentation platform, the positioning mechanism, and the high pressure water supply. Data reduction connected with these surveys should also be substantially completed. It is intended that a computer program be written in order to make such data reduction fast and accurate, requiring only directly measured quantities plus values read from the nitrogen-air mixture diagrams as inputs. Aeronautical Research Associates of Princeton will be consulted regarding the calculation of turbulent exchange parameters arising from these survey results, in order that the exchange parameters determined may have maximum application to all portions of the program and to future investigations.

In addition, significant progress should be made in the determination of flat plate heat flux and pressure distributions. These quantities will be investigated at various axial positions in both properly expanded and underexpanded jets. These tests will be preceded by completion of the revised plates and further testing of their ability to withstand the high heating environment to which they are to be subjected.

REFERENCES

1. "Theoretical and Experimental Investigation of Arc Plasma-Generation Technology", ASD TDR62-729, Part I, January 1963.

2. Birkhoff, G. and E. H. Zarantonello, "Jets, Wakes, and Cavities", N.Y., Academic Press, 1957.

3. Bond, C. E. et al., "The Development of a Ten-Megawatt Multi-Arc and Its Operational Use in Hypersonic Re-entry Vehicle Studies", RAD TM-62-5, 22 February 1962.

4. "30-Kilowatt Plasma-Jet Rocket-Engine Development, Second Year Development Program Summary Report" (u), NASA CR-54-044 15 July 1964, Confidential.

5. Grey, J1, P. F. Jacobs, and M. P. Sherman, "Calorimetric Probes for the Measurement of Extremely High Temperatures", The Review of Scientific Instruments, $\underline{33}$ (1962), 7.

6. Bade, W.L., "Experimental Tests of Arc Jet Energy Balance," AVCO Internal Memorandum, 3/9/60.

7. Warren, W. R., "An analytical and Experimental Study of Compressible Free Jets", PhD Thesis, Princeton University, Princeton, N.J.,1957.

8. Fay, J. A. and F. R. Riddell, "Theory of Stagnation Point Heat Transfer in Dissociated Air", Journal of Aeronautical Sciences", $\underline{25}$ (1958), 2

9. Wethern R. J., "Method of Analyzing Laminar Arc Tunnel Heat Transfer Data," AIAA Journal, $\underline{1}$ (1963), 7, p. 1665.

10. Beck, J. V., and H. Hurwicz, "Effect of Thermocouple Cavity on Heat Sink Temperature", Journal of Heat Transfer, Trans. ASME, Series C, $\underline{82}$, Feb. 1960, p. 27.

11. Greyrad Corporation, "A Manual of Information of the Extreme-Temperature Gas Sampling Probe", Publication G-1A, June 15, 1962.

12. Bade, W. L. and H. L. Schick, "Velocity Distribution Produced by Normal Impingement of a Subsonic Plasma Jet Upon a Plane Surface", Avco Internal Memorandum, 8 May 1959.

DISTRIBUTION

Director
Advanced Research Projects Agency
Washington, D.C.

6

Director
U.S. Naval Research Laboratory
Washington, D. C.
Attention: Code 1570

150

Defense Documentation Center
Cameron Station
Alexandria, Va.   22314

20

J. Bennett
L. Cass
. Comfort
M. Gorlansky
M. Hermann
H. Hoercher
P. John
M. Malin
T. Mix
. O'Connor

HYPERVELOCITY CITY KILL MECHANISMS PROGRAM (U)

Aerothermal Phase

Quarterly Technical Progress Report
for Period Ending
30 September 1964

Coleman duP. Donaldson
R. Evan Gray
Richard S. Snedeker

SUMMARY

The work performed by ARAP in assisting NRL in the monitoring of the Aerothermal Phase is reviewed. Several experimental studies designed to provide back-up information for the more extensive efforts of the other groups involved are described. Recent developments in ARAP's own basic research program, including the completion of reports covering the study of jet impingement phenomena, are also discussed.

INTRODUCTION

During the six-month period just past, a portion of ARAP's over-all program of research into the basic aspects of aerothermal processes under the NOL contract has been essentially completed, while investigations in other areas have continued. The results of an experimental study of impinging jets are being reported in two reports as ARAP Report Nos. 63 and 64. One of these is now complete, and both will be distributed in the near future. Other areas in which experimental investigations are continuing are those dealing with the phenomena of coupled flows and the problem of vehicle hardening by means of interior foam packing. Theoretical studies of the former have been extended to consideration of mixing of two gases in an effort to gain a better understanding of shear layer mixing in general and coupled flows in particular. ARAP has continued, during this period, to assist NOL in the over-all management and coordination of its aerothermal phase. As a part of this effort, several additional investigations have been carried out on problems of current interest. In addition, meetings among the active participants in the Aerothermal Phase have been held in order to set program goals in the light of the most recent developments.

MANAGEMENT AND COORDINATION

As in the past, ARAP's effort in this area has consisted in the performance of certain theoretical and analytical studies designed to provide information or data in support of the more extensive work being conducted by other Aerothermal Phase research groups. In particular, further tests were conducted on the general behavior of composite materials subjected to localized heating such as that due to a jet impingement of a hot jet. The material, typical of that used in certain reentry vehicle heat shields, consisted of a backing of aluminum and molded phenolic nylon separated by separate layers of epoxy resin and rubber. Sample pieces of this material 10" wide with a total thickness of about 3/4-inch were subjected to the spot heating of an oxyacetylene flame impinging on the aluminum side. In order to determine the likelihood of possible destructive internal pressure buildup due to decomposition

outgassing of the bonding material, a pressure tap and a thermocouple were inserted in the bonding material directly below the impingement point. Other thermocouples were provided at intervals away from this point so that the temperature-time history could be recorded throughout the heated region. Earlier tests of this kind which were not instrumented had shown that a failure due to bond decomposition could occur, but the composite material in that case was altered to induce such an effect by using a very thin aluminum layer. On applying the flame to the instrumented sample of unaltered material, it was found that the thermal deformations which were apparently of different magnitude in the aluminum and phenolic nylon layers were sufficient when combined with the decreased bond strength at higher temperatures to cause the mechanical separation of the layers before any appreciable pressure build-up could occur. As a result, a further test was planned using a sample mounted rigidly in a frame which both sealed and clamped the edges in order to avoid over-all mechanical deformation. It is felt that this arrangement will simulate better the case of a large expanse of material surrounding a spot of localized heating.

Another study which has been undertaken under the management and coordination portion of ARAP's effort is one designed to estimate the magnitude of certain interference effects which may be encountered in the course of the free and impinging arc-jet studies being conducted by AVCO. Two principal effects appear to be of possible importance. The first of these is a localized effect due to the presence of the probe itself in the flow. In a shear flow such as that in a jet, a probe produces local flow distortions which can result in erroneous readings. The magnitude of such errors, in turn, depends upon the size of the probe relative to the flow. Another potential source of interference is the entire geometry of the test setup. In this case, the whole jet flow field can be distorted as it passes nearby objects. This effect can be complicated by asymmetries produced in the entrainment flow field by other parts of the apparatus. In order to check the magnitude of such effects, ARAP has begun a series of measurements using probes of the AVCO design in several sizes. By making comparisons between each of these probes and a reference probe, it should be possible to isolate the probe size effect. In addition, a test setup designed to simulate AVCO's will be used and compared to one of different geometry in an attempt to evaluate the over-all interference effect.

During the reporting period, three meetings took place among those groups engaged in the Aerothermal Phase (NRL, AVCO, GE, and ARAP). These meetings primarily involved the review and discussion of recent results, current activities, and immediate future goals. The problem of evaluating foam packing materials as hardeners, which is currently under study at GE, was discussed at these meetings and the results of GE's simulated environment tests with foam packed models were presented. In this area, ARAP will carry out a basic experimental study designed to determine the behavior of various foam materials when they are subjected to dynamic and thermal loading.

JET IMPINGEMENT, WALL JET, AND FREE SHEAR LAYER STUDIES

Theoretical. A major analytical study of the characteristics of free shear flow was completed during this reporting period. A free shear flow occurs when a free stream of gas moving at some velocity passes over a cavity of stagnant gas. The shear which develops between the moving and still gas causes a mixing region to develop downstream of the initial encounter of the two gases. Expressions have been derived and programmed for a digital computer, and results have been obtained on the following properties of such a free shear flow:

1. The location of the dividing streamline

2. The growth of the mixing region

3. The energy transferred across the mixing region

4. The stagnation point heating caused by the free shear flow impinging on a blunt edged wall.

Initially, this work was confined to mixing of a single uniform gas. Subsequently, the mixing of two distinct gases, one in the main stream and the other in the cavity were incorporated into the analysis. The consideration of a different gas in the cavity stems from the possibility of decomposition products being present due to internal heating. Thus, it is now possible to solve for the above-mentioned characteristics as functions of the properties of the two gases as well as their stagnation enthalpy ratio and Mach number of the main flow.

A comprehensive report which will present the analysis and results for a number of cases is in preparation and will be issued as a separate document.

Experimental. The principal part of ARAP's experimental program under the Aerothermal Phase has been the thorough investigation of jet impingement phenomena. This study has been particularly important in view of the role of heat transfer by jet impingement for both small hole (low $A/V^{2/3}$) and large hole or "coupled" (large $A/V^{2/3}$) conditions of the punctured reentry vehicle. During the past six-month period, the primary effort has been directed to the completion of this experimental phase and the preparation of two comprehensive reports in which the detailed results are presented. The first of these reports is complete and is to be issued as ARAP Report No. 63. It covers the free jet and normal impingement studies which constitute the bulk of the program. A second report covering results for oblique impingement is to be issued as ARAP Report No. 64 and is now nearing completion. Most of the pertinent results of these studies have been reviewed in previous status reports.

In view of the increased understanding gained in recent months of the general nature of the free shear layer as applied to the coupled flow problem, it has been decided to place less emphasis on further experimental studies in this area at the present time. However, a correspondingly more thorough investigation of the behavior of foam packing materials has been planned and is about to begin.

ARPA 149 TECHNICAL REPORTS

1. Raytheon Company, "Soviet ICBM Re-Entry Body Study,"
    BR-1065, 21 November 1960 (S-RD)

2. Progress Report No. 1, "Hypervelocity Kill Mechanisms
    Program," NRL Memorandum Report 1136, January 1961 (S-RD)

3. AVCO Corporation, "Feasibility Study of a Flight Test
    Aggravation Program, Hypervelocity Kill Mechanism Program-
    Aerothermal Phase," TAD-TR-29-61-4. 13 February 1961 (S)

4. Progress Report No. 2, "Hypervelocity Kill Mechanisms
    Program," NRL Memorandum Report 1161, April 1961 (S-RD)

5. Progress Report No. 3, "Hypervelocity Kill Mechanisms
    Program," NRL Memorandum Report 1209, July 1961 (S-RD)

6. Summary Report, "Fifth Hypervelocity Kill Mechanisms
    Progress Meeting," of 29-30 June 1961, NRL Memorandum
    Report 1220, August 1961 (S-RD)

7. Progress Report No. 4, "Hypervelocity Kill Mechanisms
    Program," NRL Memorandum Report 1240, Quarterly Progress
    for Period Ending 20 September 1961 (S-RD)

8. "Force Tests on Modified General Electric Mark III Nose
    Cone Models at Mach Number 16," AEDC-TN-61-151, von
    Karman Gas Dynamics Facility, ARO, Inc., November 1961 (S)

9. Progress Report No. 5, "Hypervelocity Kill Mechanisms
    Program," NRL Memorandum Report 1261, Volume I and Volume II,
    Annual Technical Progress Report December 1961 (S-RD)

10. Progress Report No. 6, "Hypervelocity Kill Mechanisms
    Program," NRL Memorandum Report 1269, Quarterly Progress
    for the Period Ending 20 December 1961 (S-RD)

11. NRL Memorandum Report 1314, "Investigation of ICBM
    Vulnerability to ARPAT Dart," 30 April 1961 (S-RD)

12. General Electric Company, "Hypervelocity Kill Mechanisms
    Feasibility Study-Internal Heating," Document No. 62SD560
    28 May 1962 (S)

13. Progress Report No. 7 "Hypervelocity Kill Mechanisms
    Program," NRL Report 5813, Semiannual Technical Progress
    Report for period ending 20 March 1962 - June 1962 (S-RD)

14. Progress Report No. 8, "Hypervelocity Kill Mechanisms
    Program," NRL Report 5840, Quarterly Progress Report for
    Period ending 20 June 1962 (S-RD)

15. Progress Report No. 9, "Hypervelocity Kill Mechanisms Program," NRL Report 5913, Annual Technical Progress Report for period ending 30 September 1962 (S-RD) Vols. I and II

16. Progress Report No. 10, "Hypervelocity Kill Mechanisms Program," NRL Report 5931, Quarterly Progress Report for period ending 20 December 1962 (S-RD)

17. General Electric Company, "Results of Rocket Exhaust HKM Internal Heating Tests, Document No. 63SD564 of 20 May 1963 (S)

18. Progress Report No 11, "Hypervelocity Kill Mechanisms Program', NRL Report 5990, Semiannual Technical Progress Report for Period Ending 20 March 1963. (S-RD)

19. Progress Report No 12, "Hypervelocity Kill Mechanisms Program," NRL Quarterly Progress Report 6011, August 1963 (S)

20 NRL Report No. 6032 "Hypervelocity Impact Damage to Spaced Structures by Massive Projectiles," October 1963 (S)

21. General Electric Company, "Results of Wallops Island HKM Internal Heating Flight Tests," Document No. 63SD885, 4 November 1963 (S)

22. Picatinny Arsenal T.R. No. 3118, "Vulnerability of Nuclear Warheads to Aerothermal Effects," December 1963 (S-RD)

23. Progress Report No. 13 "Hypervelocity Kill Mechanisms Program', NRL Report 6077, February 1964 (S)

24. "Propulsion System Damage Study", Volume I, Summary, Conclusions, and Recommendations; ASD-TDR-64-2, January 1964 (S)

25. "Propulsion System Damage Study", Volume II, Vulnerability Analyses; ASD-TDR-64-2, January 1964 (S)

26. "Propulsion System Damage Study", Volume III, Impact-Damage Studies; ASD-TDR-64-2, January 1964 (S)

27. "A Damage Effects Investigation on a 10-Degree Half-Angle Cone at Mach 10" TDR No. AEDC-TDR-64-80, von Karman Gas Dynamics Facility, ARO Inc. May 1964 (S)

28. Progress Report No. 15 "Hypervelocity Kill Mechanisms Program," NRL Report 6214, Semiannual Technical Progress Report for Period Ending 31 March 1964 (S)

29. Summary Report; Malta Rocket Exhaust Internal Heating Tests, HKM Program, Document No. 64SD891; D.E. Nestler; July 17, 1964.

No. of Copies

Director   6
Advanced Research Projects Agency
Washington, D.C. 20301

Director of Defense Research and Engineering   1
Washington, D.C. 20301

Director   1
Weapons Systems Evaluation Group
Room 1E 875, Pentagon
Washington, D.C. 20301

Central Intelligence Agency   1
Washington, D.C. 20505

Defense Documentation Center   20
Building #5, Cameron Station
Alexandria, Virginia 22314

Commander   2
Ballistic Systems Division, AFSC, USAF
Norton Air Force Base, Calif.

Commander   2
Space Systems Division
AFSC, USAF, AF Unit Post Office
Los Angeles, California 90045

Commander   1
Hq. AFCCDD (ESRB)
LG Hanscom Field
Bedford, Mass. 07131
Attn: MAJOR Hippler

Commander   2
Detachment 4, ASD, AFSC
U.S. Air Force
Eglin Air Force Base, Florida 32542
Attn: Mr. Dale Davis
       Technical Library (PGTRI)

Commander   2
Air Force Special Weapons Center
Kirtland Air Force Base, New Mexico 87117
Attn: MAJOR M.R. Nedler,(SWRA)
       CAPT. Gillespie (S WRA-3175)

Commander   2
Field Command
Defense Atomic Support Agency (DASA)
Sandia Base, P.O. Box 5800
Albuquerque, New Mexico 87115

No. of Copies

Air University Library   1
U.S. Air Force
Maxwell Air Force Base
Alabama 36112

Commander   3
Aeronautical Systems Division, AFSC, USAF
Wright-Patterson Air Force Base, Ohio 45433
Attn: ASRCEA/LT D.L. Wells
        ASRNGW-1 Leo Krautmann
        AF Technical Information Center

Headquarters   1
United States Air Force
Air Force Technical Applications Center/TD, Wash, D.C.

Director   2
Ballistic Research Laboratories
Aberdeen Proving Ground, Aberdeen, Maryland, 21005
Attn: Dr. R. J. Eichelberger
        Dr. C. Glass

Officer in Charge   1
U.S. Continental Army Command
Office of Special Weapons Developments
Fort Bliss, Texas 79916
Attn: CAPT. T.W. Love

Commanding Officer   1
U.S. Army Air Defense Combat Development Agency
Fort Bliss, Texas 79916
Attn: CAPT. J. Monza

Commanding Officer   1
Army Material Command RD
Washington, D.C. 20315
Attn: Mr. G. Stetson

Commanding Officer   2
Picatinny Arsenal
Dover, New Jersey 07801
Attn: Mr. Fred Saxe
        Dr. A. Nordio

Commander   5
U.S. Army Missile Command
Redstone Arsenal
Huntsville, Alabama 35809

No. of Copies

Chief of Naval Operations (OP-761) 1
Department of the Navy
Washington, D. C. 20350

Chief of Naval Operations (OP9221D) 1
Department of the Navy
Washington, D. C.
Attn: Mr. E. Cecil 20350

Chief
Bureau of Naval Weapons (RTAD) 1
Attn: D.J. Brockway
Washington, D. C. 20360

Commanding Officer 1
U.S. Naval Air Development Center
Johnsville, Pennsylvania

Commanding Officer 1
U.S. Naval Weapons Evaluation Facility
Kirtland Air Force Base
New Mexico
Attn: Code 3432
        Mr. C.B. Massengill

Director 3
U.S. Naval Research Laboratory
Washington, D. C. 20390
Attn: Mr. W. W. Atkins

Director, National Aeronautics & Space Administration
Langley Research Center, 1
Langley Field, Virginia 23365
Attn: Mr. R. Hopko

University of California 1
Lawrence Radiation Laboratory
Technical Information Division
P.O. Box 808, Livermore, California 94557
Attn: Clovis G. Craig

Aeronautical Research Associates of Princeton, Inc. 2
50 Washington Road
Princeton, N. J. 08540
Attn: Dr. C. duP. Donaldson

Aerospace Corporation 4
P. O. Box 95085
Los Angeles 45, California
Attn: Library Technical Documents Group
        Dr. D. Singer
        Mr. J. Brown
        Mr. R. B. Mortensen

No. of Copies

AVCO Corporation   2
Research and Advanced Development Division
201 Lowell Street
Wilmington, Massachusetts 01887
Attn: Mr. R.S. Timmins

Battelle Memorial Institute   2
505 King Avenue
Columbus 1, Ohio 43201
Attn: Battelle - Defender

Bell Telephone Laboratories, Inc.   1
Whippany, New Jersey
Attn: Mr. D. Pope

Douglas Aircraft Company, Inc.   1
Missiles and Space Systems
3000 Ocean Park Boulevard
Santa Monica, California
Attn: Mr. T.J. Wolinski

General Atomic   1
P.O. Box 608
San Diego 12, California
Attn: Mr. A. J. Navoy

General Electric Company   2
Missile and Space Vehicle Department
3198 Chestnut Street
Philadelphia, Penna. 19104
Attn: Mr. D. Nestler

Hughes Aircraft Company   2
Culver City, California
Attn: Mr. G. Henry

Institute of Defense Analysis   1
1666 Connecticut Avenue, N.W.
Washington, D. C. 20009

Rand Corporation   1
1700 Main Street
Santa Monica, California 90406 Attn: Library 79

Shock Hydrodynamics, Inc.   1
15010 Ventura Boulevard
Sherman Oaks, Calif. 91403
Attn: Mr. K.N. Kreyenhagen

No. of Copies

Boeing Aircraft Company   1
Box 3703
Seattle, Washington
Attn: Mr. Ray Elam

DOCUMENT CONTROL DATA - R&D
(Security classification of title, body of abstract and indexing annotation must be entered when the overall report is classified)

1 ORIGINATING ACTIVITY (Corporate author)	2a REPORT SECURITY CLASSIFICATION
U.S. Naval Research Laboratory Washington, D.C. 20390	SECRET
	2b GROUP 3

3 REPORT TITLE

Progress Report No. 17, "Hypervelocity Kill Mechanisms Program," Semiannual Technical Progress Report, for period ending 30 September 1964.

4 DESCRIPTIVE NOTES (Type of report and inclusive dates)

Semiannual technical progress report for period ending 30 September 1964.

5 AUTHOR(S) (Last name, first name, initial)

No specific authors as this volume contains contributions from many sources.

6 REPORT DATE	7a TOTAL NO OF PAGES	7b NO OF REFS
December 1964	148	57

8a CONTRACT OR GRANT NO	9a ORIGINATOR'S REPORT NUMBER(S)
ARPA Order No. 149-60	NRL Report 6265 - Vol. I
b PROJECT NO NRL Problem F04-11	
c	9b OTHER REPORT NO(S) (Any other numbers that may be assigned this report)
d	

10 AVAILABILITY LIMITATION NOTICES All distribution of this report is controlled. Qualified DDC users shall request through Director, U.S. Naval Research Laboratory, Washington, D.C. 20390

11 SUPPLEMENTARY NOTES This report contains semiannual progress reports from several contributors to this program.	12 SPONSORING MILITARY ACTIVITY ARPA

13 ABSTRACT (SECRET)

The work of this program has involved comprehensive studies designed to evaluate the feasibility of defeating the mission of an intercontinental ballistic missile by fragment impact and/or by subsequent re-entry heating effects. These effects include: direct kill by impact, extent of aggravation or increase in damage caused by aerothermal effects on an R/V during re-entry, aerodynamic instability of nose cones caused by damage to the heat shield and structure, impact and thermal damage to internal components and warheads, and perturbations on the performance of ICBM booster vehicles.

DD FORM **1473**
1 JAN 64

14 KEY WORDS	LINK A		LINK B		
	ROLE	WT	ROLE	W	
Hypervelocity Kill Mechanisms					
Intercontinental Ballistic Missiles					
Fragment Impact					
Re-entry Heating					
Aerothermal Effects					
Aerodynamic Instability of Nose Cones					
ICBM Booster Vehicles					
Impact Damage to ICBM's					

INSTRUCTIONS

1. ORIGINATING ACTIVITY: Enter the name and address of the contractor, subcontractor, grantee, Department of Defense activity or other organization (corporate author) issuing the report.

2a. REPORT SECURITY CLASSIFICATION: Enter the overall security classification of the report. Indicate whether "Restricted Data" is included. Marking is to be in accordance with appropriate security regulations.

2b. GROUP: Automatic downgrading is specified in DoD Directive 5200.10 and Armed Forces Industrial Manual. Enter the group number. Also, when applicable, show that optional markings have been used for Group 3 and Group 4 as authorized.

3. REPORT TITLE: Enter the complete report title in all capital letters. Titles in all cases should be unclassified. If a meaningful title cannot be selected without classification, show title classification in all capitals in parenthesis immediately following the title.

4. DESCRIPTIVE NOTES: If appropriate, enter the type of report, e.g., interim, progress, summary, annual, or final. Give the inclusive dates when a specific reporting period is covered.

5. AUTHOR(S): Enter the name(s) of author(s) as shown on or in the report. Enter last name, first name, middle initial. If military, show rank and branch of service. The name of the principal author is an absolute minimum requirement.

6. REPORT DATE: Enter the date of the report as day, month, year; or month, year. If more than one date appears on the report, use date of publication.

7a. TOTAL NUMBER OF PAGES: The total page count should follow normal pagination procedures, i.e., enter the number of pages containing information.

7b. NUMBER OF REFERENCES: Enter the total number of references cited in the report.

8a. CONTRACT OR GRANT NUMBER: If appropriate, enter the applicable number of the contract or grant under which the report was written.

8b, 8c, & 8d. PROJECT NUMBER: Enter the appropriate military department identification, such as project number, subproject number, system numbers, task number, etc.

9a. ORIGINATOR'S REPORT NUMBER(S): Enter the official report number by which the document will be identified and controlled by the originating activity. This number must be unique to this report.

9b. OTHER REPORT NUMBER(S): If the report has been assigned any other report numbers (either by the originator or by the sponsor), also enter this number(s).

10. AVAILABILITY/LIMITATION NOTICES: Enter any limitations on further dissemination of the report, other than those imposed by security classification, using standard statements such as:

(1) "Qualified requesters may obtain copies of this report from DDC."

(2) "Foreign announcement and dissemination of this report by DDC is not authorized."

(3) "U. S. Government agencies may obtain copies of this report directly from DDC. Other qualified DDC users shall request through

_____"

(4) "U. S. military agencies may obtain copies of this report directly from DDC. Other qualified users shall request through

_____"

(5) "All distribution of this report is controlled. Qualified DDC users shall request through

_____"

If the report has been furnished to the Office of Technical Services, Department of Commerce, for sale to the public, indicate this fact and enter the price, if known.

11. SUPPLEMENTARY NOTES: Use for additional explanatory notes.

12. SPONSORING MILITARY ACTIVITY: Enter the name of the departmental project office or laboratory sponsoring (paying for) the research and development. Include address.

13. ABSTRACT: Enter an abstract giving a brief and factual summary of the document indicative of the report, even though it may also appear elsewhere in the body of the technical report. If additional space is required, a continuation sheet shall be attached.

It is highly desirable that the abstract of classified reports be unclassified. Each paragraph of the abstract shall end with an indication of the military security classification of the information in the paragraph, represented as (TS), (S), (C), or (U).

There is no limitation on the length of the abstract. However, the suggested length is from 150 to 225 words.

14. KEY WORDS: Key words are technically meaningful terms or short phrases that characterize a report and may be used as index entries for cataloging the report. Key words must be selected so that no security classification is required. Identifiers, such as equipment model designation, trade name, military project code name, geographic location, may be used as key words but will be followed by an indication of technical context. The assignment of links, roles, and weights is optional.

Z-8

Naval Research Laboratory
Technical Library
Research Reports Section

DATE: December 20, 2002

FROM: Mary Templeman, Code 5227

TO: **Code 6300 Dr Gubser**

CC: Tina Smallwood, Code 1221.1 *fd 1/6/03*

SUBJ: Review of NRL Reports

Dear Sir/Madam:

Please review NRL Report 6214, 6077, 6011, 6265-V1 and 6265-V2 for:

☑ Possible Distribution Statement

☑ Possible Change in Classification

Thank you,

Mary Templeman
(202)767-3425
maryt@library.nrl.navy.mil

The subject report can be:

☒ Changed to Distribution A (Unlimited)

☒ Changed to Classification *unclassified*

☐ Other:

_____ 1/2/03
Signature   Date